UNIVERSITY OF CALIFORNIA, SAN DIEGO

Understanding and Mimicking Developmental Mechanics to Enhance Cardiomyocyte Maturation and Therapeutic Translation

A dissertation submitted in partial satisfaction of the requirements for the degree Doctor of Philosophy

in

Bioengineering

by

Jennifer L. Young

Committee in charge:

Professor Adam J. Engler, Chair
Professor Adah Almutairi
Professor Shu Chien
Professor Karen L. Christman
Professor Sylvia Evans

2013

The dissertation of Jennifer L. Young is approved, and it is acceptable in quality and form for publication on microfilm and electronically:

_____

_____

_____

_____

_____
Chair

University of California, San Diego

2013

DEDICATION

To my family, friends and academic advisors
who contributed to this work in their own unique ways.

EPIGRAPH

"The important thing in science is not so much to obtain new facts as to discover new ways of thinking about them."

- Sir William Bragg

"You have to know how to accept rejection and reject acceptance."

- Ray Bradbury

"If a man will begin with certainties, he shall end in doubts; but if he will be content to begin with doubts he shall end in certainties."

-Sir Francis Bacon

TABLE OF CONTENTS

LIST OF FIGURES AND TABLES

Chapter 2

Chapter 3

Chapter 4

ACKNOWLEDGEMENTS

I would like to thank my doctoral adviser and committee chair, Professor Adam J. Engler, for guiding and supporting me throughout my doctoral journey. Without his contributions, this work would not have been possible.

I would also like to acknowledge my committee chair Professor Karen L. Christman, whose expertise with *in vivo* studies greatly aided this project. A great thank you to Professor Shu Chien for guiding me as a committee member, and giving invaluable advice about cellular mechanotransduction. I would like to acknowledge committee chairs Professor Sylvia Evans for her expertise in cardiovascular development and *in vivo* studies, and Professor Adah Almutairi for her expertise in polymer sciences. All of the aforementioned committee members contributed greatly to this work, and I am truly grateful for their generosity in sharing their expertise relating to my project.

I wish to also acknowledge the Bioengineering Department at UCSD for giving me the opportunity to participate in the Ph.D. program. I would like thank all of my funding sources for supporting me throughout my degree- American Heart Association (0865150F to A.J.E), National Institutes of Health (1DP02OD006460 and R21HL106529 to A.J.E.), and American Heart Association Pre-Doctoral Fellowship (10PRE4160143 to J.L.Y) and Achievement Rewards for College Scientists Fellowship (ARCS; to J.L.Y.).

I would like to thank all of the friends I have made at UCSD, who offered invaluable support throughout my time at this university. A special thank you to my lab mates for their help and great times in lab; Dr. Yu Suk Choi, Dr. Gretchen Meyer, Dr. Alexander Fuhrmann, Dr. Somyot Chirasatitsin, Andrew Holle, Ludovic Vincent, Gaurav

Kaushik, Hermes Taylor-Weiner, Jessica Wen, Matthew Ondeck, Kelsey Thomas, Ayla Sessions, Kyle Kretchmer, Justin Tse, Jacquelyn Schaefer and Andrew Lee.

Chapter 2, in full, is a reformatted version of the published article as it appears in *Biomaterials*, volume 32, number 4, pages 1002-1009, February 2011. The dissertation author was the primary investigator and author of this paper, and thanks co-author Dr. Adam J. Engler for his contributions. The authors would like to thank Dr. Donald Elbert (Washington University in Saint Louis) for advice with degradation modeling, Dr. Jean Sanger (Upstate Medical University) for assistance with cardiomyocyte isolation, Dr. Jason Li (Asylum Research) and Dr. Somyot Chirasatitsin for technical assistance with atomic force microscopy, and Dr. Anthony Mrse for assistance with NMR spectroscopy. This work was supported by grants from the American Heart Association (0865150F to A.J.E), NIH (1DP02OD006460 to A.J.E.), and American Heart Association Pre-Doctoral Fellowship (10PRE4160143 to J.L.Y) and Achievement Rewards for College Scientists Fellowship (ARCS; to J.L.Y.).

Chapter 3, in part, is currently being prepared for submission for publication of the material. The dissertation author is the primary investigator and author, and thanks co-author Kyle Kretchmer and Dr. Adam J. Engler for their contributions to the work. The authors would also like to thank Dr. Alexander Zambon for his expertise with using GO-ELITE to analyze microarray data. This work was supported by grants from the American Heart Association (0865150F to A.J.E), National Institutes of Health (R21HL106529 to A.J.E.), American Heart Association Pre-Doctoral Fellowship (10PRE4160143 to J.L.Y), Achievement Rewards for College Scientists Fellowship

(ARCS; to J.L.Y.) and California Institute for Regenerative Medicine (CIRM) Bridges Program (TB1-01186 to K.K).

Chapter 4, in full, is a reformatted version of the published article in *Acta Biomaterialia,* http://dx.doi.org/10.1016/j.actbio.2013.03.019, 2013. The dissertation author was the primary investigator and author of this paper, and thanks co-authors Jeremy Tuler, Rebecca Braden, Pamela Schüp-Magoffin, Jacquelyn Schaefer, Kyle Kretchmer, Dr. Karen Christman and Dr. Adam Engler for their contributions. The author would like to thank Dr. Alex Furhmann (UC San Diego) for use of his AFM analysis code, Dr. Marek Dobke for his kind gift of Restylane® samples and pathology expertise in examining the data shown here, Kenneth Kim and Qiongyu Chen (UCSD Hematology Core) for their hematology expertise, and Dr. William D. Dupont (Vanderbilt University) for use of his statistical power analysis software. This work was supported in part by the National Institutes of Health (R21HL106529 to A.J.E.), American Heart Association (0865150F to A.J.E. and 10PRE4160143 to J.L.Y.), and Achievement Rewards for College Scientists (ARCS; to J.L.Y.).

VITA

2008	Bachelor of Science, University of California, Davis; Davis, CA
2009-2010	Graduate Teaching Assistant, Department of Bioengineering University of California, San Diego
2013	Doctor of Philosophy, University of California, San Diego; La Jolla, CA

FIELDS OF STUDY

Major Field: Bioengineering

Studies in Drug Delivery and Tissue Engineering
Professor J. Kent Leach, Ph.D. (UC Davis)

Studies in Extracellular Matrix and Stem Cell Cardiomyogenesis
Professor Adam J. Engler, Ph.D. (UC San Diego)

PUBLICATIONS

Young, J.L.; Christman, K.L.; Engler, A.J. "Stem Cells for Cardiac Tissue Engineering" ed. Song, L. et al. "Stem Cell and Tissue Engineering" World Scientific Publishing Co., Hackensack, NJ, 2011.

Young, J.L. and Engler, A.J. "Hydrogels with Time-Dependent Mechanical Properties Enhance Cardiomyocyte Differentiation *In Vitro*" *Biomaterials* 32(4): 1002-1009, 2011.

Young, J.L.; Tuler, J.; Braden, R.; Schüp-Magoffin, P.; Schaefer, J.; Kretchmer, K.; Christman, K.L.; Engler, A.J. "*In Vivo* Response to Dynamic Hyaluronic Acid Hydrogels " *Acta Biomaterialia* 9(7): 7151-7157, 2013.

ABSTRACT OF DISSERTATION

Understanding and Mimicking Developmental Mechanics to
Enhance Cardiomyocyte Maturation and Therapeutic Translation

by

Jennifer L. Young
Doctor of Philosophy in Bioengineering
University of California, San Diego, 2013

Professor Adam J. Engler, Chair

Tissue-specific elastic modulus (*E*), or 'stiffness,' arises from developmental changes in the extracellular matrix (ECM) and suggests that progenitor cell differentiation may be optimal when physical conditions mimic tissue progression. For the myocardium, changes in extracellular matrix over time results in a ~10-fold stiffening in the chicken embryo. To mimic this temporal stiffness change *in vitro*, thiolated

hyaluronic acid (HA-SH) hydrogels were crosslinked with poly(ethylene glycol) diacrylate, and their dynamics were modulated by changing crosslinker molecular weight and component compositions. With the hydrogel appropriately tuned to stiffen as heart muscle does during development, embryonic cardiomyocytes grown on collagen-coated HA hydrogels exhibited a 3-fold increase in mature cardiac specific markers and form up to 60% more maturing muscle fibers than they do when grown on compliant but static polyacrylamide hydrogels over 2 weeks.

While active mechanotransduction aided maturation, the specific proteins responsible for responding to time-dependent stiffness remain unknown. In order to assess matrix-mediated mechanotransduction, the expression and phosphorylation state of 800 protein kinases was examined for embryonic cardiomyocytes plated on matrices with either dynamic or static cardiac tissue-specific stiffness. Microarray analysis of protein kinases showed differential expression as a function of mechanics; many cardiogenic pathways exhibited time-dependent up-regulation on dynamic versus static matrices, including PI3K/Akt and p38 MAPK, while GSK3β, a known inhibitor of cardiomyocyte maturation was down regulated.

Though improved cardiomyocyte maturation was observed *in vitro*, host interactions, matrix polymerization, and the stiffening kinetics remain uncertain *in vivo*, and each plays a critical role in therapeutic applications using HA-SH. Subcutaneously injected HA-SH hydrogels showed minimal systemic immune response and host cell infiltration and exhibited time-dependent porosity and stiffness changes at a rate similar to hydrogels polymerized *in vitro*. When injected intramyocardially, visible granulomas and macrophage infiltration were present 1 month post-injection, likely due to reactive

thiol groups. Altogether these data demonstrate the development of a novel hydrogel system that displays dynamic developmental cues in order to enhance embryonic cardiomyocyte maturation *in vitro*; however, the *in vivo* applicability of this material in vascularized tissue appears limited.

Chapter 1

Introduction

The ability of cells to sense and respond to matrix-mediated mechanical stimuli has become more widely appreciated within the last decade, resulting in a new paradigm for understanding cellular behavior. *In vitro,* a variety of cell responses can be altered by matrix elasticity, or stiffness, including migration (1-5), adhesion (6-8), proliferation (9-11) and–if a stem cell–differentiation (1, 6, 10, 12, 13). *In vivo,* tissue morphogenesis and disease remodeling can result in drastic changes in extracellular matrix (ECM) stiffness (14-17). Consequently, experiments involving stem or progenitor cells, as well as therapeutic interventions, must take matrix mechanics into account in order to more completely mimic a given cell's niche. Differential matrix-mediated cell responses are a result of mechanotransduction, the process in which a cell converts outside mechanical stimuli into internal chemical changes. While cell behaviors have traditionally been exploited using chemical cues, this chapter will introduce the concept that cells can

respond to the mechanical cues of their niche, describe the temporal variation of these cues during development and outline how one can mimic these changes in a reductionist manner *in vitro*. In particular, this dissertation focuses on cardiac mechanics in regards to tissue development, cellular maturation and therapeutic interventions, which is introduced here as well.

1.1 Cardiac Development and Mechanics

Development of the cardiovascular system is highly complex, as it is responsible for supplying nutrients and oxygen to the embryo and transporting waste and cells, all while undergoing drastic morphological changes. Active mechanical forces derived from torsion, bending and fluid shear stress are responsible for the proper development of the heart and resident cells (18). Passive mechanical properties, e.g. Young's Modulus, have also been shown to play a role in the morphogenesis of the heart as well as differentiation and development of cardiac cells (14, 19-24). These mechanical cues are of course coupled with the expression of precisely-timed chemical cues, e.g. NKX-2.5 (25), BMP4 (26) and ROCK (27-30), which will be discussed in the next section. All of these changes result in well-documented developmental stages, which in avian species have been characterized by their "HH" stage–named for Hamburger and Hamilton (31, 32) and in non-human mammals by their embryonic day (E) post-fertilization (33).

Cardiac precursor cells derive from the mesodermal germ layer of the embryo, and are guided by various transcription factors to migrate and fuse the paired primordia in order to form the primitive heart tube (HH stages 5-9 in the chick embryo; E7.5-8 in the mouse embryo; day 15-20 in the human embryo). The heart tube loops into a 'C-shaped'

then ‘S-shaped’ tube (HH stages 10-24 in the chick, E8-9 in mouse, day 20-28 in human), chambers are formed (HH stages 19-24 in chick, E9-10 in mouse, day 28-32 in human), and lastly, development of cardiac cushions and valves as well as septation of the atria, ventricles and outflow track occurs (HH stages 25-34 in chick, E10-birth in mouse, and days 32-birth in human). These changes during heart development have been linked to the fluid forces present. It has even been proposed that the purpose of the early embryonic heartbeat is not the delivery of nutrients, but rather to produce fluid forces that shape the cardiovascular system; when fluid flow was disrupted, embryos still developed normally for some time through the diffusion of essential molecules (34-37). *In vivo* visualization of fluid dynamics shaping the zebrafish heart has allowed researchers to quantify these large shear forces required for heart development, and they found that when these flows were disturbed, heart chamber development, looping and valve formation were severely affected, indicating that developmental fluid forces are an essential epigenetic factor in cardiogenesis (38).

Next, chamber formation occurs by the bending, twisting and ballooning of the heart tube. Biophysical explanations of these mechanical processes include tissue-imposed forces (30), forces created via actin polymerization (39) and changes in cell shape (40, 41). As discussed above, heart looping occurs in two stages, as the straight heart tube first becomes c-shaped, then s-shaped. Many researchers focus on the c-looping stage, which is composed of two types of deformation: ventral bending and rightward rotation (42). Rotation of the heart tube has been shown to be dependent on the forces applied by the mesodermal splanchnopleure (SPL) and the omphalomesenteric veins (OVs) of the embryo, as when these structures were removed, the ventricle untwists

completely (30). Forces exerted by actin polymerization have been connected to the ventral bending of c-looping and are thought to play a role by altering cell shape (39). When embryos were treated with cytoskeletal disruption agents, looping failed to occur, consistent with a cell shape-mediated process (39). Additional evidence stems from the fact that prominent actin bundles are present around the myocardial cell borders and that polymerization forces can reach up to a few hundred Pascal (Pa) capable of producing >50% strain in the myocardium (20, 39, 43, 44). Regional changes in cell shape have been observed during looping and ballooning of the heart, correlating with locations of curvature, i.e. elongated cells at the outer convex curvature and cuboidal cells at the inner concave curvature (40, 41).

Concomitant with these drastic active mechanical and morphological events are changes in extracellular matrix (ECM) composition. As cells are secreting and assembling new matrix, passive mechanical properties are altered (14), which in turn will affect cell how cells feel their environment and thus, respond to new mechanical loads. This will be discussed in more detail in section 1.4, and is motivation for chapter 1.

1.2 Signal Transduction in Cardiomyocyte Maturation

The precise spatial and temporal patterning of the heart outlined above is achieved partially through the activation of signal transduction pathways (outlined in (45-47)). Signal transduction occurs when molecules secreted by a cell instruct the behavior of adjacent cells via initiation of specific protein kinase pathways. As mentioned previously, cardiac cells derive from the mesodermal germ layer, which are largely guided by signals

arising from the endoderm. Cardiogenic transcription factors, such as NKX-2.5 (48), the GATA family of factors (26, 49-51), and Tbxs 2, 3, and 5 (52), are induced by both positive- and negative-acting signals, which are summarized here and are important to cardiac cell matrix-based studies which will be described in Chapters 2 and 3.

Bone morphogenic proteins 2 and 4 (BMP2 and 4) and fibroblast growth factors (FGFs) have been shown to synergistically work together and play a crucial role in cardiogenesis, both *in vitro* (26, 53-55) and *in vivo* (54-58). BMP2 and 4 act through either the TAK1-MKK23/6-p38/JNK or the *Smad* pathways to induce expression of activating transcription factor-2 (ATF-2), which turns on other cardiac-specific transcription factors (47, 59). FGFs act through the *Ras*/MAPK, the phospholipase C-γ/Ca^{2+}, and the phosphatidylinositol 3 kinase (PI3K)/protein kinase B (PKB/Akt) pathways (60, 61), which induces expression of cardiac transcription factors via ERKs (62), controls myfibrillogenesis and contractility via calcium handling (63) or promotes growth, proliferation and metabolism via protein kinase activity (64), respectively. The PI3K/Akt pathway plays a major role in positively regulating survival, proliferation, growth, regeneration and metabolism of cardiomyocytes in both the adult and embryonic heart (64). During development, Akt regulates proliferation through downstream targets glycogen synthase kinase-3β (GSK-3β) (65) and forkhead transcription factors (FOXOs) (66, 67).

Wnts 3a, 8c and 11 have also been shown to play an important role in cardiogenesis (45, 68). *Wnt* 11, a positive-acting signal, induces the *Wnt*/Ca^{2+} (69) and *Wnt*/polarity (70) pathways, which activate Akt and JNK, respectively (71). *Wnts* 3a and

8c, however, are negative-acting signals because they activate the *Wnt*/β-catenin pathway, which inhibits cardiogenesis at a later stage during induction via expression of GSK-3β (72, 73). Thus, cardiogenic induction requires precisely timed deactivation of these *Wnts* by inhibitory molecules *Dickkopf-1* (DKK-1) and *Crescent* (72). *In vitro* embryonic stem cell differentiation experiments have shown the importance of temporal activation of the JAK/STAT pathway, in which STAT3 is down-regulated at the onset of differentiation, and up-regulated prior to and during beating, while JAK2 is up-regulated in beating cells (74). Each one of these pathways will be explored in Chapter 3 to assess its contribution to matrix-mediated signaling that regulates cardiogenesis.

As mentioned earlier, heart tube formation and looping via establishment of a left-right embryonic axis are the first two major morphological events that occur in heart development (46). While these processes are very complex and will not be discussed in full detail, many factors that play a role in heart tube development have been identified: TGFβ-related molecules *Nodal* and *Lefty* (75-78), *Hedgehog* (*Hh*) genes (79, 80), activins (81) and BMPs (79). After heart tube looping, ventricular chamber development occurs, which is initiated by the formation of trabeculated myocardium, tissue containing protrusions (trabeculae) that forms within the ventricular lumen and aids in blood flow prior to the development of a contractile myocardium (46, 82, 83). Two signal transduction pathways have been identified in the process of trabeculation (46): the retinoic acid (RA) pathway (84, 85), which activates the Homeobox genes (86), and the neuregulin/ErBb pathway (87-90), which activates the PI3K/Akt via focal adhesion kinase (FAK) (91). Lastly, heart valves are formed by expression of *Wnts* via the *Wnt*/β-

catenin pathway (92); *Notch* via TGF-β2 and BMP (93, 94); vascular endothelial growth factor (VEGF) (95, 96) via Ras/MEK/ERK (47), phospholipase C-γ/Ca^{2+}, or PI3K/Akt pathways (97); BMPs (98, 99); Hyaluronic Acid (HA) via Ras and ErBb (100, 101); neurofibromin via Ras/Raf/MEK/ERK (102); and EGF via ErBb (103). While the roles of the aforementioned pathways have been extensively studied in regards to development and differentiation, both *in vitro* and/or *in vivo*, the activation of specific pathways due to mechanical cues, i.e. mechanotransduction, has been less studied. In chapter 3, I will present a means to examine protein kinase activation with respect to culture substrate stiffness, and examine the effects on development of chicken embryonic cardiomyocytes. While beyond the scope of this dissertation, information obtained from examining substrate stiffness-mediated signal transduction could be harnessed to affect cell behavior and/or improve maturation via pathway inhibition, for example.

1.3 Cardiomyocyte Development *In Vitro*

As cells sort and differentiate throughout development, they secrete and assemble extracellular matrix (ECM), giving rise to tissue-specific stiffness, e.g. brain 0.1-1 kPa (104), muscle 8-17 kPa, and bone 25-40 kPa (12). Early microindentation experiments linked the importance of material properties and residual stress present in the myocardium and cardiac jelly in the outer curvature with the morphogenetic process of cardiac looping (20, 21). These researchers postulated the heart would increase stiffness throughout development as sarcomere formation and tissue organization progress. Since then, cardiac tissues have been found to stiffen throughout development (24, 105, 106),

while others have shown that substrate stiffness regulates cardiomyocyte maturation and behavior *in vitro* (22, 23, 106, 107).

When mid- to late-stage embryonic chicken cardiomyocytes were plated on a 10 kPa compliant hydrogel, intracellular and matrix strains were matched, resulting in many striated myofibrils and prolonged beating in culture compared to cells plated on matrices that were too soft or too stiff (22). Similar results were found with neonatal rat cardiomyocytes, in which cells were able to generate greater mechanical force, larger calcium transients and more stored calcium when plated on 10 kPa hydrogels (23). In dense co-cultures of neonatal rat cardiac myocytes and fibroblasts, compliant substrates of stiffness resembling neonatal (22 kPa) and adult tissue (50kPa) were shown to enhance myofibril formation, morphology, beating and force of contraction (106). Similar results were found in co-cultures of chicken embryonic cardiac myocytes and fibroblasts on an 18 kPa compliant material (107); however these studies cannot separate the fact that cells are in syncytium, a state in which cardiomyocytes are in contact and thus can rapidly propagate action potentials through intercalated discs as well as through supporting fibroblasts, likely enhancing their function (108).

Functional data reveals the product of some intracellular perturbation, and many have attempted to uncover these molecular, organizational or structural changes explaining variable force generation and contractility. In regards to the extracellular matrix, force transmission to the cytoskeleton can occur via integrins present at focal adhesions and costameres, protein assemblies that connect sarcomeres to the cell membrane. Myofibrils, which are made of repeating units (sarcomeres), are the contractile machinery of cardiomyocytes (109-111), and as they are connected to force-

generating sites, their development is likely altered by substrate stiffness (22, 112-115). Thus, many studies focus on myofibril development in regards to stiffness and how this in turn regulates the maturation and function of cultured cardiomyocytes. Together, these data indicate an important role for passive mechanical properties of the myocardium in the development of constituent cells, and thus culture systems must reflect these specific characteristics.

1.4 Dynamic Cell Culture Systems and Cellular Responses

Biomaterials, specifically in the form of hydrogels, have become increasingly popular for use in tissue engineering approaches. Hydrogels have proven to be extremely versatile because their mechanical properties, ligand presentation and composition can be made to closely mimic the native microenvironment of tissues. In this dissertation, mechanical properties of hydrogels are of particular interest because they have recently been shown to affect a wide variety of cellular behaviors (7, 12, 13, 116, 117). Conventional hydrogel systems are static and can provide a useful model for examining very specific properties, e.g. ligands (7, 118, 119), stiffness (12) and sequestered growth factors (120, 121). However, with the knowledge that many biological tissue processes are highly dynamic, in both space and time (14-17), the need for responsive hydrogels has arisen.

The first dynamic hydrogels were degradable, i.e. softening materials, which allow for controllable or cell-mediated degradation, an important requirement for implantable biomaterials, as well as growth factor release to provide continual molecular

signaling (122). A classic degradable hydrogel system consists of a natural or synthetic monomer backbone that has incorporated functional moieties capable of hydrolysis (123-127). Cell-secreted proteases, e.g. matrix metalloproteases (MMPs), can also be a means to target incorporated specific peptides and degrade the hydrogel (128-132). Additionally, other common forms of degradable hydrogels are triggered by alterations in pH (133), temperature (134) or light (135-138); however, the effects on cells should be considered.

While softening matrices are important to understand many biological events, stiffening has been shown in development (14) and disease (15-17). Mimicking stiffening can be achieved by similar means to softening hydrogels, i.e. light, pH, temperature, or various molecular means (DNA, chemicals, AFM stiffness clamp, etc.) (138-143). One example is the collagen-alginate hydrogel system, which can crosslink via addition of divalent cations, thereby stiffening as calcium is added to the hydrogel. However, calcium-mediated signaling could alter cell responses, especially in cardiomyocytes, the crosslinks would be ionic rather than covalent, and addition would be difficult *in vivo* (144). pH and temperature changes have also been proposed to modulate network elasticity (145, 146), but these change niche hydrophobicity, as well as potentially alter cell metabolism from prolonged culture in less than optimal media conditions. The use of light has also recently been shown to stiffen methacrylated HA (MeHA) hydrogels, which can be used in a time-dependent manner to produce step-wise crosslinking via UV-activated, free radical polymerization (139). DTT-crosslinked MeHA hydrogels are stable when injected (147), but *in vivo* application is limited by the requirement of UV. Anothe interesting application of switchable hydrogel stiffness is

achieved by DNA-hybrid hydrogels (141, 148, 149). Using the thermal properties of DNA annealing and binding, crosslinks can be made or broken as desired. While the main focus of determining cellular responses to these dynamic hydrogel systems are viability and migration, the aim of this dissertation is to understand how cell development is affected by mechanically-instructive signals.

1.5 Cardiovascular Disease and Regenerative Medicine

As a leading cause of death in the United States, congestive heart failure (CHF) has prompted a wide array of preventative strategies. CHF is commonly preceded by myocardial infarction (MI) in which a major coronary vessel becomes occluded, resulting in inadequate oxygen supply to the heart tissue downstream of the blockage site (150). Within this ischemic tissue, cardiac cells die and a stiff fibrotic scar forms from increased fibroblast-secreted collagen (15, 151). This stiff fibrotic scar impairs the ability of the heart to adequately contract, which causes hypertrophy, wall thinning, and eventually CHF and death. At the root of these functional consequences occurs altered signal transduction among, for instance, the Akt, MAPKs and GSK3β pathways (152, 153), which were interestingly identified in section 1.2 as important players for proper myocardial development. One promising therapeutic approach has involved injecting stem cells into the injured tissue after acute MI has occurred. This procedure, called cellular cardiomyoplasty, has the aim of restoring function and regenerating tissue, thereby avoiding the likely outcome of CHF. While this therapy seemed to provide some promise, *in vivo* trials demonstrated that transplanting cells alone is not sufficient to

achieve uniformly positive results (15, 151, 154-157). Even more alarming, recent studies have reported that hMSCs injected into the ischemic myocardium post-MI formed small calcified lesions (158). This likely stems from the observation that ECM stiffness can direct stem cell differentiation fate; when cultured on materials that mimic the stiffness of brain, muscle and bone, stem cells give rise to neurogenic, myogenic and osteogenic lineages, respectively (12). Thus, cells in the infarct see a matrix that is 3- to 4-fold stiffer than healthy muscle (15), a range that more accurately mimics bone (12), hence their formation of calcified lesions (158). The apparently aberrant behavior of these cells may be best explained by the altered elastic and chemical properties of the diseased tissue providing matrix cues to cells that deviate from the healthy state.

The presence of a soft, deformable ECM is critically important for prolonged function of mature cardiomyocytes *in vitro* as they arrest their rhythmic beating on traditional static culture systems, i.e. cells plated on ECM-coated glass or plastic. On these rigid substrates, cardiomyocytes lose the ability to contract because they become overstrained (22), lose focal adhesions and exhibit altered actomyosin assembly (159). Isolated myocytes cultured on rigid substrates also cannot undergo proper myofibrillogenesis, but rather develop large stress fibers and become overly-adherent to the substrate (118, 160). When softer substrates were used, myofibrillogenesis was able to take place, in addition to rhythmic beating (161). Unlike these studies using more mature myocytes, cell-based MI therapies have employed undifferentiated cells assuming that they could remodel the niche better than mature cells as they differentiate. In order to produce the most effacious treatment, one must first understand mechanical cues

contributing to cardiomyocyte development and maturation, which was highlighted in previous sections.

1.6 Summary

The aims of this dissertation are (1) to characterize the stiffening dynamics of the developing myocardium, (2) to mimic these mechanics *in vitro* using a hydrogel-based approach and characterize biomaterial properties of the hydrogel, (3) to investigate maturation of embryonic cardiomyocytes on dynamically-stiffening hydrogels compared to static hydrogels, (4) to investigate mechanosensitive pathways activated based on matrix mechanics, and (5) to investigate the *in vivo* feasibility of the hydrogel system to be utilized in the heart for a tissue engineering approach. Chapter 2 of this dissertation describes the characterization of the developing myocardium, synthesis of a dynamically stiffening hydrogel, and cellular responses. In chapter 3, protein kinase signaling in the maturation of embryonic cardiomyocytes plated on stiffening and non-stiffening hydrogels is investigated. Lastly, chapter 4 examines the *in vivo* applicability of the hydrogel system described in chapter 2.

1.7 References

1. Tse JR, Engler AJ (2010) Preparation of hydrogel substrates with tunable mechanical properties. *Curr Protoc Cell Biol* Chapter 10:Unit 10.16.

2. Zaari N, Rajagopalan P, Kim SK, Engler AJ, Wong JY (2004) Photopolymerization in Microfluidic Gradient Generators: Microscale Control of

Substrate Compliance to Manipulate Cell Response. *Adv Mater* 16:2133–2137.

3. Peyton SR, Putnam AJ (2005) Extracellular matrix rigidity governs smooth muscle cell motility in a biphasic fashion. *J Cell Physiol* 204(23-24):198–209.

4. Choi YS, Vincent LG, Lee AR, Kretchmer KC, Chirasatitsin C, Dobke MK, Engler AJ (2012) The alignment and fusion assembly of adipose-derived stem cells on mechanically patterned matrices. *Biomaterials* 33(29):6943–6951.

5. Vincent LG, Choi YS, Alonso-Latorre B, del Álamo JC, Engler AJ (2013) Mesenchymal stem cell durotaxis depends on substrate stiffness gradient strength. *Biotechnology Journal* 8(4):472–484.

6. Rowlands AS, George PA, Cooper-White JJ (2008) Directing osteogenic and myogenic differentiation of MSCs: interplay of stiffness and adhesive ligand presentation. *Am J Physiol Cell Physiol* 295(4):C1037–44.

7. Huebsch N, Arany PR, Mao AS, Shvartsman D, Ali OA, Bencherif SA, Rivera-Feliciano J, Mooney DJ (2010) Harnessing traction-mediated manipulation of the cell/matrix interface to control stem-cell fate. *Nature Materials* 9(6):518–526.

8. Shih Y-RV, Tseng K-F, Lai H-Y, Lin C-H, Lee OK (2011) Matrix stiffness regulation of integrin-mediated mechanotransduction during osteogenic differentiation of human mesenchymal stem cells. *J Bone Miner Res* 26 (4):730–738.

9. Ghosh K, Pan Z, Guan E, Ge S, Liu Y, Nakamura T, Ren X-D, Rafailovich M, Clark RAF (2007) Cell adaptation to a physiologically relevant ECM mimic with different viscoelastic properties. *Biomaterials* 28(4):671–679.

10. Evans ND, Minelli C, Gentleman E, LaPointe V, Patankar SN, Kallivretaki M, Chen X, Roberts CJ, Stevens MM (2009) Substrate stiffness affects early differentiation events in embryonic stem cells. *Eur Cell Mater* 18:1–13–discussion 13–14.

11. Marklein RA, Burdick JA (2010) Spatially controlled hydrogel mechanics to modulate stem cell interactions. *Soft Matter* 6(1):136–143.

12. Engler AJ, Sen S, Sweeney HL, Discher DE (2006) Matrix Elasticity Directs Stem Cell Lineage Specification. *Cell* 126(4):677–689.

13. Saha K, Keung AJ, Irwin EF, Li Y, Little L, Schaffer DV, Healy KE (2008) Substrate Modulus Directs Neural Stem Cell Behavior. *Biophysj* 95(9):4426–4438.

14. Jacot JG, Martin JC, Hunt DL (2010) Mechanobiology of cardiomyocyte development. *Journal of Biomechanics* 43(1):93–98.

15. Berry MF, Engler AJ, Woo YJ, Pirolli TJ, Bish LT, Jayasankar V, Morine KJ, Gardner TJ, Discher DE, Sweeney HL (2006) Mesenchymal stem cell injection after myocardial infarction improves myocardial compliance. *Am J Physiol Heart Circ Physiol* 290(6):H2196–203.

16. Georges PC, Hui J-J, Gombos Z, McCormick ME, Wang AY, Uemura M, Mick R, Janmey PA, Furth EE, Wells RG (2007) Increased stiffness of the rat liver precedes matrix deposition: implications for fibrosis. *American Journal of Physiology - Gastrointestinal and Liver Physiology* 293(6):G1147–G1154.

17. Zhang S, Sun A, Ma H, Yao K, Zhou N, Shen L, Zhang C, Zou Y, Ge J (2011) Infarcted myocardium-like stiffness contributes to endothelial progenitor lineage commitment of bone marrow mononuclear cells. *Journal of Cellular and Molecular Medicine* 15(10):2245–2261.

18. Gjorevski N, Nelson CM (2010) The mechanics of development: Models and methods for tissue morphogenesis. *Birth Defects Research Part C: Embryo Today: Reviews* 90(3):193–202.

19. Zamir EA, Srinivasan V, Perucchio R, Taber LA (2003) Mechanical asymmetry in the embryonic chick heart during looping. *Ann Biomed Eng* 31(11):1327–1336.

20. Zamir EA, Taber LA (2004) Material Properties and Residual Stress in the Stage 12 Chick Heart During Cardiac Looping. *J Biomech Eng* 126(6):823–830.

21. Zamir EA, Taber LA (2004) On the Effects of Residual Stress in Microindentation Tests of Soft Tissue Structures. *J Biomech Eng* 126(2):276–283.

22. Engler AJ, Carag-Krieger C, Johnson CP, Raab M, Tang HY, Speicher DW, Sanger JW, Sanger JM, Discher DE (2008) Embryonic cardiomyocytes beat best on a matrix with heart-like elasticity: scar-like rigidity inhibits beating. *Journal of Cell Science* 121(22):3794–3802.

23. Jacot JG, McCulloch AD, Omens JH (2008) Substrate stiffness affects the functional maturation of neonatal rat ventricular myocytes. *Biophys J* 95(7):3479–3487.

24. Jacot JG, Kita-Matsuo H, Wei KA, Chen HSV, Omens JH, Mercola M, McCulloch AD (2010) Cardiac myocyte force development during differentiation and maturation. *Annals of the New York Academy of Sciences* 1188(1):121–127.

25. Lints TJ, Parsons LM, Hartley L, Lyons I, Harvey RP (1993) Nkx-2.5: a novel murine homeobox gene expressed in early heart progenitor cells and their

myogenic descendants. *Development* 119(2):419–431.

26. Schultheiss TM, Burch JB, Lassar AB (1997) A role for bone morphogenetic proteins in the induction of cardiac myogenesis. *Genes & Development* 11(4):451–462.

27. Zhao Z, Rivkees SA (2004) Rho-associated kinases play a role in endocardial cell differentiation and migration. *Developmental Biology* 275(1):183–191.

28. Sakabe M, Ikeda K, Nakatani K, Kawada N, Imanaka-Yoshida K, Yoshida T, Yamagishi T, Nakajima Y (2005) Rho kinases regulate endothelial invasion and migration during valvuloseptal endocardial cushion tissue formation. *Dev Dyn* 235(1):94–104.

29. Wozniak MA, Chen CS (2009) Mechanotransduction in development: a growing role for contractility. *Nat Rev Mol Cell Biol* 10(1):34–43.

30. Voronov DA, Alford PW, Xu G, Taber LA (2004) The role of mechanical forces in dextral rotation during cardiac looping in the chick embryo. *Developmental Biology* 272(2):339–350.

31. Hamburger V, Hamilton HL (1992) A series of normal stages in the development of the chick embryo. *Dev Dyn* 195(4):231–272.

32. Männer J (2009) The anatomy of cardiac looping: A step towards the understanding of the morphogenesis of several forms of congenital cardiac malformations. *Clin Anat* 22(1):21–35.

33. Bruneau BG (2008) The developmental genetics of congenital heart disease. *Nature* 451(7181):943–948.

34. Burggren WW (2004) What Is the Purpose of the Embryonic Heart Beat? or How Facts Can Ultimately Prevail over Physiological Dogma. *Physiol Biochem Zool* 77(3):333–345.

35. Chapman WB (1918) The effect of the heart-beat upon the development of the vascular system in the chick. *Am J Anat* 23(1):175–203.

36. Patterson C (2005) Even Flow: Shear Cues Vascular Development. *Arteriosclerosis, Thrombosis, and Vascular Biology* 25(9):1761–1762.

37. Santhanakrishnan A, Miller LA (2011) Fluid Dynamics of Heart Development. *Cell Biochem Biophys* 61(1):1–22.

38. Hove JR, Köster RW, Forouhar AS, Acevedo-Bolton G, Fraser SE, Gharib M (2003) Intracardiac fluid forces are an essential epigenetic factor for embryonic cardiogenesis. *Nature* 421(6919):172–177.

39. Latacha KS, Rémond MC, Ramasubramanian A, Chen AY, Elson EL, Taber LA (2005) Role of actin polymerization in bending of the early heart tube. *Dev Dyn* 233(4):1272–1286.

40. Manasek FJ, Burnside MB, Waterman RE (1972) Myocardial cell shape change as a mechanism of embryonic heart looping. *Developmental Biology* 29(4):349–371.

41. Auman HJ, Coleman H, Riley HE, Olale F, Tsai H-J, Yelon D (2007) Functional Modulation of Cardiac Form through Regionally Confined Cell Shape Changes. *PLoS Biol* 5(3):e53.

42. Männer J (2000) Cardiac looping in the chick embryo: A morphological review with special reference to terminological and biomechanical aspects of the looping process. *Anat Rec* 259(3):248–262.

43. Upadhyaya A, Chabot JR, Andreeva A, Samadani A, van Oudenaarden A (2003) Probing polymerization forces by using actin-propelled lipid vesicles. *Proceedings of the National Academy of Sciences* 100(8):4521–4526.

44. Taylor E (2001) Mechanics of motor proteins and the cytoskeleton. *Nature* 413(6856):572–572.

45. Wagner M, Siddiqui MAQ (2007) Signal Transduction in Early Heart Development (I): Cardiogenic Induction and Heart Tube Formation. *Experimental Biology and Medicine* 232(7):852–865.

46. Wagner M, Siddiqui MAQ (2007) Signal Transduction in Early Heart Development (II): Ventricular Chamber Specification, Trabeculation, and Heart Valve Formation. *Experimental Biology and Medicine* 232(7):866–880.

47. Rose BA, Force T, Wang Y (2010) Mitogen-Activated Protein Kinase Signaling in the Heart: Angels Versus Demons in a Heart-Breaking Tale. *Physiological Reviews* 90(4):1507–1546.

48. Moses KA, DeMayo F, Braun RM, Reecy JL, Schwartz RJ (2002) Embryonic expression of anNkx2-5/Cre gene usingROSA26 reporter mice. *Genesis* 31(4):176–180.

49. Laverriere A, MacNeill C, Mueller C, Poelmann RE, Burch JB, Evans T (1994) GATA-4/5/6, a subfamily of three transcription factors transcribed in developing heart and gut. *Journal of Biological Chemistry* 269(37):23177–23184.

50. Andrée B, Duprez D, Vorbusch B, Arnold H-H, Brand T (1998) BMP-2 induces ectopic expression of cardiac lineage markers and interferes with somite formation in chicken embryos. *Mechanisms of Development* 70(1-2):119–131.

51. Peterkin T (2003) GATA-6 maintains BMP-4 and Nkx2 expression during cardiomyocyte precursor maturation. *Nature* 22(16):4260–4273.

52. Yamada M, Revelli J-P, Eichele G, Barron M, Schwartz RJ (2000) Expression of Chick Tbx-2, Tbx-3, and Tbx-5 Genes during Early Heart Development: Evidence for BMP2 Induction of Tbx2. *Developmental Biology* 228(1):95–105.

53. Ladd AN, Yatskievych TA, Antin PB (1998) Regulation of Avian Cardiac Myogenesis by Activin/TGFβ and Bone Morphogenetic Proteins. *Developmental Biology* 204(2):407–419.

54. Barron M, Gao M, Lough J (2000) Requirement for BMP and FGF signaling during cardiogenic induction in non-precardiac mesoderm is specific, transient, and cooperative. *Dev Dyn* 218(2):383–393.

55. Lough J, Barron M, Brogley M, Sugi Y, Bolender DL, Zhu X (1996) Combined BMP-2 and FGF-4, but Neither Factor Alone, Induces Cardiogenesis in Non-Precardiac Embryonic Mesoderm. *Developmental Biology* 178(1):198–202.

56. Alsan BH, Schultheiss TM (2002) Regulation of avian cardiogenesis by Fgf8 signaling. *Development* 129(8):1935–1943.

57. Zhu X, Sasse J, McAllister D, Lough J (1996) Evidence that fibroblast growth factors 1 and 4 participate in regulation of cardiogenesis. *Dev Dyn* 207(4):429–438.

58. Lopez-Sanchez C, Climent V, Schoenwolf G, Alvarez I, Garcia-Martinez V (2002) Induction of cardiogenesis by Hensen's node and fibroblast growth factors. *Cell Tissue Res* 309(2):237–249.

59. Monzen K, Nagai R, Komuro I (2002) A Role for Bone Morphogenetic Protein Signaling in Cardiomyocyte Differentiation. *Trends in Cardiovascular Medicine* 12(6):263–269.

60. Bottcher RT (2005) Fibroblast Growth Factor Signaling during Early Vertebrate Development. *Endocrine Reviews* 26(1):63–77.

61. Dailey L, Ambrosetti D, Mansukhani A, Basilico C (2005) Mechanisms underlying differential responses to FGF signaling. *Cytokine & Growth Factor Reviews* 16(2):233–247.

62. Tsang M, Dawid IB (2004) Promotion and Attenuation of FGF Signaling Through the Ras-MAPK Pathway. *Science Signaling* 2004 (228):pe17:1-5.

63. Pucéat M, Jaconi M (2005) Ca2+ signalling in cardiogenesis. *Cell Calcium* 38(3-4):383–389.

64. Sussman MA, Völkers M, Fischer K, Bailey B, Cottage CT, Din S, Gude N, Avitabile D, Alvarez R, Sundararaman B, Quijada P, Mason M, Konstandin MH, Malhowski A, Cheng Z, Khan M, McGregor M (2011) Myocardial AKT: The Omnipresent Nexus. *Physiological Reviews* 91(3):1023–1070.

65. Kerkela R, Kockeritz L, MacAulay K, Zhou J, Doble BW, Beahm C, Greytak S, Woulfe K, Trivedi CM, Woodgett JR, Epstein JA, Force T, Huggins GS (2008) Deletion of GSK-3β in mice leads to hypertrophic cardiomyopathy secondary to cardiomyoblast hyperproliferation. *The Journal of Clinical Investigation* 118(11):3609.

66. Skurk C (2005) The FOXO3a Transcription Factor Regulates Cardiac Myocyte Size Downstream of AKT Signaling. *Journal of Biological Chemistry* 280(21):20814–20823.

67. Ni YG, Wang N, Cao DJ, Sachan N, Morris DJ, Gerard RD, Kuro-o M, Rothermel BA, Hill JA (2007) FoxO transcription factors activate Akt and attenuate insulin signaling in heart by inhibiting protein phosphatases. *Proceedings of the National Academy of Sciences* 104(51):20517–20522.

68. Gessert S, Kühl M (2010) The Multiple Phases and Faces of Wnt Signaling During Cardiac Differentiation and Development. *Circulation Research* 107(2):186–199.

69. Sheldahl LC, Slusarski DC, Pandur P, Miller JR, Kühl M, Moon RT (2003) Dishevelled activates Ca2+ flux, PKC, and CamKII in vertebrate embryos. *The Journal of Cell Biology* 161(4):769–777.

70. Pandur P, Lasche M, Eisenberg LM, Kuhl M (2002) Wnt-11 activation of a non-canonical Wnt signalling pathway is required for cardiogenesis. *Nature* 418(6898):636–641.

71. Miller JR (2002) The Wnts. *Genome Biology* 3(1): reviews 3001.1.

72. Schneider VA, Mercola M (2001) Wnt antagonism initiates cardiogenesis in Xenopus laevis. *Genes & Development* 15(3):304–315.

73. Naito AT, Akazawa H, Takano H, Minamino T, Nagai T, Aburatani H, Komuro I (2005) Phosphatidylinositol 3-Kinase–Akt Pathway Plays a Critical Role in Early Cardiomyogenesis by Regulating Canonical Wnt Signaling. *Circulation Research* 97(2):144–151.

74. Foshay K, Rodriguez G, Hoel B, Narayan J, Gallicano GI (2005) JAK2/STAT3 Directs Cardiomyogenesis Within Murine Embryonic Stem Cells In Vitro. *Stem Cells* 23(4):530–543.

75. Brand T (2003) Heart development: molecular insights into cardiac specification

and early morphogenesis. *Developmental Biology* 258(1):1–19.

76. Harvey RP (1998) Links in the Left/Right Axial Pathway. *Cell* 94(3):273–276.

77. Raya Á, Belmonte JCI (2004) Sequential transfer of left–right information during vertebrate embryo development. *Current Opinion in Genetics & Development* 14(5):575–581.

78. Hamada H, Meno C, Watanabe D, Saijoh Y (2002) Establishment of vertebrate left-right asymmetry. *Nat Rev Genet* 3(2):103–113.

79. Monsoro-Burq A-H, Le Douarin NM (2001) BMP4 Plays a Key Role in Left–Right Patterning in Chick Embryos by Maintaining Sonic Hedgehog Asymmetry. *Molecular Cell* 7(4):789–799.

80. Gianakopoulos PJ, Skerjanc IS (2005) Hedgehog Signaling Induces Cardiomyogenesis in P19 Cells. *Journal of Biological Chemistry* 280(22):21022–21028.

81. Levin M, Pagan S, Roberts DJ, Cooke J, Kuehn MR, Tabin CJ (1997) Left/Right Patterning Signals and the Independent Regulation of Different Aspects ofSitusin the Chick Embryo. *Developmental Biology* 189(1):57–67.

82. Icardo JM, Fernandez-Terán A (1987) Morphologic Study of Ventricular Trabeculation in the Embryonic Chick Heart. *Acta Anatomica* 130(3):264–274.

83. Sedmera D, Pexieder T, Vuillemin M, Thompson RP, Anderson RH (2000) Developmental patterning of the myocardium. *Anat Rec* 258(4):319–337.

84. Niederreither K, Vermot J, Messaddeq N, Schuhbaur B, Chambon P, Dolle P (2001) Embryonic retinoic acid synthesis is essential for heart morphogenesis in the mouse. *Development* 128(7):1019–1031.

85. Chazaud C, Chambon P, Dolle P (1999) Retinoic acid is required in the mouse embryo for left-right asymmetry determination and heart morphogenesis. *Development* 126(12):2589–2596.

86. Conlon RA (1995) Retinoic acid and pattern formation in vertebrates. *Trends in Genetics* 11(8):314–319.

87. Meyer D, Birchmeier C (1995) Multiple essential functions of neuregulin in development. *Nature* 378(6555):386–390.

88. Gassmann M, Casagranda F, Orioli D, Simon H, Lai C, Klein R, Lemke G (1995) Aberrant neural and cardiac development in mice lacking the ErbB4 neuregulin receptor. *Nature* 378(6555):390–394.

89. Lee K-F, Simon H, Chen H, Bates B, Hung M-C, Hauser C (1995) Requirement for neuregulin receptor erbB2 in neural and cardiac development. *Nature* 378(6555):394–398.

90. Negro A (2004) Essential Roles of Her2/erbB2 in Cardiac Development and Function. *Recent Progress in Hormone Research* 59(1):1–12.

91. Kuramochi Y, Guo X, Sawyer DB (2006) Neuregulin activates erbB2-dependent src/FAK signaling and cytoskeletal remodeling in isolated adult rat cardiac myocytes. *J Mol Cell Cardiol* 41(2):228–235.

92. Hurlstone AFL, Haramis A-PG, Wienholds E, Begthel H, Korving J, van Eeden F, Cuppen E, Zivkovic D, Plasterk RHA, Clevers H (2003) The Wnt/β-catenin pathway regulates cardiac valve formation. *Nature* 425(6958):633–637.

93. Timmerman LA, Grego-Bessa J, Raya Á, Bertrán E, Pérez-Pomares JM, Díez J, Aranda S, Palomo S, McCormick F, Izpisúa-Belmonte JC, de la Pompa JL (2004) Notch promotes epithelial-mesenchymal transition during cardiac development and oncogenic transformation. *Genes & Development* 18(1):99–115.

94. Dickson MC, Slager HG, Duffie E, Mummery CL, Akhurst RJ (1993) RNA and protein localisations of TGF beta 2 in the early mouse embryo suggest an involvement in cardiac development. *Development* 117(2):625–639.

95. Armstrong EJ, Bischoff J (2004) Heart Valve Development: Endothelial Cell Signaling and Differentiation. *Circulation Research* 95(5):459–470.

96. Dor Y, Camenisch TD, Itin A, Fishman GI, McDonald JA, Carmeliet P, Keshet E (2001) A novel role for VEGF in endocardial cushion formation and its potential contribution to congenital heart defects. *Development* 128(9):1531–1538.

97. Abedi H, Zachary I (1997) Vascular Endothelial Growth Factor Stimulates Tyrosine Phosphorylation and Recruitment to New Focal Adhesions of Focal Adhesion Kinase and Paxillin in Endothelial Cells. *Journal of Biological Chemistry* 272(24):15442–15451.

98. Keyes W, Logan C, Parker E, Sanders E (2003) Expression and function of bone morphogenetic proteins in the development of the embryonic endocardial cushions. *Anat Embryol* 207(2):135–147–147.

99. Somi S, Buffing AAM, Moorman AFM, Van Den Hoff MJB (2004) Dynamic patterns of expression of BMP isoforms 2, 4, 5, 6, and 7 during chicken heart development. *Anat Rec* 279A(1):636–651.

100. Camenisch TD, Spicer AP, Brehm-Gibson T, Biesterfeldt J, Augustine ML,

Calabro Jr. A, Kubalak S, Klewer SE, McDonald JA (2000) Disruption of hyaluronan synthase-2 abrogates normal cardiac morphogenesis and hyaluronan-mediated transformation of epithelium to mesenchyme. *J Clin Invest* 106(3):349–360.

101. Schroeder JA, Jackson LF, Lee DC, Camenisch TD (2003) Form and function of developing heart valves: coordination by extracellular matrix and growth factor signaling. *Journal of Molecular Medicine* 81(7):392–403.

102. Brannan CI, Perkins AS, Vogel KS, Ratner N, Nordlund ML, Reid SW, Buchberg AM, Jenkins NA, Parada LF, Copeland NG (1994) Targeted disruption of the neurofibromatosis type-1 gene leads to developmental abnormalities in heart and various neural crest-derived tissues. *Genes & Development* 8(9):1019–1029.

103. Jackson LF (2003) Defective valvulogenesis in HB-EGF and TACE-null mice is associated with aberrant BMP signaling. *The EMBO Journal* 22(11):2704–2716.

104. Flanagan LA, Ju Y-E, Marg B, Osterfield M, Janmey PA (2002) Neurite branching on deformable substrates. *Neuroreport* 13(18):2411.

105. Lahmers S, Wu Y, Call DR, Labeit S, Granzier H (2004) Developmental Control of Titin Isoform Expression and Passive Stiffness in Fetal and Neonatal Myocardium. *Circulation Research* 94(4):505–513.

106. Bhana B, Iyer RK, Chen WLK, Zhao R, Sider KL, Likhitpanichkul M, Simmons CA, Radisic M (2010) Influence of substrate stiffness on the phenotype of heart cells. *Biotechnol Bioeng* 105(6):1148–1160.

107. Bajaj P, Tang X, Saif TA, Bashir R (2010) Stiffness of the substrate influences the phenotype of embryonic chicken cardiac myocytes. *J Biomed Mater Res* 95A(4):1261–1269.

108. Kohl P, Camelliti P, Burton FL, Smith GL (2005) Electrical coupling of fibroblasts and myocytes: relevance for cardiac propagation. *Journal of Electrocardiology* 38(4):45–50.

109. Sanger JW, Kang S, Siebrands CC, Freeman N, Du A, Wang J, Stout AL, Sanger JM (2005) How to build a myofibril. *J Muscle Res Cell Motil* 26(6-8):343–354.

110. Sanger JW, Wang J, Fan Y, White J, Sanger JM (2010) Assembly and Dynamics of Myofibrils. *Journal of Biomedicine and Biotechnology* 2010(7):1–8.

111. Gregorio CC, Antin PB (2000) To the heart of myofibril assembly. *Trends in Cell Biology* 10(9):355–362.

112. Friedrich BM, Buxboim A, Discher DE, Safran SA (2011) Striated Acto-Myosin

Fibers Can Reorganize and Register in Response to Elastic Interactions with the Matrix. *Biophysj* 100(11):2706–2715.

113. Quach NL, Rando TA (2006) Focal adhesion kinase is essential for costamerogenesis in cultured skeletal muscle cells. *Developmental Biology* 293(1):38–52.

114. Geiger B, Spatz JP, Bershadsky AD (2009) Environmental sensing through focal adhesions. *Nat Rev Mol Cell Biol* 10(1):21–33.

115. Sparrow JC, Schoumlck F (2009) The initial steps of myofibril assembly: integrins pave the way. *Nat Rev Mol Cell Biol* 10(4):293–298.

116. Pelham RJ, Wang YL (1998) Cell locomotion and focal adhesions are regulated by the mechanical properties of the substrate. *Biol Bull* 194(3):348–9– discussion 349–50.

117. Gilbert PM, Havenstrite KL, Magnusson KEG, Sacco A, Leonardi NA, Kraft P, Nguyen NK, Thrun S, Lutolf MP, Blau HM (2010) Substrate Elasticity Regulates Skeletal Muscle Stem Cell Self-Renewal in Culture. *Science* 329(5995):1078–1025.

118. Engler AJ, Griffin MA, Sen S, Bönnemann CG, Sweeney HL, Discher DE (2004) Myotubes differentiate optimally on substrates with tissue-like stiffness: pathological implications for soft or stiff microenvironments. *J Cell Biol* 166(6):877–887.

119. Miyamoto S, Kathz B-Z, LaFrenie RM, Yamada KM (1998) Fibronectin and Integrins in Cell Adhesion, Signaling, and Morphogenesis. *Annals of the New York Academy of Sciences* 857:119–129.

120. Sakiyama-Elbert SE, Hubbell JA (2000) Development of fibrin derivatives for controlled release of heparin-binding growth factors. *Journal of Controlled Release* 65(3):389–402.

121. Discher DE, Mooney DJ, Zandstra PW (2009) Growth factors, matrices, and forces combine and control stem cells. *Science* 324(5935):1673–1677.

122. Anseth KS, Metters AT, Bryant SJ, Martens PJ, Elisseeff JH, Bowman CN (2002) In situ forming degradable networks and their application in tissue engineering and drug delivery. *Journal of Controlled Release* 78(1-3):199–209.

123. Metters AT, Bowman CN, Anseth KS (2000) A statistical kinetic model for the bulk degradation of PLA-b-PEG-b-PLA hydrogel networks. *Journal of Physical Chemistry B* 104(30):7043–7049.

124. Martens P, Holland T, Anseth KS (2002) Synthesis and characterization of

degradable hydrogels formed from acrylate modified poly(vinyl alcohol) macromers. *Polymer* 43(23):6093–6100.

125. De Groot CJ, Van Luyn MJA, Van Dijk-Wolthuis WNE, Cadée JA, Plantinga JA, Den Otter W, Hennink WE (2001) In vitro biocompatibility of biodegradable dextran-based hydrogels tested with human fibroblasts. *Biomaterials* 22(11):1197–1203.

126. Sahoo S, Chung C, Khetan S, Burdick JA (2008) Hydrolytically Degradable Hyaluronic Acid Hydrogels with Controlled Temporal Structures. *Biomacromolecules* 9(4):1088–1092.

127. Boontheekul T, Kong H-J, Mooney DJ (2005) Controlling alginate gel degradation utilizing partial oxidation and bimodal molecular weight distribution. *Biomaterials* 26(15):2455–2465.

128. Kraehenbuehl TP, Zammaretti P, Van der Vlies AJ, Schoenmakers RG, Lutolf MP, Jaconi ME, Hubbell JA (2008) Three-dimensional extracellular matrix-directed cardioprogenitor differentiation: Systematic modulation of a synthetic cell-responsive PEG-hydrogel. *Biomaterials* 29(18):2757–2766.

129. Gobin AS, West JL (2002) Cell migration through defined, synthetic extracellular matrix analogues. *The FASEB Journal* 16(7):751–753.

130. Lutolf MP, Raeber GP, Zisch AH, Tirelli N, hubbell JA (2003) Cell-Responsive Synthetic Hydrogels. *Adv Mater* 15(11):888–892.

131. Lutolf MP (2003) Synthetic matrix metalloproteinase-sensitive hydrogels for the conduction of tissue regeneration: Engineering cell-invasion characteristics. *Proceedings of the National Academy of Sciences* 100(9):5413–5418.

132. Patterson J, hubbell JA (2010) Enhanced proteolytic degradation of molecularly engineered PEG hydrogels in response to MMP-1 and MMP-2. *Biomaterials* 31(30):7836–7845.

133. Elsner N, Kozlovskaya V, Sukhishvili SA, Fery A (2006) pH-Triggered softening of crosslinked hydrogen-bonded capsules. *Soft Matter* 2(11):966.

134. Kim MR, Park TG (2002) Temperature-responsive and degradable hyaluronic acid/Pluronic composite hydrogels for controlled release of human growth hormone. *Journal of Controlled Release* 80(1-3):69–77.

135. Kloxin AM, Kasko AM, Salinas CN, Anseth KS (2009) Photodegradable Hydrogels for Dynamic Tuning of Physical and Chemical Properties. *Science* 324(5923):59–63.

136. Kloxin AM, Benton JA, Anseth KS (2010) In situ elasticity modulation with

dynamic substrates to direct cell phenotype. *Biomaterials* 31(1):1–8.

137. Frey MT, Wang Y-L (2009) A photo-modulatable material for probing cellular responses to substrate rigidity. *Soft Matter* 5(9):1918–1924.

138. Burdick JA, Chung C, Jia X, Randolph MA, Langer R (2005) Controlled degradation and mechanical behavior of photopolymerized hyaluronic acid networks. *Biomacromolecules* 6(1):386–391.

139. Guvendiren M, Burdick JA (2012) Stiffening hydrogels to probe short- and long-term cellular responses to dynamic mechanics. *Nat Commun* 3(792):1-9.

140. Crow A, Webster KD, Hohlfeld E, Ng WP, Geissler P, Fletcher DA (2012) Contractile Equilibration of Single Cells to Step Changes in Extracellular Stiffness. *Biophysical Journal* 102(3):443–451.

141. Lin DC, Yurke B, Langrana NA (2005) Inducing Reversible Stiffness Changes in DNA-crosslinked Gels. *Journal of Materials Research* 20(6):1456–1464.

142. Burdick JA, Murphy WL (2012) Moving from static to dynamic complexity in hydrogel design. *Nat Commun* 3:1–8.

143. Kim J, Hayward RC (2012) Mimicking dynamic in vivo environments with stimuli-responsive materials for cell culture. *Trends in Biotechnology* 30(8):426–439.

144. Gillette BM, Jensen JA, Wang M, Tchao J, Sia SK (2010) Dynamic Hydrogels: Switching of 3D Microenvironments Using Two-Component Naturally Derived Extracellular Matrices. *Adv Mater* 22(6):686–691.

145. Yoshikawa HY, Rossetti FF, Kaufmann S, Kaindl T, Madsen J, Engel U, Lewis AL, Armes SP, Tanaka M (2011) Quantitative Evaluation of Mechanosensing of Cells on Dynamically Tunable Hydrogels. *J Am Chem Soc* 133(5):1367–1374.

146. Yamato M, Utsumi M, Kushida A, Konno C, Kikuchi A, Okano T (2001) Thermo-Responsive Culture Dishes Allow the Intact Harvest of Multilayered Keratinocyte Sheets without Dispase by Reducing Temperature. *Tissue Engineering* 7(4):473–480.

147. Ifkovits JL, Tous E, Minakawa M, Morita M, Robb JD, Koomalsingh KJ, Gorman JH, Gorman RC, Burdick JA (2010) Injectable hydrogel properties influence infarct expansion and extent of postinfarction left ventricular remodeling in an ovine model. *Proceedings of the National Academy of Sciences* 107(25):11507–11512.

148. Jiang FX, Yurke B, Schloss RS, Firestein BL, Langrana NA (2010) Effect of Dynamic Stiffness of the Substrates on Neurite Outgrowth by Using a DNA-

Crosslinked Hydrogel. *Tissue Engineering Part A* 16(6):1873–1889.

149. Jiang FX, Yurke B, Firestein BL, Langrana NA (2008) Neurite Outgrowth on a DNA Crosslinked Hydrogel with Tunable Stiffnesses. *Ann Biomed Eng* 36(9):1565–1579.

150. Figueroa MS, Peters JI (2006) Congestive heart failure: Diagnosis, pathophysiology, therapy, and implications for respiratory care. *Respir Care* 51(4):403–412.

151. Murry CE, Soonpaa MH, Reinecke H, Nakajima H, Nakajima HO, Rubart M, Pasumarthi KB, Virag JI, Bartelmez SH, Poppa V, Bradford G, Dowell JD, Williams DA, Field LJ (2004) Haematopoietic stem cells do not transdifferentiate into cardiac myocytes in myocardial infarcts. *Nature* 428 (6983):664–668.

152. Haq S, Choukroun G, Lim H, Tymitz KM, del Monte F, Gwathmey J, Grazette L, Michael A, Hajjar R, Force T, Molkentin JD (2001) Differential Activation of Signal Transduction Pathways in Human Hearts With Hypertrophy Versus Advanced Heart Failure. *Circulation* 103(5):670–677.

153. Wang Y (2007) Mitogen-Activated Protein Kinases in Heart Development and Diseases. *Circulation* 116(12):1413–1423.

154. Nygren JM, Jovinge S, Breitbach M, Säwén P, Röll W, Hescheler J, TaneeraJ, Fleischmann BK, Jacobsen SE (2004) Bone marrow-derived hematopoietic cells generate cardiomyocytes at a low frequency through cell fusion, but not transdifferentiation. *Nat Med* 10(5):494–501.

155. Lunde K, Solheim S, Aakhus S, Arnesen H, Abdelnoor M, Forfang K, ASTAMI investigators (2005) Autologous stem cell transplantation in acute myocardial infarction: The ASTAMI randomized controlled trial. Intracoronary transplantation of autologous mononuclear bone marrow cells, study design and safety aspects. *Scand Cardiovasc J* 39(3):150–158.

156. Chachques JC, Acar C, Herreros J, Trainini JC, Prosper F, D'Attellis N, Fabiani JN, and Carpentier AF (2004) Cellular cardiomyoplasty: clinical application. *Ann Thorac Surg* 77(3):1121–1130.

157. Janssens S, Dubois C, Bogaert J, Theunissen K, Deroose C, Desmet W, Kalantzi M, Herbots L, Sinnaeve P, Dens J, Maertens J, Rademakers F, Dymarkowski S, Gheysens O, Van Cleemput J, Bormans G, Nuyts J, Belmans A, Mortelmans L, Boogaerts M, Van de Werf F (2006) Autologous bone marrow-derived stem-cell transfer in patients with ST-segment elevation myocardial infarction: double-blind, randomised controlled trial. *Lancet* 367(9505):113–121.

158. Breitbach M, Bostani T, Roell W, Xia Y, Dewald O, Nygren JM, Fries JW, Tiemann K, Bohlen H, Hescheler J, Welz A, Bloch W, Jacobsen SE, Fleischmann BK (2007) Potential risks of bone marrow cell transplantation into infarcted hearts. *Blood* 110(4):1362–1369.

159. Simpson DG, Decker ML, Clark WA, Decker RS (1993) Contractile activity and cell-cell contact regulate myofibrillar organization in cultured cardiac myocytes. *J Cell Biol* 123(2):323–336.

160. Griffin MA, Sen S, Sweeney HL, Discher DE (2004) Adhesion-contractile balance in myocyte differentiation. *J Cell Sci* 117(24):5855–5863.

161. Eschenhagen T, Fink C, Remmers U, Scholz H, Wattchow J, Weil J, Zimmermann W, Dohmen HH, Schäfer H, Bishopric N, Wakatsuki T, Elson EL (1997) Three-dimensional reconstitution of embryonic cardiomyocytes in a collagen matrix: a new heart muscle model system. *FASEB J* 11(8):683–694.

Chapter 2

Hydrogels with Time-Dependent Material Properties Enhance Cardiomyocyte Differentiation *In Vitro*

Abstract

Tissue-specific elastic modulus (*E*), or 'stiffness,' arises from developmental changes in the extracellular matrix (ECM) and suggests that progenitor cell differentiation may be optimal when physical conditions mimic tissue progression. For cardiomyocytes, maturing from mesoderm to adult myocardium results in a ~9-fold stiffening originating in part from a change in collagen expression and localization. To mimic this temporal stiffness change *in vitro*, thiolated-hyaluronic acid (HA) hydrogels were crosslinked with poly(ethylene glycol) diacrylate, and their dynamics were modulated by changing crosslinker molecular weight. With the hydrogel appropriately

tuned to stiffen as heart muscle does during development, pre-cardiac cells grown on collagen-coated HA hydrogels exhibit a 3-fold increase in mature cardiac specific markers and form up to 60% more maturing muscle fibers than they do when grown on compliant but static polyacrylamide hydrogels over 2 weeks. Though ester hydrolysis does not substantially alter hydrogel stiffening over 2 weeks *in vitro*, model predictions indicate that ester hydrolysis will eventually degrade the material with additional time, implying that this hydrogel may be appropriate for *in vivo* applications where temporally changing material properties enhance cell maturation prior to its replacement with host tissue.

2.1 Introduction

Cell behavior on compliant hydrogels often more closely approximates *in vivo* behavior compared to cells on rigid culture substrates, e.g. glass or plastic (1). This occurs in part because cells can 'feel' that the hydrogel's elastic modulus (*E*), or 'stiffness' (measured in Pascal, Pa) more closely matches their native microenvironment as they contract against it. Mechanically-regulated responses are numerous but can include even the most fundamental processes, such as stem cell maturation (2-4), where muscle markers emerge in stem cells grown on hydrogels of muscle stiffness. Moreover, stiffness can affect tissue morphogenesis (5) and (6), e.g. tube formation (7), or migration of cells within explants (8). Such behavior may also provide a mechanical explanation for the concept of 'tissue affinity,' where cells differentially sort within the body to form larger structures (9). Yet over this time period in which cells sort, they also secrete and assemble their extracellular matrix (ECM) (10), and together they gives rise to the

stiffness associated with mature tissues (6, 11).

Mature, contractile heart cells, i.e. cardiomyocytes, have traditionally been cultured on thick collagen gels to maintain rhythmic contraction (12, 13), but more recently it was shown with synthetic gels that stiffness is a critical regulator of contraction (14). This may be due in part to its modulation of cytoskeletal assembly in the form of myofibril striation and alignment, both of which can affect beating rate (15, 16). As with most other cell types, these behaviors in culture become most *in vivo*-like when cells are grown on a substrate that mimics the stiffness of their native environment (1). For example on a 10 kPa hydrogel, which mimics adult myocardial stiffness (17) and is similar to other muscle types (18-20), intra- and extracellular strains become matched and can prolong rhythmic beating in culture (16). When too stiff or soft, cardiomyocytes overstrain themselves or do little work on the substrate, respectively, which in both cases result in few striated myofibrils and a loss of rhythmic contraction. In fact many diseases also stiffen the ECM, e.g. fibrotic stiffening of heart muscle post-heart attack (17), and induce hyper-strained myocytes that do not function properly. When coupled with stem cells for therapeutic use, failure to consider the altered material properties of disease can lead to undesired outcomes including the formation of calcified lesions (21), which emphasizes the importance of the mechanical properties of materials in regulating cell contraction.

Despite improved myocyte function on materials with biomimetic stiffness, the heart does not begin as a contractile 10 kPa material but instead originates from a much softer tissue layer called mesoderm <500 Pa (22), which can require up to two weeks to develop in chicken (23, 24). In general, maturation from mesoderm to myocardium can

require some finite amount of time and suggests that rigid or even soft materials with static properties, e.g. thick collagen (12, 13) or synthetic gels (14-16), may not provide the most appropriate physical environment in which to study stem or progenitor cells *in vitro*. While the kinetics of stiffening are uncertain, development of immature cells into cardiomyocytes is likely due in part to this time-dependent mechanical change from softer mesoderm into stiffer heart tissue (25). This stiffness change then supports the appropriate level of tension required to assemble an adequate amount of myofibrils, i.e. the contractile unit of muscle (13). However, no biologically-appropriate material has been demonstrated to exhibit time-dependent stiffening in which to test this hypothesis, especially one that is tuned to mimic the mechanics of developing myocardium. Since immature cells require muscle-like stiffness in which to develop into muscle (3) as opposed to the rigid, fibrotic tissues in which they are often used therapeutically (17, 21), understanding the effect of time-dependent stiffening on cell maturation may be a critical design parameter for future material-based therapies that involve the addition of co-injected cells.

2.2 Materials and Methods

2.2.1 Materials

Hyaluronic Acid (HA) was obtained from Calbiotech (CA) and thiolated using a cleavable, carbohydrate selective, sulfhydryl-reactive crosslinker, PDPH (3-[2-Pyridyldithio]propionyl hydrazide) (Thermo Scientific-Pierce), MES Buffer (Thermo

Scientific-Pierce), DMSO (Sigma), EDC (1-ehtyl-3-[3-dimentylaminopropyl] carbodiimide hydrochloride) (Sigma), and DTT (dithiothreitol, Sigma). Alternatively, thiolated HA of similar functionality was also obtained from Glycosan Biosystems (UT). Poly(ethylene glycol) diacrylate (PEGDA) of different molecular weight was used as a crosslinker (M_w ~ 3400 Da from Glycosan Biosystems, UT and M_w ~ 258, 700 and 2000 Da from Sigma). For protein attachment on gels, EDC, NHS (N-Succinylamide) (Sigma) and type I rat tail collagen (BD Biosciences) in HEPES buffer (Sigma) was used. Polyacrylamide (PA) hydrogels were prepared from crosslinker *n*,*n*'-methylene-bis-acrylamide and acrylamide monomers (Fisher Scientific), and the same protein was covalently attached using a photoactivating crosslinker, sulfo-SANPAH (Pierce).

To fluorescently label collagen or cells on the surface of the hydrogel for imaging purposes, primary monoclonal mouse type I collagen antibody (C2456, Sigma), alpha-actinin (A7811, Sigma), rhodamine phallodin (R415, Invitrogen), Hoescht (33342, Sigma) and Alexa Flour 488 or 568 conjugated goat anti-mouse secondary antibody (Invitrogen) were used. Samples were mounted using Fluoromount-G (SouthernBiotech). For ELISA, secondary goat anti-mouse HRP-conjugated antibody (62–6520, Zymed) and 3,3′,5,5′-Tetramethylbenzidine (TMB, Sigma) were used.

To examine myocardial stiffness and subsequent use in cell studies, chicken embryos were obtained from McIntyre Poultry Farm (Lakeside, CA). For histological analysis, hearts were embedded in optimal cutting temperature (OCT) solution (TissueTek) and stained using phosphomolybdic acid (Electron Microscopy Sciences-EMS), sirius red in 0.1% saturated picric acid (EMS), and mounted with Cytoseal (Richard Allen Scientific). For cardiomyocyte isolation, tissue was digested using 0.05%

trypsin-EDTA (Invitrogen) and purified using a 70 μm cell strainer (BD Falcon). Cells were stored in normal heart medium (89% MEM alpha:l-glutamine (+), ribo-/deoxyribo-nucelosides (−), Invitrogen; 10% fetal bovine serum, Hyclone; and 1% penicilin:streptomycin, Invitrogen).

For reverse transcription PCR (RT-PCR), 10 mm dNTP (Roche), 100 mm DTT (Invitrogen), 5X First Strand Buffer (Invitrogen), 50 mm Random Hexamers (Qiagen), 200 U/μL Reverse Transcriptase (Invitrogen), and DEPC water (OmniPur, EMD) were used. For quantitative PCR (qPCR), SYBR Green (Applied Biosystems) and primers obtained from Integrated DNA Technologies (IDT) (Table S1) were used.

2.2.2 Hyaluronic Acid Thiolation

Fermentation-derived HA Fermentation-derived HA (sodium salt) of intermediate molecular weight, e.g. 769 kD, was digested in order to obtain low molecular weight HA of M_w ~ 200 kD as previously described (26). Briefly, 1 mg/mL HA was dissolved in 37 °C water of pH 0.5 (adjusted by the addition of 10 m HCl) and mixed at 130 rpm for 6 h. pH was then adjusted to 7.0 with 1 m NaOH, dialyzed against water for 4 days (12 kD molecular weight cutoff), and centrifuged before the supernatant was lyophilizated. HA was dissolved in MES Buffer at 5–10 mg/mL and 25 μL of 20 mm PDPH in DMSO was added per 1 mL of HA solution. The reaction was carried out at room temperature for 30–60 min. 12.5 μL of 0.5 m EDC in MES buffer was added per 1 mL of HA solution. The solution was mixed and incubated at room temperature for 2 h to overnight with mixing. The solution was centrifuged in order to remove any precipitate that formed during the reaction. Any non-reacted PDPH molecule was removed by dialysis or gel filtration. In

order to reduce the disulfide bond, 0.5 mL of 23 mg/mL DTT in MES buffer was added per 1 mL of PDPH-modified HA and incubated for 30 min at room temperature. The solution was dialyzed or gel filtered in order to remove any excess DTT. Samples were lyophilized, dissolved in D_2O at 1 mg/mL and analyzed via ^1H nuclear magnetic resonance (NMR) spectroscopy (JEOL ECA 500) to assess thiol substitution.

2.2.3 Gel Synthesis, Protein Attachment and Detection

To prepare HA hydrogels of the appropriate stiffness to mimic heart stiffening, 4.53% (w/v) PEGDA with M_w~ 3400 Da (polydispersity index or PDI ~ 3) in DG PBS and 1.25% thiolated HA in DG PBS were separately mixed at 37 °C with gentle shaking for up to 30 min. For swelling experiments, PEGDA with M_w ~ 258 Da, 700 Da, and/or 2000 Da (PDI ~ 1) were also used in a similar fashion. To initiate polymerization, solutions were combined at a volume ratio of 1 PEGDA solution: 4 HA solution to yield a 1% HA/0.9% PEGDA hydrogel, and 50 μL of the solution was placed between adhesive, aminosilanated and non-adhesive hydroxylated glass coverslips (27) and allowed to polymerize in a humidified 37 °C incubator for 1 h. Hydrogels bound to the aminosilanated coverslip were rinsed and stored in DG PBS in a humidified 37 °C incubator until use. To attach protein to the surface, 20 mm EDC, 50 mm NHS and 150 μg/mL type I rat tail collagen were mixed in HEPES buffer and incubated with the hydrogels overnight. Polyacrylamide gels were prepared as described previously (27). Briefly, gel crosslinker n,n'-methylene-bis-acrylamide and acrylamide monomer concentrations were varied in distilled water and polymerized between adhesive, aminosilanated and non-adhesive hydroxylated glass coverslips using 1/200 volume of

10% ammonium persulfate and 1/2000 volume of *n*,*n*,*n*',*n*'-tetramethylethylenediamine. To attach protein to the PA hydrogel surface, 0.5 mg/ml sulfo-SANPAH (Pierce) in 50 mm HEPES pH 8.5.

Enzyme-linked immunosorbent assay (ELISA) was used to compare the amount of rat tail type I collagen binding to HA and PA hydrogels when using optimal coating densities of 1 μg/cm^2 as previously described (27). Primary monoclonal mouse type I collagen antibody was incubated at 1:500 in 2% ovalbumin with cells on hydrogels for 1 h at 37 °C. After rinsing, 1 mL of secondary goat anti-mouse HRP-conjugated antibody at 1:1000 and 1:5000 in 2% ovalbumin was added to the gel surface and incubated for 1hr at 4 °C. After rinsing, 0.5 mL of TMB ELISA substrate was added and incubated at room temperature for 30 min. The reaction was stopped using 1 m HCl and analyzed on a plate reader at 450 nm. Binding was confirmed and assessed by immunofluorescence using a BD Carv II confocal microscope (BD Biosciences; San Jose, CA) mounted on a Nikon Eclipse TE2000-U microscope with Metamorph 7.6 software. Image brightness was uniformly enhanced 2-fold to better illustrate the location of labeled protein.

2.2.4 Material Stiffness and Surface Topography

Force-mode atomic force microscopy (AFM) was performed on the developing myocardium and HA and PA hydrogels to examine mechanical properties. For the tissue samples, specimens were isolated from chicken embryos, bisected, and mounted on glass slides with epoxy to expose the apical surface. HA and PA hydrogel bound to aminosilanated coverslips were directly mounted on the AFM stage (3D-Bio; Asylum Research). Samples were indented to a depth of 100 nm with a pyramid-tipped cantilever

having a spring constant (20 pN/nm nominal) as determined from thermal calibration. At least 50 measurements were made randomly across the surface of each sample. Force-indentation plots were fit with a Hertz model to determine the Young's modulus (28). To assess disulfide crosslinking, HA gels were treated with 0 mm, 1 mm and 1mDTT in order to examine disulfide bond formation during gelation. Data for the elastic modulus of HA gels and the myocardium were fit with exponential decay curves to assess differences between the systems. For HA and PA hydrogels, AFM was also performed in tapping mode to image surface topography.

2.2.5 Material Stability and Degradation

Degradation of HA hydrogels was determined via equilibrium mass swelling ratio (Q_m), thickness measurements, and elastic modulus effects. For Q_m, thickness measurements, and elastic modulus determination, degradation was carried out at 37 °C in pH 7.4 and pH 9 PBS (enhanced degradative environment). For determination of Q_m, as defined by the ratio of swollen polymer to dry polymer, the weight of each sample was examined over time. At 24 hpp, multiple samples were weighed and then lyophilized in order to determine an average equilibrium swelling ratio. Swollen HA gels were weighed over time and Q_m values were calculated. We assume HA gels remain a constant material mass over the time points examined (up to 2 weeks), as these times are less than that of significant degradation. Thickness measurements were examined over time after coating HA hydrogels with collagen and fluorescently tagging and using confocal microscopy to measure distance from the top of the hydrogel to the top of the coverslip. Stiffness measurements were collected as previously described for force-mode AFM but in the

presence or absence of basic pH. Hydrogel modulus was examined as previously described for force-mode AFM.

2.2.6 Hydrolysis Modeling

One characteristic of PEGDA addition reactions is the formation of hydrolytically degradable esters, which may balance the stiffening effect of additional crosslinks. Metters and coworkers (29) previously reported an application of a Flory-Rehner hydrolytic degradation model, (30) which was used here to illustrate the kinetics of crosslinking versus ester degradation through a description of the change in hydrogel swelling. While Metters and coworkers describe a triblock system consisting of poly(lactic acid) (PLA) and PEG, i.e. PLA-PEG-PLA, where hydrolyzable ester bonds are found within the PLA block, we can apply this system to the reaction of PEGDA with HA since it creates two degradable esters existing on opposite ends of the PEGDA crosslinker. Briefly, first-order hydrolysis kinetics are assumed for ester bond degradation, having a pseudo first-order rate constant for ester bond hydrolysis, *k'*. The fraction of hydrolyzed thioether-ester groups, which form between the HA backbone and PEGDA crosslinker (*P*), is related to

$$P = 1 - e^{-jk'_E t} \tag{1}$$

The crosslinking density (ρ_c) as a function of time can then be related to (1) using knowledge of the triblock crosslink structure as follows

$$\rho_c \sim (1-P)^2 \sim e^{-2jk'_E t} \quad (2)$$

Using a simplified form of the Flory–Rehner equation, which relates volumetric swelling ratio (Q) to crosslinking density, Q can be related to time by

$$Q \sim \rho_C^{-0.6} \sim e^{1.2jk'_E t} \quad (3)$$

and plotted with experimentally-determined Q_m for the thiolated HA hydrogels between 0 and 216 hpp as shown in Fig. 6C. It is important to note that this model assumes immediate and complete crosslinking in equations (2) and (3), which describes crosslinking density only as it exponentially decays from hydrolysis. Since opposing behavior is observed initially for HA hydrogels, either additional crosslinking with time may reduce and delay hydrogel swelling or degradation kinetics are sufficiently slow as to be decoupled from additional crosslinking. Regardless, any hydrolysis-induced material erosion is not experimentally observable until after stiffening has occurred (Fig. 3C).

2.2.7 Cell and Tissue Isolation and Cell Culture

Animals received humane care in compliance with University of California, San Diego's Institutional Animal Care and Use Committee (protocol #S09200). Chicken embryonic hearts and heart cells were obtained by isolation at 72, 120, 168, 240 and 288 HPF. Age was confirmed using Hamburger–Hamilton stages (23). Hearts were obtained by dissection and either mounted for AFM, digested for cell isolation, or embedded in

optimal cutting temperature (OCT) solution for histological analysis using a Picrosirius red stain. Briefly, after sectioning samples and mounting on glass slides, tissue was rehydrated, treated with 0.2% phosphomolybdic acid, stained with sirius red in 0.1% saturated picric acid, then 0.01 m HCl, dehydrated, cleared and mounted with Cytoseal. For cardiomyocyte isolation, isolated hearts were minced using sterile razor blades and collected with 10 mL of 0.05% trypsin-EDTA (Invitrogen) and incubated in a sterile humidified 37 °C incubator (5% CO_2) for 15 min. In order to remove red blood cells, the tube was inverted and tissue was allowed to settle prior to a change of solution to 10 mL of fresh trypsin. After incubation for 15 min, the sample was centrifuged and the pellet was carefully triturated with normal heart medium (see section 2.2.1 for media components). The cell solution was passed through a 70 μm cell strainer (BD Falcon) and pre-plated on a sterile tissue culture dish for 1 h in a cell incubator in order to remove fibroblasts from the solution. The unattached cells were collected, counted, and plated at a density of 5×10^6 cells/cm^2. Cells used for qPCR and immunofluorescence were incubated according to the time course in Fig. 5. Media changes were performed every 2 days. All cell culture and tissue experiments were performed at least in triplicate.

2.2.8 Cell Maturation Assays

In order to examine cardiac ECM expression in the myocardium, chicken embryonic hearts were isolated and mRNA was extracted as follows. Cells on hydrogels were washed with PBS, lysed with trizol for 5 min at room temperature and the solution transferred to RNAase/DNAase-free eppendorf tubes. Chloroform was added and samples were vigorously shaken at room temp for 2 min. Samples were centrifuged in

order to separate phases and the aqueous phase was transferred to new tubes. RNA was precipitated by the addition of isopropanol, vortexing and allowing samples to sit at room temperature for 10 min. The samples were then centrifuged, the supernatant was removed and a gel-like RNA pellet was washed with 75% ethanol and vortexed. The samples were spun a final time and the supernatant was removed. The RNA sample was allowed to air dry for 5 min. Samples were resuspended in DEPC water (OmniPur, EMD) and absorbance was examined for RNA concentration at 260 nm OD. In order to convert mRNA into cDNA for future analysis, reverse transcription polymerase chain reaction (RT-PCR) of 37 °C for 60 min, followed by 99 °C for 5 min, followed by 5 °C for 5 min was performed. Samples consisting of 2 μg of mRNA were mixed with 20 μL of mastermix consisting of 1 μL 10 mm dNTP (Roche), 2 μL 100 mm DTT (Invitrogen), 4 μL 5X First Strand Buffer (Invitrogen), 1 μL 50 mm Random Hexamers (Qiagen), 1 μL 200 U/μL Reverse Transcriptase (Invitrogen) and 11 μL DEPC H_2O. qPCR was then performed using an Applied Biosystems 7900HT Fast Real-Time PCR machine for quantifying matrix protein expression of collagen (COL) 1A2, laminin (LN) 2 and fibronectin (FN) 1 (see Supplemental Table 1 for list of primers).

In order to examine cell maturation from the time course previously described, samples were either used to quantify cardiac gene expression or were stained with antibodies specific to cardiac proteins. Cardiac gene expression was determined via qPCR (as previously described) for Troponin T and NKX-2.5 (see Supplemental Table 1 for list of primers). Immunofluorescence was performed as follows: cells were fixed with 3.7% formaldehyde in PBS for 15 min, rinsed and permeabilized using Triton X-100 for

10 min. Cells were rinsed and incubated with primary mouse antibody for alpha-actinin (A7811, Sigma) at 1:500 in 2% ovalbumin for 30–60 min in a 37 °C cell incubator. Samples were rinsed and 1:1000 rhodamine-phallodin (R415, Invitrogen), 1:1000 Alexa Flour 488 conjugated goat anti-mouse secondary antibody (Invitrogen) and 1:5000 Hoescht (33342, Sigma) in 2% ovalbumin were added for 30 min at 37 °C. Samples were rinsed and mounted with Fluoromount-G (SouthernBiotech) and sealed with nail polish. Images were captured using a Nikon Eclipse TE2000-U fluorescent microscope with Metamorph 7.6 software. Images were analyzed using Image J to determine striation length by drawing a calibrated line through a fibril and dividing by the number of striations, and myofibril alignment by examining ellipse fits of fibrils and calculating the deviation of fibrils from long cell axis using an orientation correlation function (OCF): $OCF = 0.5 (\cos (2\theta) + 1)$, where θ is the difference between the angle of the fibril and cell axis.

2.2.9 Statistical Analyses

All statistical analyses were performed using student t-tests. Differences among groups were assessed to identify statistical differences between treatments when p is at least less than 0.05. Data where $0.05 < p < 0.1$ is indicated though not statistically different. All data is presented as mean ± standard error of the mean.

2.3 Results and Discussion

2.3.1 Characterization of the Developing Myocardium

In order to test the hypothesis that time-dependent material properties can improve cell maturation, mechanochemical parameters of the developing heart were first characterized using a chicken embryo model, which displays all the hallmarks of human heart development (24) in distinct stages (23). *Ex vivo* samples of the developing heart were isolated between 36 and 408 hours post-fertilization (HPF) of the embryo, mounted on a glass slide and an atomic force microscope (AFM) was used to indent the inner tissue surface and assess stiffness. Fig. 1A shows the developing embryonic chicken heart undergoes a 9-fold increase in elastic modulus, i.e. $E \sim 0.9 \pm 0.2$ kPa at 36 HPF to $E \sim 8.2 \pm 1.3$ kPa at 408 HPF, and an exponential curve fit of these data indicate a time constant, τ, of 57.6 HPF. One tissue component that changes significantly over this time course and may likely be responsible for heart stiffening is the extracellular matrix (ECM), a protein scaffold to which cells attach and transduce signals; since cells attach to ECM rather than polymers, knowing what the most abundant ECM protein is may aid in attaching cells to the material. Quantitative polymerase chain reaction (qPCR) was used to assess compositional changes of heart ECM proteins, e.g. collagen, laminin, and fibronectin, over this developmental time course (Fig. 1B). Collagen expression increased through 264 HPF and changed from being peripherally-localized to be uniformly distributed (Fig. 1B inset). Though peripherally-localized collagen is likely mechanically important during heart formation (25), uniform collagen expression throughout the heart may enable a consistent set of material properties for heart maturation. On the other hand,

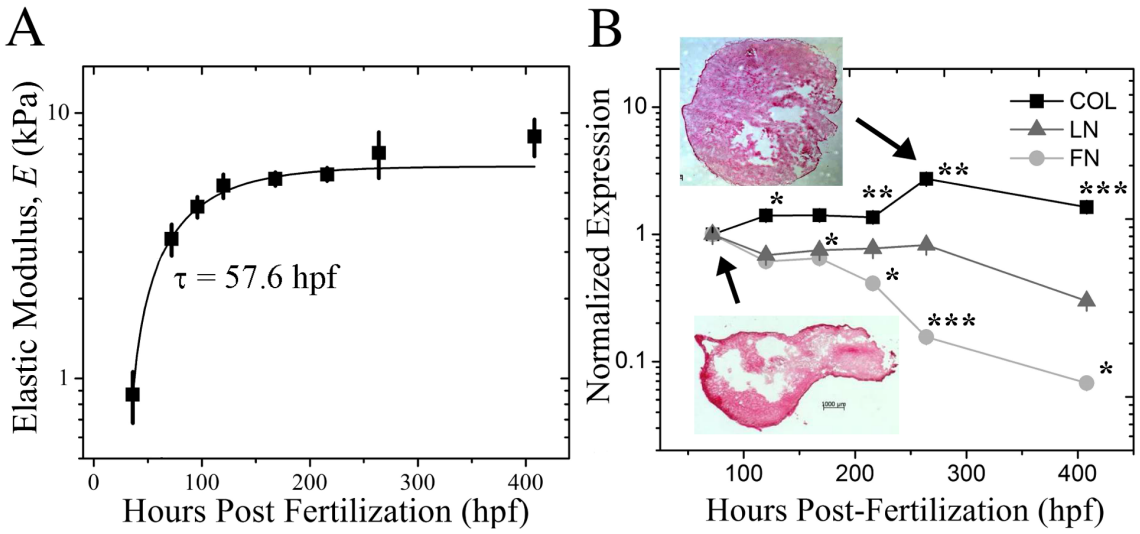

Figure 1: *Characterizing Myocardial Development in the Chicken Embryo.* (A) Myocardial elastic modulus was measured by atomic force microscopy from 36 to 408 HPF. Data was fit with an exponential curve, which exhibited a time constant, τ, of 57.6 HPF as indicated. (B) qPCR quantification of myocardial collagen (black squares), laminin (grey triangles) and fibronectin (light grey circles) expression was normalized to the initial time point at 72 HPF and plotted as a function of developmental time. Inset images show tissue samples isolated at the indicated time points and stained with Picrosirius Red to indicate collagen localization (red). *$p < 0.05$, **$p < 0.01$, ***$p < 0.001$ compared to the initial time point.

both fibronectin and laminin expression decreased by almost an order of magnitude from 72 to 408 HPF and are not as likely to contribute to tissue stiffening as much as collagen may.

2.3.2 Mimicking and monitoring time-dependent stiffness in hyaluronic acid hydrogels

We have used a modified hyaluronic acid (HA) hydrogel to recapitulate this dynamic environment *in vitro*. HA is a natural, non-immunogenic (31) ECM component that can be easily modified to display various chemistries (26, 32, 33). HA was thiolated using the carbohydrate selective, sulfhydryl-reactive crosslinker (3-[2-Pyridyldithio]propionyl hydrazide) and upon reduction, a free thiol was added to the end of the carboxyl group (see Fig. 2A1). Substitution efficiency was confirmed by ^{1}H nuclear magnetic resonance (NMR) spectroscopy, comparing methylene peaks 1 and 2 and the *N*-acetyl methyl peak 3 in Fig. 3A to determine a ~40% average thiolation. A poly(ethylene glycol) diacrylate (PEGDA) crosslinker was added to initiate a Michael-type addition reaction (34) (Fig. 2A2). Addition reaction dynamics can be controlled by PEGDA molecular weight: hydrogels composed of higher molecular weight PEGDA reduced their mass swelling ratio, i.e. the ratio of swollen to dried polymer weight (Q_m, Fig. 3B), and stiffened (Fig. 3C) faster than lower molecular weight PEGDA hydrogels. This could imply that a higher molecular weight PEGDA bound at one end may diffuse through greater space and thus is more likely to find an unbound thiol site faster to form a crosslink.

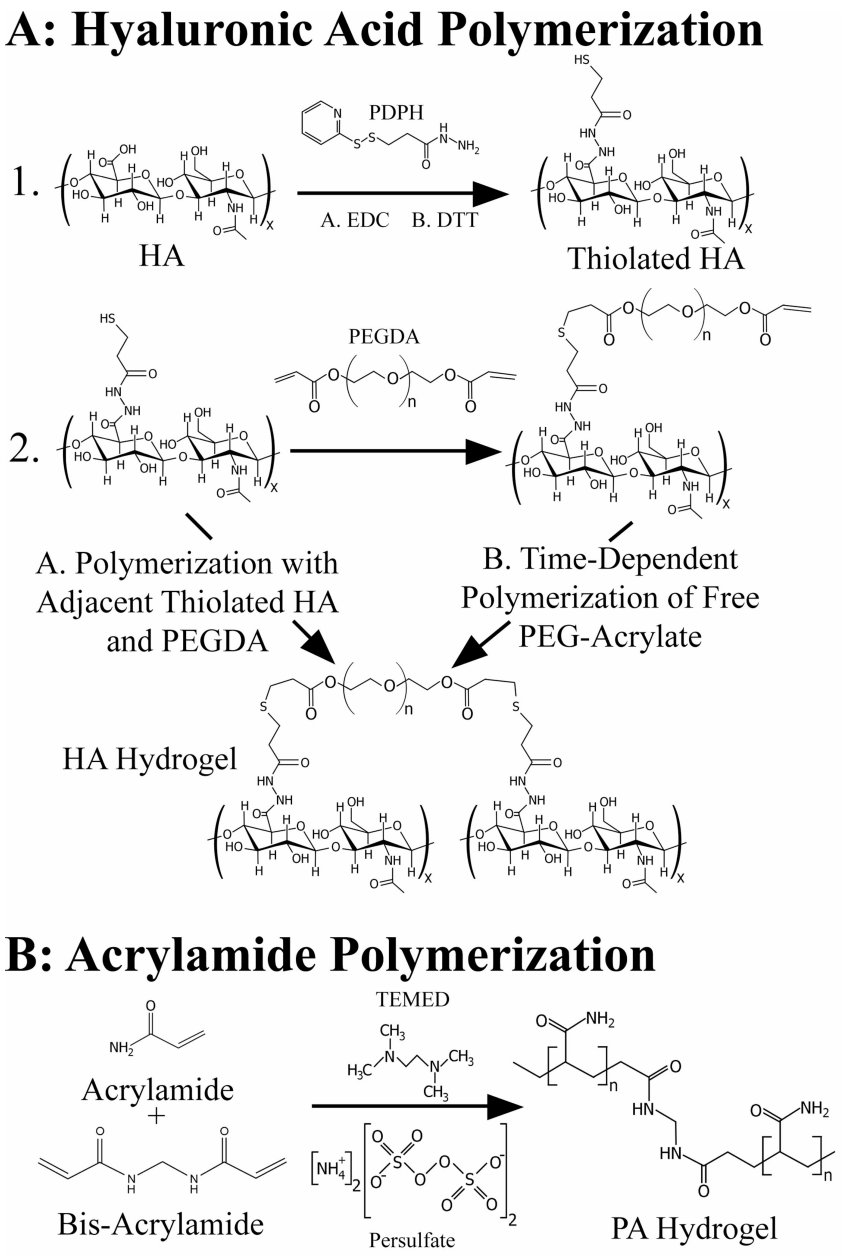

Figure 2: *Polymerization Schematic.* (A) HA is reacted with a cleavable crosslinker PDPH, EDC and DTT in order to thiolate the backbone (step 1). A hydrogel forms by two mechanisms (step 2): A. adjacent thiolated HA molecules are crosslinked via PEGDA, and B. time-dependent polymerization via a free PEG-acrylate molecule along the HA backbone to a more distant free thiol group. (B) Polyacrylamide gels are formed via free radical polymerization by mixing acrylamide, bis-acrylamide, TEMED and ammonium persulfate.

To obtain a hydrogel that stiffened similarly to heart, 0.9% PEGDA of M_w ~3400 Da and 1% thiolated HA were polymerized into hydrogel, characterized via AFM over 456 hours post-polymerization (hpp), and found to stiffen from 1.9 ± 0.1 to 8.2 ± 1.1 kPa (Fig. 3C) with a time constant of 69.6 hpp. Due to the presence of free thiol groups however, it is possible that some of the time-dependent stiffness could be due to the formation of disulfide bonds between adjacent thiolated HA chains and not the Michael-type addition reaction. Therefore, HA hydrogel stiffness was measured in the presence of 1 mm and 1 m dithiothreitol (DTT), a reducing agent of disulfide bonds. The addition of 1 mm DTT, a concentration which normally reduces protein disulfides, had a negligible effect on HA hydrogel stiffness over time compared to untreated hydrogels. 1 m DTT appears to interfere with stiffening (Fig. 5), but the high concentration may affect many other hydrogel properties. Thus, it would appear that a time-dependent Michael-type addition reaction is the likely candidate for the majority of stiffening observed here.

Hydrogel degradation via ester hydrolysis, which would actually soften the hydrogel, could compete with time-dependent crosslinking that stiffens the material. Degradation over a cell-relevant time course was monitored by placing hydrogels in either neutral (pH 7.4) or basic (pH 9) degassed (DG) PBS, the latter of which is an enhanced degradative environment for esters. Hydrogel stiffness at pH 9 was significantly lower than neutral pH, but only after more than 300 hpp (Fig. 6A)–the point at which stiffening plateaus (see Fig. 3C) indicating that even in hydrolyzing environments, significant time must elapse before degradation out competes crosslinking to soften the material. However, degradation might cause material erosion rather than

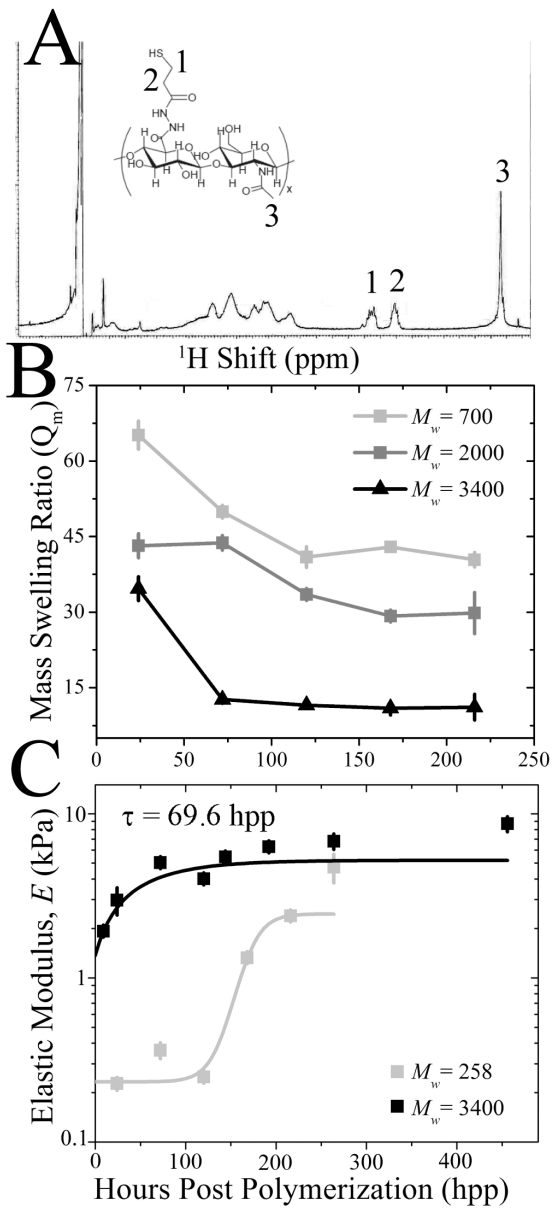

Figure 3: *HA Hydrogel Stiffening can be Tuned by Molecular Weight*. (A) ^{1}H NMR spectroscopy of thiolated HA, indicating peaks from the thiolation (1, 2) and HA backbone (3) as shown on the inset schematic of thiolated HA. (B) Mass swelling ratio (Q_m) was examined over 216 hpp among HA hydrogels prepared from PEGDA of M_w ~ 700 Da (light grey), 2000 Da (dark grey) and 3400 Da (black). (C) Elastic modulus of HA hydrogels made of M_w ~ 258 and 3400 Da PEGDA was determined by AFM as a function of time. 3400 Da hydrogels were fit with an exponential curve exhibiting a time constant, τ, of 69.6 hpp. 258 Da hydrogels were hyperbolically fit to indicate slower crosslinking.

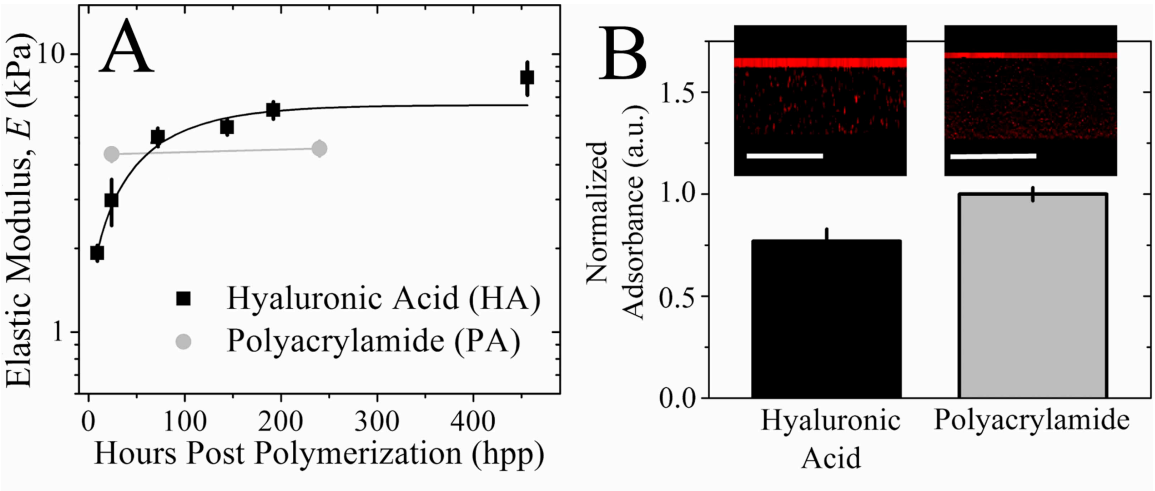

Figure 4: *Comparison of HA and PA Hydrogels.* (A) Material elastic modulus of HA (black squares) and PA (grey circles) was measured as a function of time over 456 hpp and 240 hpp, respectively. HA hydrogel data was fit with an exponential curve, which exhibited a time constant, τ, of 69.6 hpp. (B) Absorbance values at 450 nm from ELISAs performed on type I collagen-coated PA and HA hydrogels were normalized to PA hydrogels and plotted to indicate any difference in protein binding. Inset images show confocal cross-sections of each hydrogel with fluorescently-labeled type I collagen bound to the apical surface. Scale bars for HA and PA hydrogels are 64 and 72 μm, respectively.

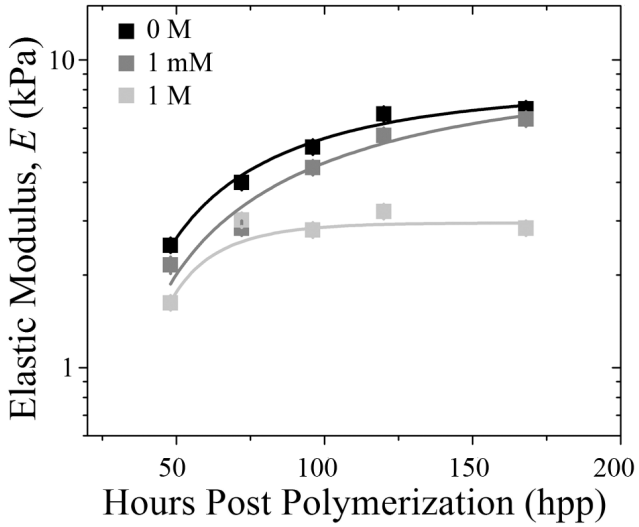

Figure 5: *Disulfide Bond Formation Does Not Substantially Contribute to Time-Dependent Stiffening*. HA hydrogels made of M_w ~3400 Da PEGDA were polymerized, subsequently treated with 0 m (black), 1 mm (grey) and 1 m (light grey) DTT, and their elastic modulus was determined by AFM as a function of time. HA hydrogel data at 1 mm and 1 m were fitted with exponential curves, exhibiting time constants, τ, of 80 and 20 hpp, respectively.

affect micro-scale stiffness, so hydrogel thickness, surface topography, and swelling were examined in neutral and basic conditions. The z-position of fluorescently-labeled collagen that was covalently bound to the hydrogel surface was monitored using confocal microscopy (see Fig. 4B inset), and over 288 hpp, the z-position of this layer on the HA hydrogel surface decreased more than ~45% in basic conditions, indicating hydrogel thinning. Changes in neutral pH were more modest indicating less thinning (Fig. 6B). Substrate topography, which can significantly affect cell responses (35), may be affected by hydrolysis-induced material erosion. Yet surface roughness, i.e. the root mean squared height change along the hydrogel surface (Fig. 7A), did not change for HA hydrogels between 24 and 192 hpp (Fig. 7C). However material erosion, if any, may be best reflected by changes in swelling (30). Measurements of the equilibrium mass swelling ratio (Q_m) showed that the HA samples regardless of pH decreased Q_m through 144 hpp and then maintained low Q_m up to 288 hpp. Such behavior is unlike the exponential increase predicted by the Flory-Rehner model for similar hydrogel systems using modest hydrolysis rate estimates where bond hydrolysis increases hydrogel water content (29, 36) (Fig. 6C). The difference may be due to that model's assumption of immediate and complete crosslinking; evidence here would suggest that complete crosslinking is not achieved until at least 216 hpp resulting in decreased Q_m with the presence of less water in the hydrogel. Thus any hydrolysis-induced erosion must at least be equally balanced with additional crosslinking through 288 hpp, but after which time hydrolysis may dominate.

In contrast to time-dependent hydrogels, polyacrylamide (PA) hydrogel crosslinking is provided by persulfate-generated free radical polymerization (Fig. 2B).

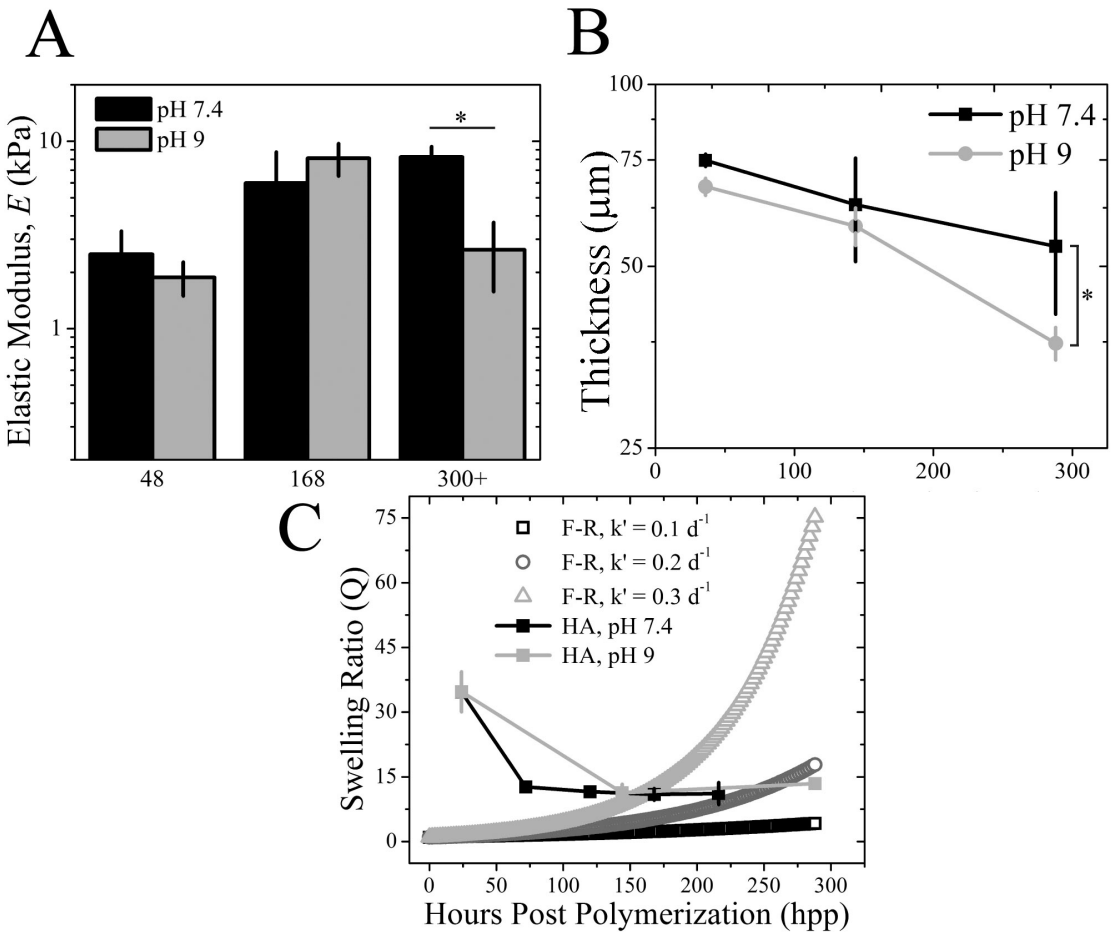

Figure 6: *HA Hydrogel Stiffening Initially Outcompetes Ester Hydrolysis*. (A) HA hydrogel elastic modulus was measured in both pH conditions over time and was reduced only in pH 9 samples after 300 + hpp. *$p < 0.05$. (B) HA hydrogel thickness was examined over 288 hpp in pH 7.4 (black squares) and 9 (grey circles) by confocal microscopy. Modest hydrogel thinning was observed for pH 7.4 but was >45% for pH 9. *$p < 0.005$. (C) Equilibrium mass swelling ratio of HA hydrogels at pH 7.4 (black) and 9 (light grey) was determined up to 288 hpp. Data is plotted as compared to a modified Flory-Rehner (F–R) model of hydrolysis for volumetric swelling where the F-R ester bond hydrolysis constant, *k'*, was varied. $k' = 0.1$ day^{-1} (open black squares), $k' = 0.2$ day^{-1} (open dark grey circles) and $k' = 0.3$ day^{-1} (open light grey triangles).

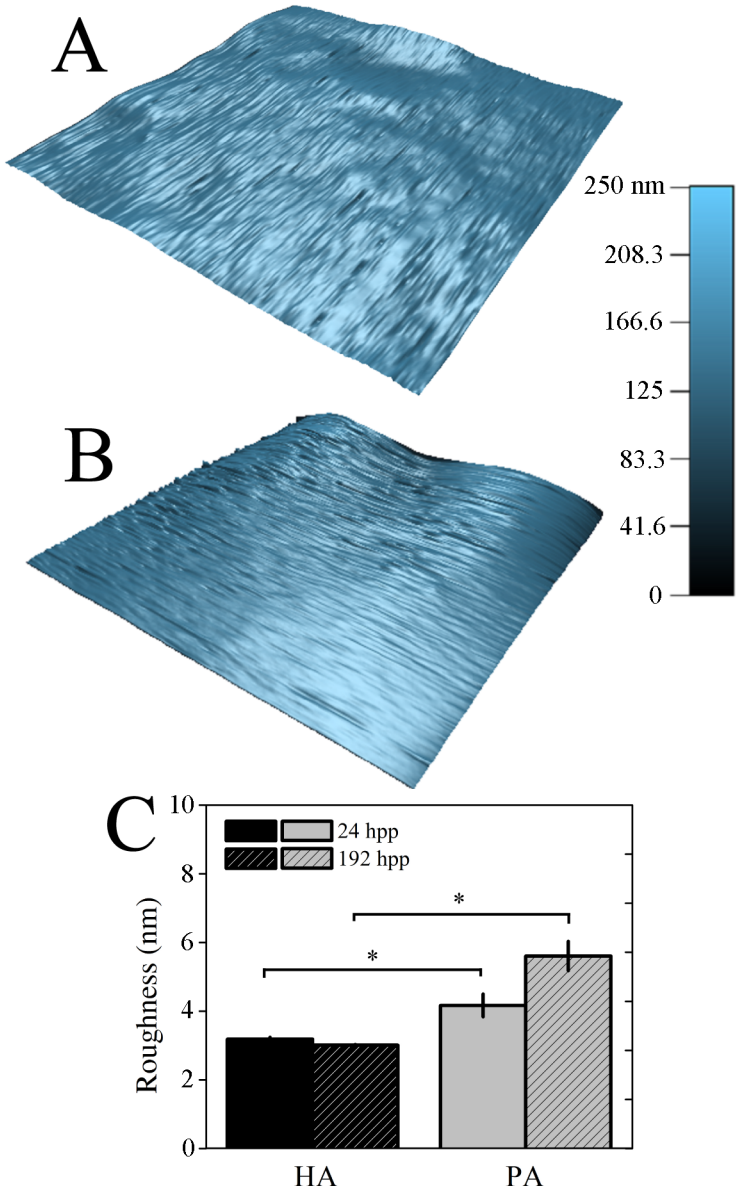

Figure 7: *HA Hydrogels Surface Topography Does Not Change Over Time.* 3-dimensional surface topography maps of HA (A) and PA (B) hydrogels at 196 hpp. (C) Surface roughness, as measured by root mean squared distance, was computed from topographical maps and plotted at both 24 and 192 hpp for HA and PA hydrogel systems. *$p < 0.05$.

This creates hydrogels with stiffness that remains constant over time (Fig. 4A; grey circles), making it a suitable control for HA hydrogels. However, both hydrogels require the attachment of ECM protein to facilitate cell adhesion. Type I collagen was covalently linked to the hydrogel surfaces using NHS chemistry, and to ensure similar attachment on both hydrogels, an enzyme-linked immunosorbent assay (ELISA) was performed. Despite the different surface chemistry, PA hydrogels contained only 23.1 ± 1.9% more collagen than HA hydrogels (Fig. 4B), and confocal cross-sectional images show that fluorescently-labeled collagen is evenly distributed along the tops of both hydrogels (Fig. 4B inset), suggesting that the surfaces may appear to be similar to cells.

2.3.3 Improved Cardiac Cell Marker Expression on Hydrogels with Time-Dependent Stiffness

To examine to what extent material stiffening regulates cardiomyocyte development, embryonic cells were isolated from myocardial or precursors tissues at 72, 120, 168, 240, and 288 HPF and cultured *in vitro* on both hydrogel systems until reaching a total age of 312 HPF. Cells isolated at each time point were plated on hydrogels of appropriate elastic modulus for that specific time point, i.e. cells plated at 72 and 288 HPF were cultured on 1 and 8 kPa hydrogels, respectively, to match previously determined tissue elastic modulus measurements with the only difference being that PA hydrogels did not stiffen while HA hydrogels continued to stiffen over time. Over this time course, expression of the immature marker NKX-2.5 and the mature cardiac specific marker Troponin T were first monitored in the intact heart and found to decrease and

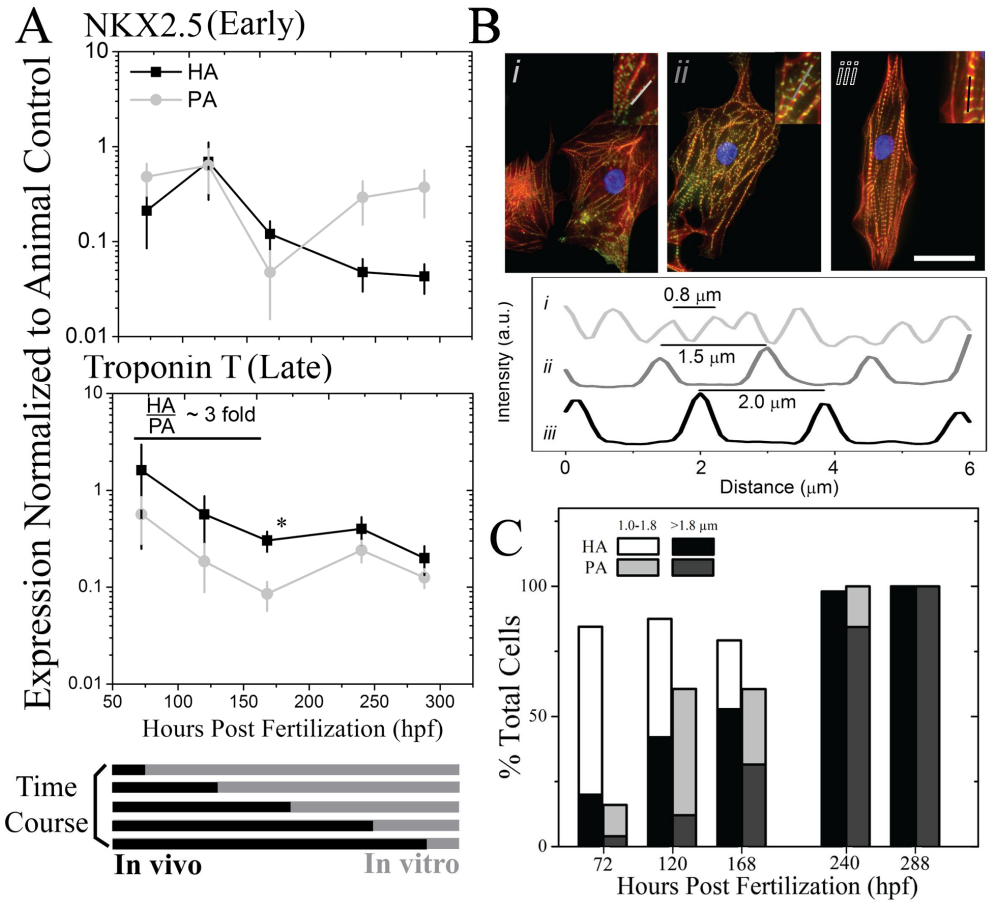

Figure 8: *Cardiomyocyte Maturation Is Improved on HA versus PA Hydrogels.* (A) Cells from early through late myocardial development were plated onto HA (black squares) and PA (grey circles) hydrogels such that total cell age (*in vivo* and *in vitro*) was 312 HPF. Early and late cardiac markers NKX-2.5 (top) and Troponin T (bottom) were measured by qPCR in cells plated on PA and HA hydrogels and normalized to the animal expression level at 312 HPF for the respective gene (see Fig. 7). Normalized expression below, at, or above 1 indicates lower, similar, or higher expression than the animal control, respectively. *$p < 0.05$ between HA and PA hydrogels. (B) Representative immunofluorescent images of cells stained for actin (red), alpha-actinin (green), and nuclei (blue) illustrate the stages of myofibril development in terms of striation length: pre-myofibrils at ~ 0.8 μm (i), maturing myofibrils at ~ 1.5 μm (ii), and mature myofibrils at ~2.0 μm (iii). Inset images indicate the myofibril that was examined in the corresponding intensity plot profile. Scale bar is 25 μm. (C) Cells were cultured in accordance to the time course in (A), and the percentage of cells containing nascent (1.0–1.8 μm; HA in white, PA in light grey) or mature myofibrils of (>1.8 μm; HA in black, PA in dark grey) was quantified. Pre-myofibrils (<1.0 μm), consist of the remaining percentage of cells, were not plotted. $n > 25$ cells were analyzed per time point per hydrogel.

increase, respectively (Fig. 9). After 312 HPF, Troponin T expression, normalized to final tissue expression, was 3-fold higher on HA than PA hydrogels in cells isolated before 150 HPF (Fig. 8A bottom). Expression of NKX-2.5, normalized to already low expression in the animal at late time points, was less than 1 (Fig. 8A top), indicating that all young, pre-cardiac cells had reduced expression of immature markers but only cells grown on HA hydrogels expressed mature cardiac markers. A better assessment of cardiac muscle formation, however, is the assembly of contractile units, i.e. myofibrils, which show a striped pattern of alternating actin and myosin. These fibrils can be described by three major stages to indicate muscle maturity: pre-myofibrils, maturing myofibrils, and mature myofibrils where the alternating pattern is less than 1 μm, 1–1.8 μm, and 1.8–2.2 μm (13), respectively, as is illustrated in Fig. 8B with staining for actin and cardiac specific α-actinin. Though all cells stained positively for cardiac specific α-actinin, quantifying myofibril striation distance indicated that greater than 75% of pre-cardiac cells plated on HA hydrogels contained maturing or mature myofibrils for cells isolated before 150 HPF (Fig. 8C). Conversely, pre-cardiac cells on PA hydrogels mostly contained pre-myofibrils (40–85%) at these early time points, resulting in up to a 60% difference. Myofibril alignment with respect to the long axis of the cell is also an indication of muscle maturity (13) (Fig. 10A) and was quantified via an orientation correlation function (OCF) (18); when OCF is 1, fiber alignment is in the direction of the long axis of the cell and when close to 0, orientation is misaligned, i.e. perpendicular to the cell axis. The OCF of cells grown *in vivo* for the longest time examined, i.e. 244 HPF, showed that cells had the highest alignment, consistent with the most mature cells coming directly from the animal. Yet again for cells isolated before 168 HPF, HA hydrogels

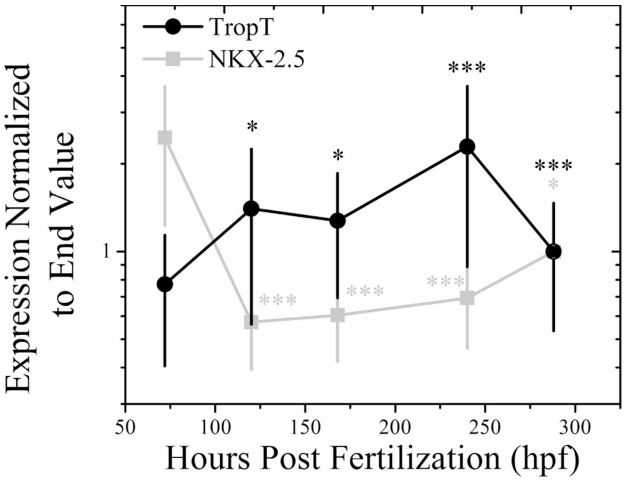

Figure 9: *Expression of Cardiac Markers in the Chick Myocardium*. Early and late cardiac markers NKX2.5 (grey squares) and Troponin T (black circles) were measured by qPCR in animals during development, normalized to the final time point at 288 HPF, and plotted. *$p < 0.05$, **$p < 0.01$, ***$p < 0.001$ compared to the initial time point.

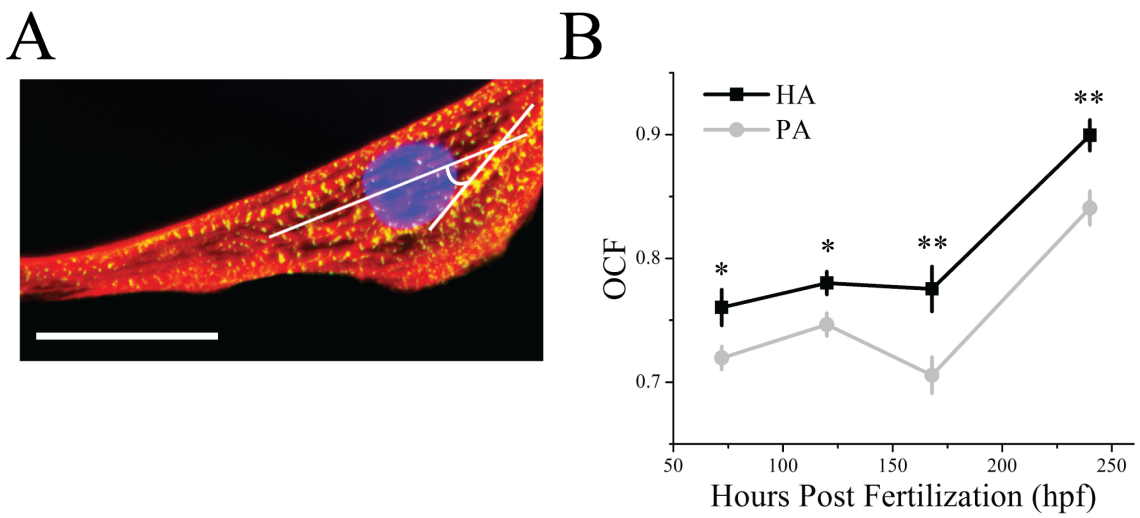

Figure 10: *Myofibrils are Most Oriented on HA Hydrogels.* (A) Myofibril orientation was examined by calculating an orientation correlation function (OCF) where θ is the difference between the myofibril angle and the long axis of the cell as indicated in white in the image of a representative cell. Scale bar is 25 μm. (B) Quantification of OCF over time for cells cultured on HA (black squares) or PA hydrogels (grey circles). Note that an OCF of 1 and 0.5 indicates parallel and diagonal alignment, respectively, in reference to the long axis of the cell. *$p < 0.05$, **$p < 0.005$ compared between HA and PA hydrogels.

produced cells with better aligned myofibrils compared to PA hydrogels as OCF was consistently higher (Fig. 10B).

2.4 Conclusions

In vitro studies presented here demonstrate the importance of dynamic material cues in guiding cell maturation while modeling implies that this hydrogel may be appropriate for *in vivo* applications due to its eventual but not immediate hydrolysis. Moreover, this study illustrates the importance not just of material properties as design criterion for therapies but of how these properties change during development, an especially critical point when a therapy intends to produce mature cells from immature precursor cells. Despite tuning HA hydrogel stiffening to mimic the mechanics of heart development here, developmental changes that lead to tissue stiffening occur ubiquitously, and this HA-based system can likely be tuned to match stiffening that occurs in many other biological contexts.

2.5 Acknowledgements

Chapter 2, in full, is a reformatted version of the published article as it appears in *Biomaterials*, volume 32, number 4, pages 1002-1009, February 2011. The dissertation author was the primary investigator and author of this paper, and thanks co-author Dr. Adam J. Engler for his contributions. The authors would like to thank Dr. Donald Elbert (Washington University in Saint Louis) for advice with degradation modeling, Dr. Jean Sanger (Upstate Medical University) for assistance with cardiomyocyte isolation, Dr. Jason Li (Asylum Research) and Dr. Somyot Chirasatitsin for technical assistance with

atomic force microscopy, and Dr. Anthony Mrse for assistance with NMR spectroscopy. This work was supported by grants from the American Heart Association (0865150F to A.J.E), NIH (1DP02OD006460 to A.J.E.), and American Heart Association (10PRE4160143) and ARCS pre-doctoral fellowships (to J.L.Y.).

2.6 Appendix

Table 1: *qPCR Primers used to Measure Gene Expression.* All qPCR primers (IDT Technologies) used are listed in the table with their PCR product size and were designed to eliminate potential contributions from genomic DNA. Human primers for fibronectin1 (FN 1) were also used in order to created a standard curve from human plasmid DNA.

Gene (Accession #)	Primer sequence	Size (bp)
Collagen 1 A2 (NM_001079714.2)	FP: 5'-TGACACTGGTGCAACAGGAAGAGA-3' RP: 5'-TCACCACGTTCACCAGGAATACCA-3'	156
Laminin B2 (NM_204166.1)	FP: 5'-ACAGGATGCCAATTTCAACGCCAG-3' RP: 5'-ATGCTGTCGAAGGCACCAAGGAAA-3'	141
Fibronectin 1 (Ckn) (XM_421868.2)	FP: 5'-ACTACAGCCAGCAGCTTTGTTGTC-3' RP: 5'-TCAGGGATGTTGACAGAAGTGGCT-3'	146
Troponin T2 (NM_205449.1)	FP: 5'-AAGAAGGGTGGCAAGAAGCAAACG-3' RP: 5'-TCAGTTTGTCTTCGCTGAGGTGGT-3'	103
NKX-2.5 (NM_205164.1)	FP: 5'-ACAAGAAAGAACTGTGTGCCCTGC-3' RP: 5'-TCTGCTGCTTGAACCTTCTCTCCA-3'	154
GAPDH (NM_204305.1)	FP: 5'-ACTGTCAAGGCTGAGAACGGGAAA-3' RP: 5'-TGATAACACGCTTAGCACCACCCT-3'	187
Fibronectin 1 (Human) (NM_212482)	FP: 5'-AAACTTGCATCTGGAGGCAAACCC-3' RP: 5'-AGCTCTGATCAGCATGGACCACTT-3'	158

2.7 References

1. Discher DE, Mooney DJ, Zandstra PW (2009) Growth factors, matrices, and forces combine and control stem cells. *Science* 324(5935):1673–1677.

2. Saha K, Keung AJ, Irwin EF, Li Y, Little L, Schaffer DV, Healy KE (2008) Substrate modulus directs neural stem cell behavior. *Biophys J* 95(9):4426–4438.

3. A.J. Engler, S. Sen, H.L. Sweeney, D.E. Discher (2006) Matrix elasticity directs stem cell lineage specification. *Cell* 126(4):677–689.

4. Huebsch N, Arany PR, Mao AS, Shvartsman D, Ali OA, Bencherif SA, Rivera-Feliciano J., Mooney DJ (2010) Harnessing traction-mediated manipulation of the cell/matrix interface to control stem-cell fate. *Nat Mater* 9(6):518–526.

5. Lutolf MP, Hubbell JA (2005) Synthetic biomaterials as instructive extracellular microenvironments for morphogenesis in tissue engineering. *Nat Biotechnol* 23(1):47–55.

6. Nelson CM, Bissell MJ (2006) Of extracellular matrix, scaffolds, and signaling: tissue architecture regulates development, homeostasis, and cancer. *Annu Rev Cell Dev Biol* 22:287–309.

7. Deroanne CF, Lapiere CM, Nusgens BV (2001) In vitro tubulogenesis of endothelial cells by relaxation of the coupling extracellular matrix-cytoskeleton. *Cardiovasc Res* 49(3):647–658.

8. Guo WH, Frey MT, Burnham NA, Wang YL (2006) Substrate rigidity regulates the formation and maintenance of tissues. *Biophys J* 90(6):2213–2220.

9. Townes PL, Holtfreter J (1955) Directed movements and selective adhesion of embryonic amphibian cells. *J Exp Zool* 128(1):53–120.

10. E.D. Hay (1991) Cell biology of extracellular matrix (2nd ed.) Plenum Press, New York.

11. Montell DJ (2008) Morphogenetic cell movements: diversity from modular mechanical properties. *Science* 322 (5907):1502–1505.

12. Bird SD, Doevendans PA, van Rooijen MA, de la Riviere AB, Hassink RJ, Passier R, Mummery CL (2003) The human adult cardiomyocyte phenotype. *Cardiovasc Res* 58:423–434.

13. Sanger JW, Kang S, Siebrands CC, Freeman N, Du A, Wang J, Stout AL, Sanger JM (2005) How to build a myofibril. *J Muscle Res Cell Motil* 26(6–8):343–354.

14. Shapira-Schweitzer K, Seliktar D (2007) Matrix stiffness affects spontaneous contraction of cardiomyocytes cultured within a PEGylated fibrinogen biomaterial. *Acta Biomater* 3:33–41.

15. Jacot JG, McCulloch AD, Omens JH (2008) Substrate stiffness affects the functional maturation of neonatal rat ventricular myocytes. *Biophys J* 95(7):3479–3487.

16. Engler AJ, Carag-Krieger C, Johnson CP, Raab M, Tang HY, Speicher DW, Sanger JW, Sanger JM, Discher DE (2008) Embryonic cardiomyocytes beat best on a matrix with heart-like elasticity: scar-like rigidity inhibits beating. *J Cell Sci* 121(Pt 22):3794–3802.

17. Berry MF, Engler AJ, Woo YJ, Pirolli TJ, Bish LT, Jayasankar V, Morine KJ, Gardner TJ, Discher DE, Sweeney HL (2006) Mesenchymal stem cell injection after myocardial infarction improves myocardial compliance. *Am J Physiol Heart Circ Physiol* 290(6):H2196–H2203.

18. Engler AJ, Griffin MA, Sen S, Bonnemann CG, Sweeney HL, Discher DE (2004) Myotubes differentiate optimally on substrates with tissue-like stiffness: pathological implications for soft or stiff microenvironments. *J Cell Biol* 166(6):877–887.

19. Collinsworth AM, Zhang S, Kraus WE, Truskey GA (2002) Apparent elastic modulus and hysteresis of skeletal muscle cells throughout differentiation. *Am J Physiol Cell Physiol* 283(4):C1219–C1227.

20. Pasternak C, Wong S, Elson EL (1995) Mechanical function of dystrophin in muscle cells. *J Cell Bio* 128:355–361.

21. Breitbach M, Bostani T, Roell W, Xia Y, Dewald O, Nygren JM, Fries JW, Tiemann K, Bohlen H, Hescheler J, Welz A, Bloch W, Jacobsen SE, Fleischmann BK (2007) Potential risks of bone marrow cell transplantation into infarcted hearts. *Blood* 110(4):1362–1369.

22. Krieg M, Arboleda-Estudillo Y, Puech PH, Kafer J, Graner F, Müller DJ, Heisenberg CP (2008) Tensile forces govern germ-layer organization in zebrafish. *Nat Cell Biol* 10(4):429–436.

23. Hamburger V, Hamilton HL (1951) A series of normal stages in the development of the chick embryo. *J Morph* 88:49–62.

24. Hibbs RG (1956) Electron microscopy of developing cardiac muscle in chick embryos. *Am J Anat* 99(1):17–51.

25. Zamir EA, Srinivasan V, Perucchio R, Taber LA (2003) Mechanical asymmetry in the embryonic chick heart during looping. *Ann Biomed Eng* 31(11):1327–1336.

26. Shu XZ, Liu Y, Luo Y, Roberts MC, Prestwich GD (2002) Disulfide cross-linked hyaluronan hydrogels. *Biomacromolecules* 3(6):1304–1311.

27. Tse JR, Engler AJ (2010) Preparation of hydrogel substrates with tunable mechanical properties. *Curr Protoc Cell Biol* [Chapter 10]:Unit 10.16.

28. Radmacher M (2007) Studying the mechanics of cellular processes by atomic force microscopy. *Methods Cell Biol* 83:347–372.

29. Metters AT, Anseth KS, Bowman CN (2001) A statistical kinetic model for the bulk degradation of PLA-b-PEG-b-PLA hydrogel networks: Incorporating network non-idealities. *J Phys Chem B* 105(34):8069–8076.

30. Flory PJ (1953) Principles of polymer chemistry. Cornell University Press.

31. Humphrey JH (1943) Antigenic properties of hyaluronic acid. *Biochem J* 37(4):460–463.

32. Burdick JA, Chung C, Jia X, Randolph MA, Langer R (2005) Controlled degradation and mechanical behavior of photopolymerized hyaluronic acid networks. *Biomacromolecules* 6(1):386–391.

33. Serban MA, Yang G, Prestwich GD (2008) Synthesis, characterization and chondroprotective properties of a hyaluronan thioethyl ether derivative. *Biomaterials* 29(10):1388–1399.

34. Serban MA, Scott A, Prestwich GD (2008) Use of hyaluronan-derived hydrogels for three-dimensional cell culture and tumor xenografts. *Curr Protoc Cell Biol* [Chapter 10]:Unit 10.14.

35. Dalby MJ, Gadegaard N, Tare R, Andar A, Riehle MO, Herzyk P, Wilkinson CD, Oreffo RO (2007) The control of human mesenchymal cell differentiation using nanoscale symmetry and disorder. *Nat Mater* 6(12):997–1003.

36. Metters AT, Bowman CN, Anseth KS (2000) A statistical kinetic model for the bulk degradation of PLA-b-PEG-b-PLA hydrogel networks. *J Phys Chem B* 104(30):7043–7049.

Chapter 3

Mechanosensitive Kinases Regulate Stiffness-Induced Cardiomyogenesis

Abstract

As cells migrate and differentiate throughout development, they secrete and assemble extracellular matrix, giving rise to time-dependent, tissue-specific stiffness, i.e. cardiac muscle stiffens ~10-fold during maturation. When mimicked *in vitro* with a thiolated hyaluronic acid (HA) hydrogel, myocardial matrix stiffening enhanced cardiac specific gene expression and myofibril organization in isolated embryonic cardiomyocytes vs. static hydrogels. While active mechanotransduction aided maturation, the specific proteins responsible for responding to time-dependent stiffness remain unknown. In order to assess matrix-mediated mechanotransduction, we examined the expression and phosphorylation state of 800 protein kinases of embryonic cardiomyocytes plated on matrices with either dynamic or static cardiac tissue-specific stiffness. Microarray analysis of protein kinases showed differential expression as a function of mechanics, confirmed by ratiometric western blotting. Many cardiogenic

pathways exhibited time-dependent up-regulation on dynamic versus static matrices, including PI3K/Akt and p38 MAPK, while GSK3β, a known inhibitor of cardiomyocyte maturation, was down regulated. These data indicate that mechanically driven maturation is at least partially achieved via active mechanosensing at focal adhesions. Identifying mechanosensitive pathways that are active in cardiomyogenesis can lead to a better understanding of how stem cell differentiation and development are mediated by extracellular matrix properties.

3.1 Introduction

Extracellular matrix (ECM) elasticity, or stiffness, regulates a variety of cell signaling pathways and subsequent responses, e.g. differentiation (1-4), via myosin-based contractility (5), but these pathways likely undergo significant temporal regulation throughout development as cells secrete and assemble ECM (6). This gives rise to mature tissue stiffness (7, 8) and alters contractility over time, i.e. greater stiffness requires increased contractile work that cells must exert on the matrix. The change in work done by cells manifests itself in the form of changes in mechanosensitive signaling pathways, such as with cardiomyocytes on stiffer substrates exhibiting more myosin II-based contractility (1-4, 9). While the effects from aberrantly stiff matrix, e.g. fibrosis, usually leads to dysfunction via impaired myosin II function (10), stiffness changes during development can lead to more appropriate signaling as it does normally *in vivo*. Static substrate stiffness is known to influence migration (1, 11, 12), adhesion (2, 13, 14), proliferation (15-17), and differentiation (1-4), but beyond stiffness alone, temporal

changes in stiffness that mirror *in vivo* stiffening are known to impact cardiac maturation as shown in Chapter 2 (18). When these behaviors are integrated over many cells, stiffening can affect tissue morphogenesis (7, 19, 20), e.g. tubulogenesis (21) and heart development (22), making stiffness not just a significant niche component, but one that must be appropriately mimicked over time *in vitro*.

While temporal changes are likely important in almost every developmental context, they are especially important for cardiomyocytes, which contract more effectively when grown on substrates mimicking the stiffness of their native microenvironment versus rigid glass (23). Improved contractility in mature cardiomyocytes may be due in part to the modulation of myofibril organization and alignment, both of which can affect beating rate, and are known to be regulated by static matrix stiffness (9, 10). On a hydrogel with a stiffness of 10 kiloPascal (kPa; Pascal is a unit of stiffness), which approximates the adult myocardium (24), intra- and extracellular strains become matched, thereby prolonging rhythmic beating of mature cardiomyocytes in culture compared to soft or stiff substrates (10). Despite improved myocyte function on matrices with biomimetic stiffness, the heart does not begin as a contractile ~10 kPa ECM but instead originates from much softer mesoderm where stiffness is less than 500 Pa (18, 25-29) and stiffens up to E14 with a $\tau_{1/2}$~ 60 hr (18).

Mimicking myocardial stiffening dynamics using a thiolated hyaluronic acid (HA-SH)/poly(ethylene glycol) diacrylate (PEGDA) hydrogel, which stiffens from ~1 to 10 kPa with $\tau_{1/2}$~ 69 hr, and absent specific exogenous growth factors aside from serum, improved cardiomyocyte maturation by up to 60% based on gene expression and phenotypic changes was observed (18). While many signaling pathways could be

mechanosensitive, those most affected by stiffness are likely to be critical for spatiotemporal heart patterning pathways (outlined in (30-32)), including agonist pathways phosphatidylinositol 3 kinase (PI3K)/protein kinase B (PKB/Akt) (33, 34), *Wnt*/Ca^{2+} (35) and *Wnt*/polarity (36), and antagonist pathways such as the Canonical *Wnt*/β-catenin via expression of GSK-3β (37, 38). While these signaling pathways have been extensively studied in regards to development and differentiation, both *in vitro* and/or *in vivo*, stiffness-mediated activation remains unclear. To understand what role these and other pathways play in cardiac maturation as directed by temporal stiffening of ECM, a systematic examination of protein kinase pathway activation with respect to dynamic vs. static substrate stiffness was conducted and specific pathway effects on the maturation of embryonic cardiomyocytes were examined.

3.2 Materials and Methods

3.2.1 Hydrogel Polymerization

To prepare HA hydrogels of the appropriate stiffness to mimic heart stiffening, 4.53% (w/v) PEGDA (Glycosan Biosystems, UT) with M_w ~ 3400 Da (polydispersity index or PDI ~ 3) in 1X degassed phosphate buffered saline (DG PBS) and 1.25% thiolated HA (HA-SH, Glycosan Biosystems, UT) in DG PBS were separately mixed at 37 °C with gentle shaking for up to 30 min. HA-SH was analyzed via ^{1}H nuclear magnetic resonance (NMR) spectroscopy (JEOL ECA 500) to assess thiol substitution (~ 40%). To initiate polymerization, solutions were combined at a volume ratio of 1 PEGDA solution: 4 HA solution to yield a 1% HA/0.9% PEGDA hydrogel, and 50 μL of

the solution was placed between adhesive, aminosilanated and non-adhesive hydroxylated glass coverslips (39) and allowed to polymerize in a humidified 37 °C incubator for 30 min-1 hr. To attach protein to the surface, 20 mM EDC (ThermoScientific), 50 mM NHS (ThermoScientific) and 150 μg/mL type I rat tail collagen (BD Biosciences) were mixed in 1X PBS and incubated with the hydrogels overnight. Polyacrylamide gels (PA) were prepared as described previously (39). Briefly, gel crosslinker n,n'-methylene-bis-acrylamide and acrylamide (Fisher Scientific) monomer concentrations were varied in 1X PBS and polymerized between adhesive, aminosilanated and non-adhesive hydroxylated glass coverslips using 1/200 volume of 10% ammonium persulfate (Sigma) and 1/2000 volume of *n*,*n*,*n*',*n*'-tetramethylethylenediamine (TEMED, BioRad) in order to create hydrogels of Young's Modulus, *E*, of ~ 1 kPa (soft, ~ brain stiffness), 11 kPa (intermediate, ~ muscle stiffness) and 34 kPa (stiff, ~ bone stiffness), according to a previously published protocol (39). To attach protein to the PA hydrogel surface, 0.5 mg/ml of the photoactivating crosslinker, sulfo-SANPAH (Pierce), was mixed in 50 mm HEPES (EMD) of pH 8.5 and activated with 350 nm UV light for 10 min. Collagen was added as with HA hydrogels overnight.

3.2.2 Cell Isolation and Cell Culture

Animals received humane care in compliance with University of California, San Diego's Institutional Animal Care and Use Committee (protocol #S09200). Chicken embryos were obtained from McIntyre Poultry Farm (Lakeside, CA) and embryonic hearts were obtained by isolation at 72, 120, 168, 240, 312 and 336 hours post-fertilization (HPF). Age was confirmed using Hamburger–Hamilton stages (40). Hearts

were obtained by dissection and digested for cell isolation. Isolated hearts were minced using sterile razor blades and collected with 10 mL of 0.05% trypsin-EDTA (Invitrogen) and incubated in a sterile humidified 37 °C incubator (5% CO_2) for 10 min. In order to remove red blood cells, the tube was inverted and tissue was allowed to settle prior to a change of solution to another 10 mL of fresh trypsin. After incubation for 10 min, the sample was centrifuged at 1000 x g for 2.5 min and the pellet was carefully triturated with normal heart medium (89% MEM-alpha: l-glutamine (+), ribo-/deoxyribo-nucelosides (−), Invitrogen; 10% fetal bovine serum, Hyclone; and 1% penicilin:streptomycin, Invitrogen). The cell solution was passed through a 70 μm cell strainer (BD Falcon) and pre-plated on a sterile tissue culture dish for 1 hr in a cell incubator in order to remove fibroblasts from the solution. The unattached cells were collected, counted, and plated at a density of 1-2 × 10^6 cells/mm^2. Cells used for western blotting, immunofluorescence and calcium imaging were incubated for 1, 3, 5 and 11 days (total age: 96, 144, 192 and 336 HPF, respectively) on HA and 1, 11, 34 kPa PA hydrogels. Cells used for the microarray were cultured on HA and 11 kPa PA hydrogels. Media changes were performed every 2 days. All cell culture and tissue experiments were performed at least in triplicate.

3.2.3 Protein Kinase Microarray, Analysis and Validation

For the microarray, cells on hydrogels were washed twice in ice cold 1X PBS and lysed in buffer according to instructions provided by Kinexus. The lysis buffer consisted of 20 mM MOPS (Fisher Scientific) pH 7.0, 2 mM EGTA (EMD Biosciences), 5 mM EDTA (EMD Biosciences), 30 mM sodium fluoride (J.T. Baker), 60 mM β-

glycerophosphate (Sigma), pH 7.2, 20 mM sodium pyrophosphate (Fisher Scientific), 1 mM sodium orthovanadate (Sigma), and 1% Triton X-100 (Fisher Scientific). Just before use, 1 Roche Complete Mini Inhibitor Cocktail tablet (Roche) and 1 mM dithiothreitol (DTT, Amresco, OH) were added to the buffer. Lysates were sonicated four times for 10 seconds each time with 10-15 second intervals on ice in order to rupture the cells and to shear nuclear DNA. The homogenate was centrifuged at 90,000 x g for 30 min at 4°C in a Beckman Table Top TL-100 ultracentrifuge and the resulting supernatant fraction was taken. The sample was then assayed for protein concentration using a commercial Bradford assay reagent (BioRad).

For the Kinex™ Antibody Microarray analyses, a single dye, non-competitive sample binding methodology was used. The antibodies employed consist of polyclonal and monoclonal antibodies that were carefully selected and have been stringently validated (a complete list can be found on the Kinexus website at: http://www.kinexus.ca/ourServices/microarrays/antibody_microarrays/antibody_microarrays.html). Arrays contained 517 pan-specific antibodies (for protein expression) and 337 phosphorylation site-specific antibodies. For each sample, the chip contained a field of 16 sub-grids of 10 x 11 spots of diameters 120-150 μm.

Kinexus performed the Kinex™ microarray as follows. 50 μg of lysate protein from each sample was covalently labeled with a fluorescent dye, with free dye molecules removed by gel filtration. After blocking non-specific binding sites on the array, samples were incubated on the chip and unbound proteins washed away. Imaging was performed with a Perkin-Elmer ScanArray Reader laser array scanner (Waltham, MA). Signal quantification was performed with *ImaGene 8.0* from BioDiscovery (El Segundo, CA)

with predetermined settings for spot segmentation and background correction. Z scores were calculated by subtracting the overall average intensity of all spots within a sample from the raw intensity for each spot, and dividing it by the standard deviations (SD) of all of the measured intensities within each sample (41). Z ratios were then calculated by taking the difference between the averages of the protein Z scores and dividing by the SD of all of the differences for that particular comparison (D3 vs. D1 HA and PA, D5 vs. D1 HA and PA, D11 vs. D1 HA and PA, D11 HA and PA vs. D14 chicken).

Statistically significant values were determined by performing a 2-way ANOVA in Matlab and choosing interaction $p < 0.05$. Clustering was performed using Cluster 3.0 and visualized in Java TreeView. Data that was statistically significant as well as significantly expressed (-1 > z-ratio or z-ratio > 1) was visualized in clustering in order to choose the most conservative data set. GO-ELITE analysis (42) was performed in order to determine significant proteins and pathways by calculating advanced over-representation analysis statistics of data to identify a non-redundant set of ontology (i.e. gene ontology terms (43)) and pathways (i.e. WikiPathways (44)). Significant pathways were edited in PathVisio using statistically significant data (data not trimmed by value of z-ratio).

Microarray validation was achieved by performing western blots on a select set of proteins relevant to cardiomyocyte maturation, and within the statistically significantly, differentially expressed population. For western blots, cells on hydrogels were washed twice in ice cold 1X PBS and lysed with mRIPA [1% Triton-X (Fisher Scientific), 1% Sodium Deoxycholate (Sigma), 0.1% sodium dodecyl sulfate (Fisher Scientific), 150mM Sodium Chloride (Fisher Scientific), 10% glycerol (Fisher Scientific), 1.5mM

Magnesium Chloride (Fisher Scientific), 50mM Hepes (EMD) and pH adjusted to 7.5]. Just before use 1mM phenylmethylsulfonyl fluoride (EMD), 1mM ethylenediaminetetraacetic acid (EMD) and 1% Phosphatase Inhibitor Cocktail B (sc-45045, Santa Cruz Biotechnology) for 10 min at room temperature. Samples were prepared such that the loading solution consisted of 1/3 volume protein loading dye (National Diagnostics), and were subsequently heated at 90°C for 2 min and loaded into 10% resolving/5% stacking acrylamide hydrogels (Biorad) and run for 45 min - 1 hr at 150 V in 10% SDS buffer [25mM Tris (Fisher Scientific), 192mM Glycine (J.T. Baker) and 20% v/v Methanol (Fisher Scientific)].

Separated proteins were transferred onto nitrocellulose film for 1.25 hr at 100 V at 4°C and blocked overnight in blocking buffer [1% non-fat milk or 4% Sea-block (ThermoScientific), 25mM Tris (Fisher Scientific), 150mM NaCl (Fisher Scientific), 0.1%Tween-20 (Fisher Scientific)]. Specific antibodies of interest were added to blocking buffer as follows: vinculin – 1 hr, 1:1000 (V4505, Sigma); Paxillin – 1 hr, 1:1000 (MBS470022, MyBioSource); Erk 1+2 – 1 hr, 1:1000 (LS-B3687, Lifespan BioSciences); AKT1 – 1 hr, 1:1000 (AP09425PU-N, Acris Antibodies); AKT2 - 1 hr, 1:1000 (AP03032PU-N, Acris Antibodies); P38 MAPK – 1 hr, 1:1000 (AP03041SU-N, Acris Antibodies; GAPDH - 1 hr, 1:5000 (MAB374, Milipore); GSK3β - 1 hr, 1:500 (MBS462236, MyBioSource). Primary antibodies were labeled with HRP-conjugated antibodies for 1 hr [goat anti-rabbit 1:10000 (170-6515, BioRad), donkey anti-sheep 1:10000 (713-035-003, Jackson), goat anti-mouse 1:10000 (115-035-062, Jackson)]. Films were exposed using ECL reagent (Thermo Scientific and processed in a Konica

Minolta SRX-101A x-ray developer for 30 sec, 5 min and 1 hr. All westerns were quantified using ImageJ, normalized to GAPDH expression.

3.2.4 Cell Maturation Assays

In order to examine cell maturation from the time course previously described, immunofluorescence for myofibril development and calcium imaging experiments were performed. Immunofluorescence was performed as follows: cells were fixed with 3.7% formaldehyde in PBS for 30 min, rinsed and permeabilized using Triton X-100 for 10 min. Cells were rinsed and incubated with primary mouse antibody for α-actinin (A7811, Sigma) at 1:500 in 2% ovalbumin (Sigma) for 60 min in a 37 °C cell incubator. Samples were then incubated with 1:1000 rhodamine-phallodin (R415, Invitrogen) and 1:1000 Alexa Flour 488 conjugated goat anti-mouse secondary antibody (A11001, Invitrogen) in 2% ovalbumin for 30 min, followed by 1:5000 Hoescht (33342, Sigma) in DH_20 for 10 min at 37 °C. Samples were rinsed and mounted with Fluoromount-G (SouthernBiotech) and sealed with nail polish. Images were captured using a Nikon Eclipse TE2000-U fluorescent microscope with Metamorph 7.6 software. Images were analyzed using ImageJ to determine striation length by drawing a calibrated line through every visible fibril within a cell. At least 20 cells, corresponding to 100 myofibrils were analyzed per condition. Calcium imaging was performed at days 1 and 11 after plating by adding Fluo-4 AM (F-14201, Invitrogen) at 1:2000 directly to the media for 10 minutes. Videos were captured using a Nikon Eclipse TE2000-U fluorescent microscope outfitted with a LiveCell imager with Metamorph 7.6 software utilizing pre-determined exposure (light intensity set at 250-950 units and exposed for 200 ms at 120 frames/s). Videos were

analyzed in MATLAB using custom-written code to determine the power spectral density of the signal.

3.2.5 Statistical Analyses

Microarray statistical analyses were performed using a 2-way ANOVA. Differences among groups were assessed to identify statistical differences between the interaction of hydrogel types and time points when $p < 0.05$. All other statistical analyses were performed using student t-tests. Differences among groups were assessed to identify statistical differences between treatments when $p < 0.05$. All data is presented as mean ± standard error of the mean.

3.3 Results and Discussion

3.3.1 Stiffness-Mediated Maturation

To examine the role of dynamic vs. static stiffness in cardiomyocyte maturation, cells were isolated at 72 HPF (E3) from the hearts of chicken embryos and cultured *in vitro* on dynamic HA and static 1, 11, and 34 kPa PA hydrogels for 1 and 11 days (96 and 336 HPF, respectively). Cardiomyocyte morphology and maturation were examined, with the latter being assessed by sarcomere assembly of the thin filament protein actin and z-disc protein α-actinin, which alternate position within the sarcomere. Cells on soft, static matrices were rounded with few that spread over time, regardless of whether they were isolated or in clusters (Fig. 1A, top middle row). On stiff substrates similar to a fibrotic niche (24), i.e. 34 kPa matrix, cells developed a rod-shaped morphology but a dominant

fraction formed syncytia over the time course such that matrix effects could not be decoupled (Fig. 1A, bottom row). For both dynamic HA and static 11 kPa PA hydrogels, cells developed a rod-shaped morphology with most remaining as single cells (Fig. 1A, top and bottom middle rows, respectively).

Despite similar morphology, myocytes on dynamic HA matrices developed and maintained myofibrils with average z-disc spacing ~ 1.8 μm (Fig. 1B, left), indicative of mature myofibrils (45), but myocytes on static 11 kPa matrices disassembled some mature sarcomeres and assembled sarcomeres with smaller z-disc spacing, which is indicative of immature sarcomeres (< 1.8 μm (45)) and less mature myocytes (Fig. 1B, right). Myocytes on the softest substrates were precluded from measurement because cells remained rounded, thereby resulting in a limited number of myofibrils able to be quantified, whereas fibroblast proliferation on the stiffest substrates could not be controlled, resulting in mixed cell type clusters whose sarcomeres could not be easily measured, as well as complications due to discerning cell-matrix vs. cell-cell junction signaling. To determine if these differences in sarcomere assembly resulted in functional changes, calcium transients, which regulate contraction magnitude and duration (46), were observed for isolated myocytes on dynamic HA and static PA matrices. Over the duration of stiffening, the average power spectral density remained relatively constant for dynamic HA hydrogels but dropped 22% for myocytes on static PA hydrogels (Fig. 1C). When examining power spectral density as a function of frequency, contractions between 0-2 Hz were present for both substrates initially after plating (Fig. 2A, B), but over time, lower frequencies (0-0.8 Hz) dominate on 11 kPa, while on HA hydrogels, we see consistent beating vs. day 1 (Fig. 2C, D).

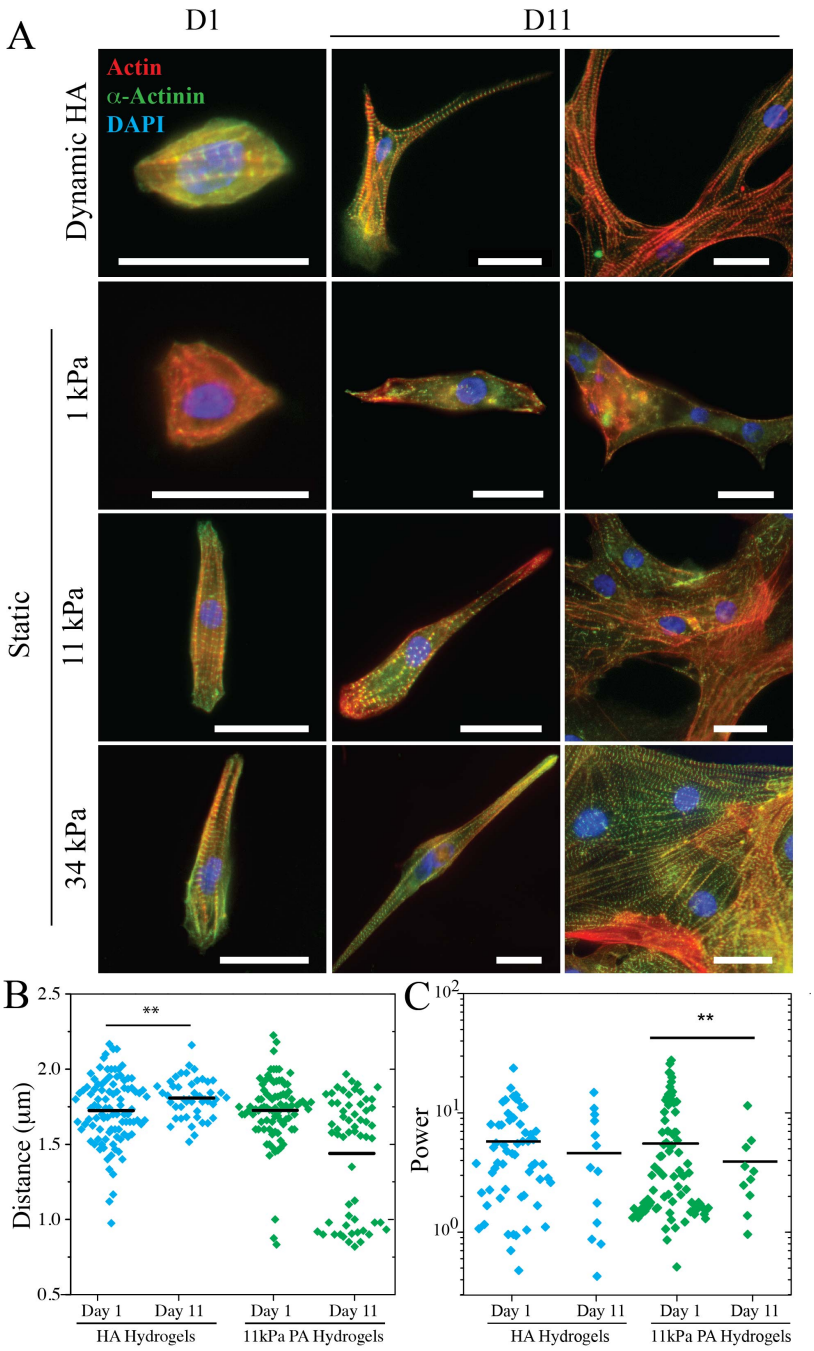

Figure 1: *Cardiomyocyte Maturation on Mechanically-Instructive Hydrogels.* (A) Immunofluorescence of α-actinin (green), actin (red) and nuceli (blue) of 72 HPF plated cardiomyocytes at 1 (D1) and 11 (D11) days after plating on dynamic HA (top row) and static 1 (second row), 11 (third row) and 34 (bottom row) kPa PA hydrogels. Day 11 images consist of single cells (middle column) and clustered cells (right column). All scale bars are 25 μm. (B) Sarcomere spacing (μm) of individual myofibrils is plotted for HA (blue) and 11 kPa PA (green) hydrogels at day 1 and 11 after plating, n>20 cells. (C) Power of beating from calcium imaging is plotted for day 1 and 11 after plating on HA and 11 kPa PA hydrogels. $^{**}p < 0.01$

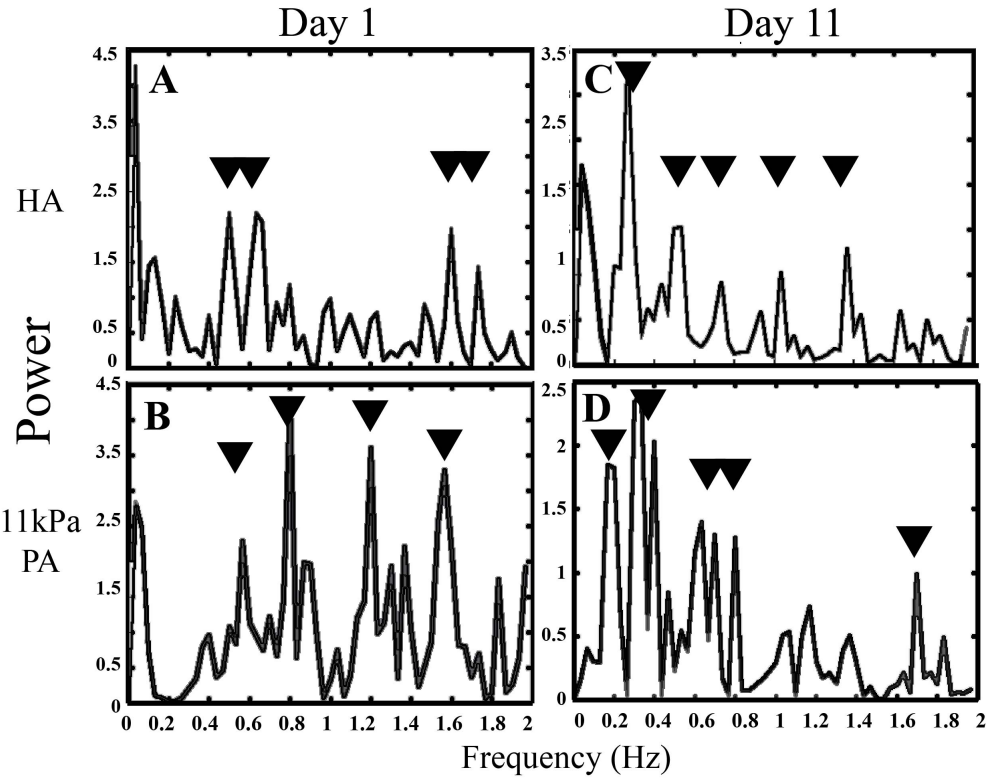

Figure 2: *Calcium Imaging of Static and Dynamic Hydrogels.* Power spectral density plotted vs. frequency is shown 1 day after plating 72 HPF myocytes on stiffening HA (A) and 11 kPa PA (B) hydrogels. Panels C and D show dynamic HA and static 11 kPa PA hydrogels after 11 days of culture, respectively. Peaks in the power spectrum are indicated by arrowheads.

Together these data indicate that not only does a matrix that is too soft or stiff versus the niche impair maturation, but that a matrix that does not change with the cells as they mature can also adversely affect maturation and maintenance of embryonic cardiomyocytes. These data also implicate signaling proteins that are responsible for changes in maturation and cytoskeletal architecture, e.g. p38 MAPK/JNK (30, 31), as possible regulators.

3.3.2 Mechanosensitive Signaling

To identify possible mechano-sensitive signaling mechanisms used in the maturation and maintenance of embryonic myocytes, a protein kinase microarray was employed to compare signaling differences in 72 HPF embryonic cardiomyocytes plated on dynamic HA and static PA hydrogels for 1, 3, 5 and 11 days (for a total age of 96, 144, 192 and 336 HPF, respectively); myocardial development as well as stiffening conclude by 336 HPF (18, 40). Normalized to the initial post-isolation time point, expression and phosphorylation of 517 and 337 proteins, respectively, were assessed. 203 proteins were found to have both statistically significant changes in expression or phosphorylation over time and between dynamic HA and static PA hydrogels based on 2-way ANOVA analysis of their z-ratios and a z-ratio greater than 1 or less than -1, i.e. proteins with significant expression or phosphorylation changes (Table 1). Using centroid linkage clustering, data was grouped based on z-ratio as shown in the heat map in Fig. 3 where time increases to the right and dynamic HA and static 11 kPa PA data are on the left and right portions of the heat map, respectively. To better annotate how cardiac-

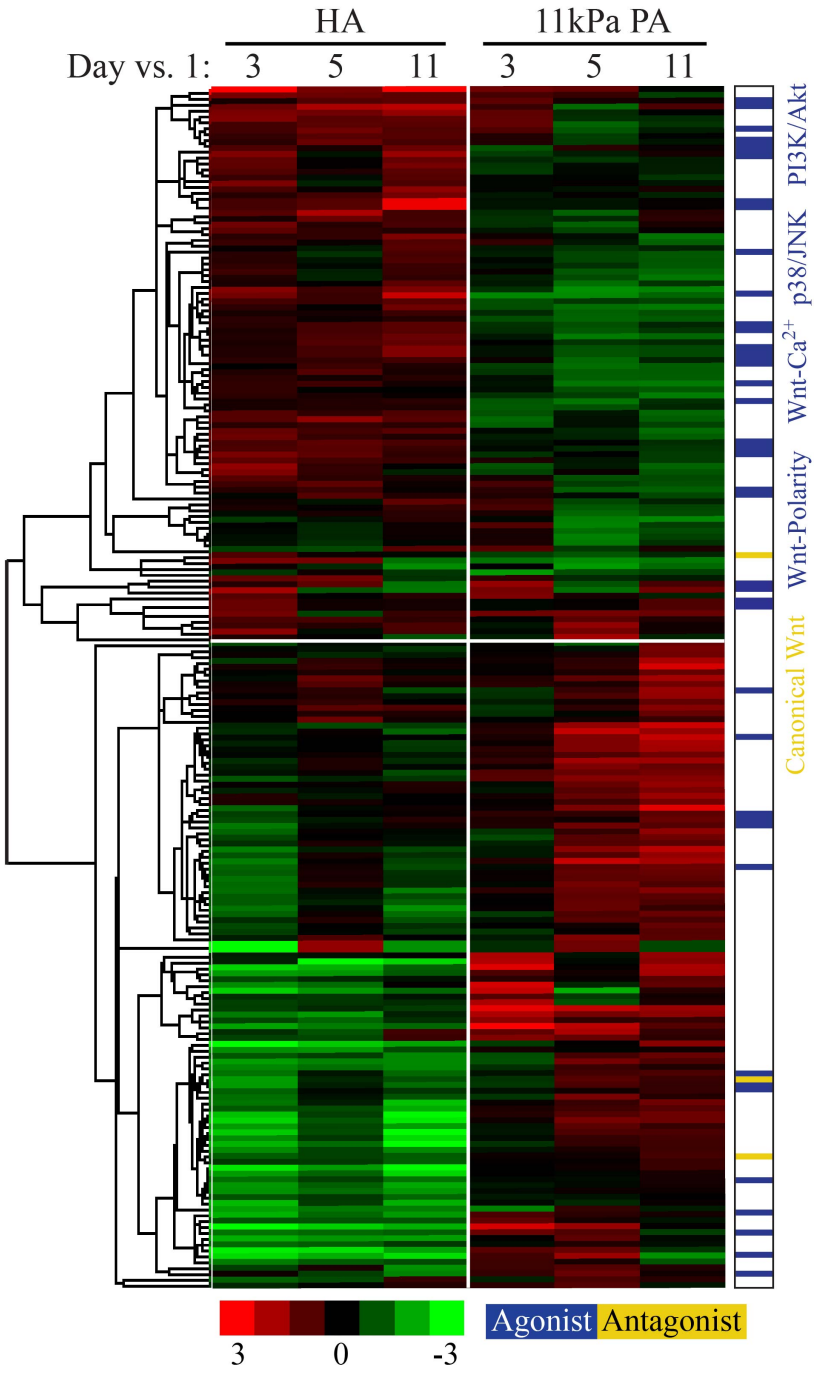

Figure 3: *Clustering of Microarray Data Reveals Differentially Expressed Protein Kinases on HA versus PA Hydrogels.* Z-ratio values of significant data (interaction $p < 0.05$) of dynamic HA and static 11 kPa PA hydrogels over 3, 5 and 11 days vs. 1 day of culture were clustered (-3 is green, 0 is black, +3 is red). Agonists of cardiac development (*Wnt*-Polarity, *Wnt*-Ca^{2+}, p38/JNK, PI3K/Akt) are highlighted in blue while antagonists (*Wnt*-Canonical) are highlighted in yellow.

specific pathways clustered within the map, cardiac development agonists (blue; PI3K/Akt, *Wnt*-Ca^{2+}, *Wnt*-Polarity and p38/JNK pathways) and antagonists (yellow; canonical *Wnt* signaling (30, 31)) are labeled in the right hand column (Fig. 3). Cardiac agonists (25 out of 94 proteins-27%) were differentially up-regulated on dynamic HA matrices over time, while only 14 out of 110 (13%) were up-regulated on static PA matrices. Additionally, cardiac antagonists were up-regulated on PA vs. HA hydrogels.

While pathway annotation indicated general differences between static and dynamic hydrogel systems, GO-ELITE (gene ontology) clustering (42, 44) identified significant changes in expression within a given pathway utilizing all statistically significant interaction p values ($p < 0.05$). Among all GO-ELITE pathways, focal adhesion signaling, which encompasses a variety of pathways including those identified as cardiac-specific, e.g. PI3K/Akt, *Wnt* signaling and p38 MAPK/JNK (30, 31), contained the greatest percentage of significantly differentially expressed or phosphorylated proteins (Fig. 4). In particular, these data verify significant up-regulation of agonist Akt and p38 MAPK signaling in dynamic HA and down-regulation in static PA hydrogels. Gene ontology clustering also indicated up-regulation of cardiac developmental antagonist GSK3β (30, 31) in static PA but not dynamic HA hydrogels. Together these data implicate that agonists are more highly expressed in cardiomyocytes plated on a dynamic matrix, while antagonists are expressed on a static matrix. Western blotting confirmed expression of proteins within these specific pathways (Fig. 5A, D); for example enhanced expression of Akt 1 (dark grey) and Akt 2 (light grey) on dynamic HA vs. static PA was observed in both methods (Fig. 5B, C). Other proteins not involved in the specific signaling pathways identified, e.g. paxillin (black; Fig. 5B, C) had a protein

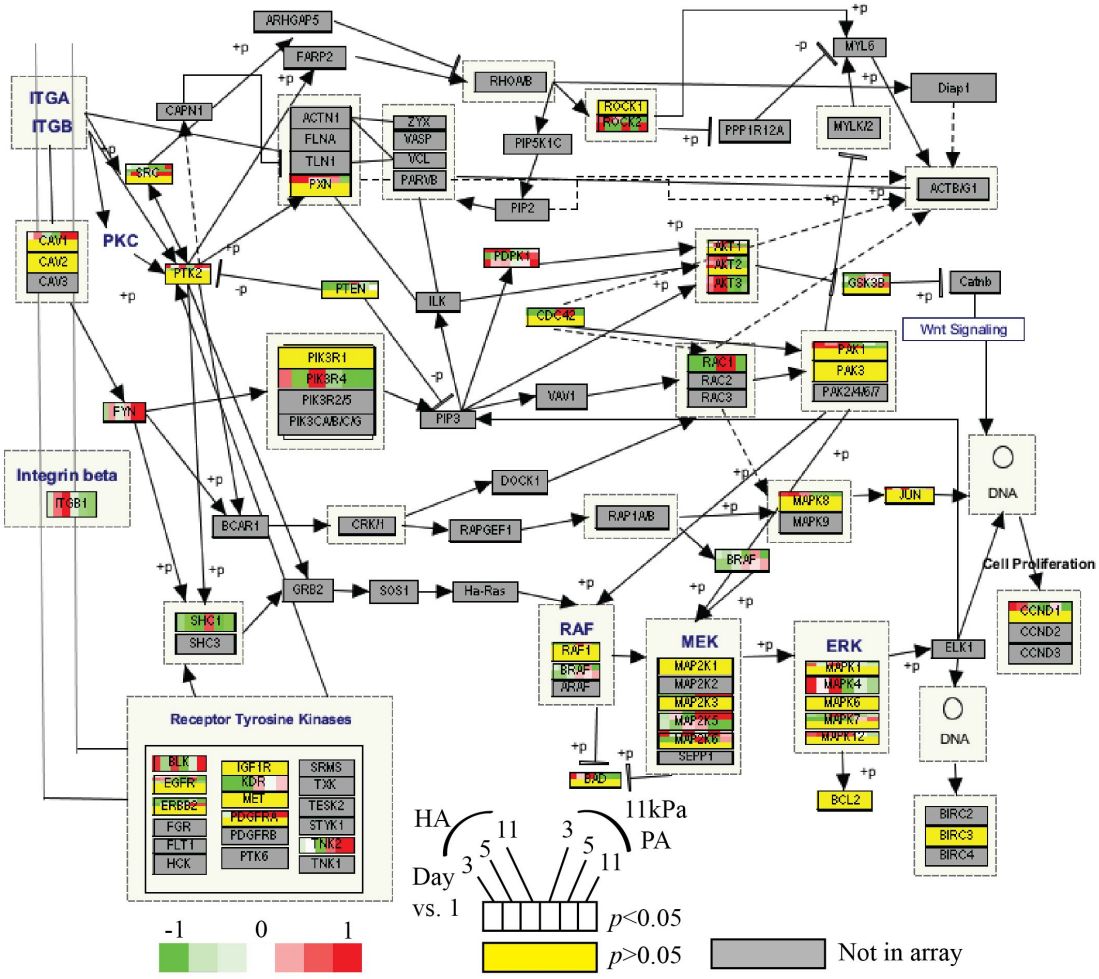

Figure 4: *Focal Adhesion Signaling Depends on the Stiffness of the Substrate.* GO-ELITE analysis of microarray data determined focal adhesion signaling from WikiPathways to be significantly changed. For interaction $p < 0.05$, protein boxes were divided into 6 smaller boxes indicating z-ratios of day, 3, 5 and 11 vs. day 1 (left to right) for HA (left three boxes) and 11 kPa PA (right three boxes) (see schematic). For interaction $p > 0.05$, the protein boxes were shaded yellow. For proteins not included in the array, the protein boxes are shaded grey. Color map is -1: green, 0: white, +1: red.

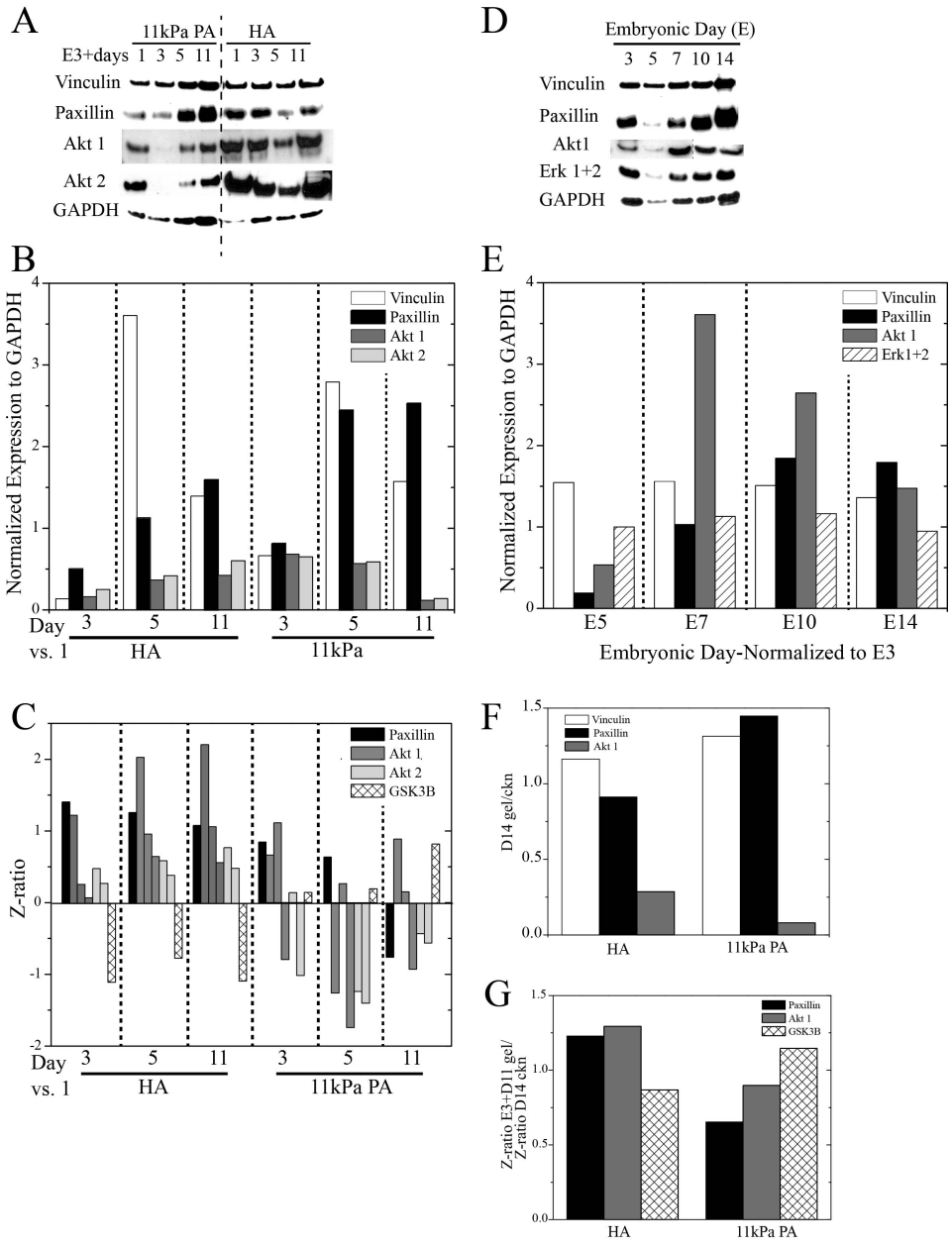

Figure 5: *Western Blot Validation of Microarray Data*. (A) Representative western blots for Vinculin (white), Paxillin (black), Akt 1 (dark grey), Akt 2 (light grey) and GAPDH for HA and 11 kPA PA hydrogels over the time course (1, 3, 5, 11 days after plating). Multiple bars for one protein signifies the use of more than one antibody. (B) Western blot data quantified. (C) Corresponding microarray data for (B), excluding vinculin (not on array) and including GSK3β (not in WB, crosshatch). (D) Representative western blots for Vinculin, Paxillin, Akt 1, Erk 1+2 (stripes) and GAPDH for chicken lysates. (E) Western blot data quantified (n=3). (F) Quantified western blot data for D11 HA and PA vs. D14 chicken lysate for Vinculin, Paxillin and Akt 1, and (G) corresponding micorrary data for Paxillin, Akt 1 and GSK3β.

expression profile that was less correlated to microarray data, i.e. enhanced expression on static PA vs. dynamic HA hydrogel, though this might be expected as cells plated on stiffer substrates have greater focal adhesions (47) [Fig. 5B, C; vinculin (white) expression correlated with paxillin (black), as expected for focal adhesion proteins]. Regardless, western blots corroborated critical signaling cascades from microarrays, e.g. Akt which inhibits GSK3β (crosshatch) expression (30).

While dynamic vs. static hydrogel comparisons are useful, comparisons with parallel maturation *in vivo* provide a more complete maturation assessment. Western blotting of embryonic myocardium lysates of 72, 120, 144, 240 and 288 HFP, corresponding to the hydrogel time course, for vinculin (white), paxillin (black), Akt 1 (dark grey), and Erk 1+2 (stripes) (Fig. 5D) indicated that paxillin (black) and Akt 1 (dark grey) change throughout development, while vinculin (white) and Erk 1+2 (stripes) remain relatively constant (Fig. 5E). Examining *in vivo* expression 288 HPF and age-matched cardiomyocytes cultured on the hydrogels showed cells that matured on dynamic HA gels were most similar to cells that matured in the animal as indicated by western blotting (Fig. 5F) and microarray (Fig. 5G).

3.4 Conclusions

In vitro studies presented here demonstrate the importance of dynamic material cues in guiding cell maturation via activation of mechanosensitive signaling pathways. Moreover, this study illustrated that many cardiogenic pathways are sensitive to mechanics, including PI3K/Akt and *Wnt*, both canonical and non-canonical. In

particular, GSK3β, a cardiomyocyte maturation inhibitor, was upregulated on static PA hydrogels but suppressed for cells on dynamic HA hydrogels; thus this molecule could be a target to better explore the link between mechanics and protein kinase signaling. While limited to cardiomyogenesis, identifying mechanosensitive pathways involved in developmental processes can lead to a better understanding of how differentiation and development are mediated by extracellular matrix properties.

3.5 Acknowledgements

Chapter 3, in part, is currently being prepared for submission for publication of the material. The dissertation author is the primary investigator and author, and thanks co-authors Kyle Kretchmer and Dr. Adam J. Engler for their contributions to the work. The authors would also like to thank Dr. Alexander Zambon for his expertise with using GO-ELITE to analyze microarray data. This work was supported by grants from the American Heart Association (0865150F to A.J.E), National Institutes of Health (R21HL106529 to A.J.E.), American Heart Association Pre-Doctoral Fellowship (10PRE4160143 to J.L.Y), Achievement Rewards for College Scientists Fellowship (ARCS; to J.L.Y.) and California Institute for Regenerative Medicine (CIRM) Bridges Program (TB1-01186 to K.K).

3.6 Appendix

Table 1*: Protein Kinases Microarray Indicate Cardiac Agonist and Antagonists.* The data in the table corresponds to the cluster image shown in Fig. 3. The boundaries denoted by the thick black lines correspond to the white lines in Fig. 3. Agonists are highlighted in blue and antagonists in yellow.

	Z-ratio					
	HA			11 kPa PA		
Name	D3	D5	D11	D3	D5	D11
RIPK1	3.118561	1.41393	3.460529	1.302378	1.178256	-0.056596
Paxillin 1	1.41654	1.268163	1.087366	0.842122	0.635712	-0.754733
PKBa (Akt1)	0.264489	0.965528	1.06965	1.111093	0.264182	0.1588
PKBa (Akt1)	1.229188	2.038357	2.217376	0.661501	-1.260495	0.894316
Acetylated Lysine	1.44282	1.304733	1.770655	1.116746	-0.506789	-0.031211
Hsp70	1.541007	1.037319	1.107019	1.150081	-0.562886	-0.493094
PAK1/2/3	0.776104	1.06329	1.04998	1.172034	-1.184353	-0.623856
CaMK4	0.779123	1.324707	0.95634	0.931652	-1.019233	-0.319275
CASP5	0.598107	1.028487	0.994088	0.390919	-0.728146	-0.041321
CaMK4	0.495511	1.22562	0.834609	0.411212	-0.706381	-0.243526
CaMKK(2)	0.943849	0.248911	1.263717	-0.984113	0.527364	0.127558
CAMK2d	1.523365	-0.229242	1.811499	-0.72495	-0.347124	0.260349
BRD2	1.136803	0.054021	1.203891	-0.452536	-0.653066	-0.326928
Erk4	1.107361	0.055422	1.394372	-0.630889	-0.118246	-0.334087
PAK1/2/3	0.948263	0.369127	1.066551	-0.690516	-0.095569	-0.345316
Plk3	0.672003	-0.134462	1.005197	-0.083173	-0.03673	-0.608942
FKHRL1	1.455873	-0.416982	0.932408	-0.063484	0.080064	-0.251109
Jun	0.842453	0.095988	1.675553	-0.063109	-0.22174	0.298127
DRAK2	0.459267	0.794971	1.376504	-0.274393	0.076223	-0.41308
PDK1	0.803476	1.024977	2.820525	-0.219629	-0.229376	0.072734
PDK1	0.803476	1.024977	2.820525	-0.219629	-0.229376	0.072734
CASK/Lin2	1.022953	2.045698	0.802445	-0.505226	-1.15088	0.438138
CASP4	0.295283	1.221252	0.786617	-0.601213	-0.465674	0.522222
TTK	1.321602	0.471881	0.869861	-0.57012	-1.146624	0.306811
Hsp90a/b	1.085824	0.564965	0.41566	-0.255948	-0.798461	0.078978
MAPKAPK2a+b	0.48936	0.587282	1.482418	0.193866	-0.157672	-1.362849
MLC(MLRC2)	0.665943	0.120591	0.966125	0.626417	-0.280281	-1.162283
DNAPK	0.104506	-0.319912	1.019119	-0.272631	-0.630259	-0.405866
PI3KR4	0.48408	-0.59191	0.84015	-0.354578	-0.830465	-1.030824
LOK	0.457298	-0.241554	0.909654	-0.0935	-0.809914	-1.021077
PSD-95	0.578636	-0.102043	0.673613	-0.234534	-0.58851	-1.04871
Src	0.725509	-0.368572	0.678135	0.117391	-1.029744	-1.218583
RSK2	0.362122	-0.423058	0.574849	-0.365098	-0.894501	-1.420319
Aurora A (AIK)	0.303025	0.054139	1.08098	-0.294044	-1.32332	-0.609501
Hsp90a/b	1.565056	0.720446	1.484229	-0.579676	-1.711245	-1.567809
CAMK2g	1.364879	0.650535	2.377233	-1.607255	-1.652867	-1.193594
Axl	0.810166	0.65317	1.048305	-0.954094	-0.670458	-0.814457
LATS1	0.537874	0.068121	1.316567	-0.925545	-1.317764	-1.450028
STK33	0.295381	0.277942	0.707861	-0.505754	-1.148913	-0.95651
CDK10	0.516296	0.140963	0.40281	-0.91955	-1.204346	-1.085317

Table 1*: Protein Kinases Microarray Indicate Cardiac Agonist and Antagonists, Continued.* The data in the table corresponds to the cluster image shown in Fig. 3. The boundaries denoted by the thick black lines correspond to the white lines in Fig. 3. Agonists are highlighted in blue and antagonists in yellow.

	Z-ratio					
	HA			11kPa PA		
Name	D3	D5	D11	D3	D5	D11
PKBg (Akt3)	0.452398	0.811281	1.052166	-0.596686	-0.954137	-0.432973
PKBg (Akt3)	0.313189	0.815993	1.018104	-0.526271	-1.053984	-0.648539
PKA R2a	0.372615	0.891271	1.262279	-0.284347	-1.469272	-1.207878
TAK1	0.318886	0.964627	1.149757	-0.023813	-0.648555	-0.518719
PKCb2	0.37785	0.805038	1.53164	-0.210172	-0.973237	-0.87325
PKCb2	0.37785	0.805038	1.53164	-0.210172	-0.973237	-0.87325
PKBb (Akt2)	0.485591	0.593907	0.779685	0.137288	-1.237538	-0.425113
PKCa	0.032825	0.7158	0.36242	-0.741567	-1.308193	-1.092303
Striatin	0.399507	0.992305	0.291171	-0.636113	-1.12192	-1.080082
SLK	0.516777	0.238874	0.459154	-0.168609	-1.14005	-1.108244
p38a MAPK	0.575381	0.733064	0.238724	-0.237214	-1.398244	-1.46398
Smac/DIABLO	0.587405	-0.038214	0.010419	-0.157447	-0.944491	-1.053084
PACSIN1	0.514819	0.300631	0.106391	-0.601623	-0.727706	-1.495214
PKBb (Akt2)	0.276853	0.391034	0.491596	-1.018768	-1.401298	-0.554514
CDC2L5 (CHED)	0.281433	0.403158	0.368731	-1.085769	-0.963701	-0.439058
PARP1	0.990711	0.570212	0.938939	-0.978055	-0.268624	-1.21526
p53	1.006419	1.736152	1.023852	-1.248786	-0.200012	-1.100283
DAPK1	0.491915	0.665172	0.506557	-1.140837	-0.202872	-0.791534
Hsp70	1.185353	0.794187	1.056422	-0.111991	-0.442507	-1.282293
Tau	1.297463	0.657086	0.3599	-0.331313	-0.419152	-1.114111
p38a MAPK	0.857238	1.100944	0.877293	-0.221055	-0.027737	-0.553582
p38a MAPK	0.919623	1.0269	0.672235	-0.114266	-0.451576	-0.613434
p38a MAPK	1.446649	1.104376	0.557517	-0.594791	0.011412	-0.718936
Histone H3	1.117656	0.788326	0.682093	0.370793	-0.249005	-0.709561
DNAPK	1.728067	0.597896	0.024918	-0.976747	-0.300776	-1.194556
Cyclin D1	1.512635	0.608261	-0.408179	-0.798171	0.119052	-1.00741
Tau	1.016748	0.511381	0.29606	0.279633	-0.965381	-0.871309
STAT5A	0.744842	1.117934	0.160584	0.836651	-0.731099	-0.953199
p38a MAPK	0.448033	0.689392	0.101709	0.489351	-1.113249	-1.142935
p38a MAPK	-0.080375	1.008698	0.409135	0.387138	-0.123883	-0.847004
NFkappaB p65	0.207677	-0.243458	1.13438	0.706522	-0.840447	-0.414968
Tau	0.320528	0.054567	0.62102	0.843564	-1.034836	-0.819794
S6Kb1	-0.138331	0.297189	0.472441	0.3297	-1.232425	-0.882128
Crystallin aB	-0.677603	-0.186794	0.47217	-0.089992	-1.506035	-1.612321
MEKK4 (MAP3K4)	-0.034323	-0.446795	0.144932	0.971659	-1.564642	-0.732007
MEK5 (MAP2K5)	-0.171479	-0.428684	0.140558	0.258188	-1.524946	-0.785424
MEKK1 (MAP3K1)	-0.196334	-0.557563	-0.080015	0.330578	-1.457612	-0.572964
B23 (NPM)	-0.745112	-0.862645	1.004867	1.024493	-0.671971	0.364066
CK1g2	0.93041	0.155272	-0.116395	-0.760403	-1.019973	-0.459042
HspBP1	1.444564	1.41566	-1.327759	-1.361431	-1.661153	-1.431718
p73	0.17493	-0.482951	-1.669515	0.021272	-1.838897	-1.257993
DFF45 + DFF35	-0.632077	0.190245	-0.659683	-1.860874	-0.921992	-0.788212
Tau	1.159635	1.36147	-0.588396	0.567417	-0.486393	-0.324366

Table 1*: Protein Kinases Microarray Indicate Cardiac Agonist and Antagonists, Continued.* The data in the table corresponds to the cluster image shown in Fig. 3. The boundaries denoted by the thick black lines correspond to the white lines in Fig. 3. Agonists are highlighted in blue and antagonists in yellow.

	Z-ratio					
	HA			11kPa PA		
Name	D3	D5	D11	D3	D5	D11
p38a MAPK	0.433488	1.117919	-1.347307	1.760173	-0.982249	0.833823
ROKa (ROCK2)	1.972204	-0.989057	-1.407477	1.413432	-1.307096	1.301044
4E-BP1	1.025276	0.004168	0.471921	1.499449	0.272316	-0.396939
PDK1	1.218788	0.187133	0.238844	-0.081323	0.074075	0.936769
PDK1	1.218788	0.187133	0.238844	-0.081323	0.074075	0.936769
Erk5	1.367647	-0.781281	0.63823	1.316673	1.402561	1.261759
Ksr1	0.842898	0.840624	0.550829	-0.037351	1.044453	0.390595
Lck	0.757186	0.444438	0.876175	-0.247151	1.716076	0.192929
MEK6 (MAP2K6)	1.614992	-0.151231	0.849289	-0.100568	1.364647	0.21265
PKR1	0.364637	0.033185	-0.979673	-0.369043	1.992409	-0.42783
MKP1	-0.836143	-0.133765	-0.146683	0.035132	-1.06497	1.232768
ZAP70	-0.061521	-0.203611	-0.609243	0.042182	-0.18419	1.393055
APG2	0.150294	-0.472691	-0.299352	0.116513	0.237445	1.321845
Bid	-0.671042	0.532931	0.12821	0.192042	0.510321	1.993602
Cdc25C	0.258885	0.646374	0.22615	0.101978	0.556267	2.556052
Hsc70	-0.057588	0.368266	-0.082892	0.080845	0.336476	1.214685
PITSLRE	-0.146578	1.225894	0.417843	0.378211	1.087375	1.93692
Hsp60	0.210503	0.976806	0.224738	0.485401	0.330767	1.349873
PKCl/i	0.260779	0.502538	-0.88319	-0.608357	0.650599	1.787113
Caveolin 1	0.061818	0.449019	-0.226282	-0.559367	0.901969	1.739942
CASP7	0.444569	0.5958	0.008601	-0.352635	0.21982	1.172298
IRAK1	0.073512	1.081855	0.885188	-0.622458	0.52171	1.573068
CASP9	-0.009595	0.408844	0.365617	-0.561613	-0.070947	1.21751
CDK1 (CDC2)	0.043758	1.29544	0.234885	-0.034385	0.260234	0.672023
CDK6	-0.434431	-0.863763	-0.718763	0.352504	1.744787	2.415047
Lck	-0.524246	0.116391	-1.183648	0.45455	2.305449	1.799592
CAMK1a	-0.151746	0.037172	-0.043639	0.310736	1.487269	2.336935
AIF	-0.387123	-0.011213	-0.685952	0.164083	1.489236	1.98385
ACK1	-0.125669	0.018257	-0.623166	0.486812	1.519447	1.914611
Mnk2	-0.078268	0.156158	-0.300941	0.392307	0.953456	1.30486
MAPKAPK2	-0.519881	0.341587	-0.530013	0.591909	1.900478	1.880025
Fyn	-0.326917	0.333247	-0.10909	0.227629	1.481577	1.191292
MEK5 (MAP2K5)	-0.207637	0.127849	-0.905763	0.97597	1.220942	1.371272
CASP1	-1.006798	-0.390332	-0.625822	1.006348	1.560494	1.588134
CDK1 (CDC2)	0.059832	0.08199	0.396044	-0.144604	1.225236	1.751633
YSK1	-0.40377	-0.138005	0.337413	-0.255201	1.02004	1.462446
MEK3 (MAP2K3)	0.420992	-0.298495	-0.006241	0.243264	1.201852	1.845549
Nlk	0.375408	0.245514	-0.008121	0.066984	0.741243	1.336288
CDK1 (CDC2)	-1.216324	-0.097755	0.176882	0.146405	1.447098	2.697508
CaMK1d	-0.74525	-0.024432	0.106416	0.501158	0.583972	1.089181
PKCd	-0.876049	-0.311605	0.422427	0.346629	0.219945	1.210451
JNK1/2/3	-1.452539	-0.141892	0.215458	0.35837	1.29291	1.006271

Table 1*: Protein Kinases Microarray Indicate Cardiac Agonist and Antagonists, Continued.* The data in the table corresponds to the cluster image shown in Fig. 3. The boundaries denoted by the thick black lines correspond to the white lines in Fig. 3. Agonists are highlighted in blue and antagonists in yellow.

	Z-ratio					
	HA			11kPA PA		
Name	D3	D5	D11	D3	D5	D11
KHS	-1.194769	0.072718	-0.0909	-0.602463	0.602155	1.69426
CDK5	-0.81786	-4.92E-04	-0.148184	-0.877076	1.007051	1.318459
PAK2	-0.552638	0.353208	-0.221834	-0.404794	0.972517	1.082372
Cyclin B1	-1.487178	-0.360937	-0.85401	-0.280898	1.645455	2.230759
Ksr1	-0.98207	0.265598	-0.546646	-0.289714	1.000431	1.750282
CDK2	-1.499435	0.079835	-0.774513	0.44826	2.357549	1.964587
PKC h	-1.186869	0.232441	-0.906284	-0.119242	1.020722	1.278831
Plk2	-1.089996	0.318755	-0.57791	0.113046	1.143469	1.212019
DDIT3(CHOP)	-1.356082	0.25179	-0.52449	0.10793	1.085071	1.116675
BMX (Etk)	-1.245008	0.448983	-0.514794	-0.104603	1.370643	0.908806
MEK7 (MAP2K7)	-1.302749	-0.125739	-1.479917	0.507675	1.199299	1.550629
PAC1	-1.075421	-0.218818	-0.851956	0.076474	1.121872	1.046202
GCK	-1.082652	-0.406333	-1.134822	-0.017798	1.201981	0.911047
ErbB2 (HER2)	-1.391078	-0.106752	-1.732703	0.076242	1.227747	0.648536
Tyk2	-1.153299	0.159261	-1.284704	-0.680616	0.897699	1.250663
CDK1 (CDC2)	-0.520045	0.404827	-0.968281	-0.196117	1.012198	0.857373
Chk1	-0.861002	0.023662	-0.551867	0.0076	0.201694	1.198285
TBK1	-0.747377	-0.050391	-0.765219	-0.622961	0.068058	1.006084
Src	-0.350373	0.896066	-0.017745	-0.284935	1.49196	1.052773
CDK2	-4.233369	1.74415	-1.701654	-0.519198	1.307565	-0.838613
CDK2	-4.233369	1.74415	-1.701654	-0.519198	1.307565	-0.838613
ATF2	-0.364917	-0.18171	0.033055	2.040451	-0.217375	1.721937
Arrestin b1	-0.378173	-2.953097	-2.546699	2.098366	-0.117612	1.608445
MST1	-2.527446	-2.072399	-1.14156	2.662114	0.063739	2.006949
Aurora A (AIK)	-1.854017	-1.7871	-1.055906	0.874698	0.203757	1.981832
MST1	-0.838552	-0.484228	-0.207971	0.491802	0.098773	1.060639
Mnk1	-1.678045	-1.264944	0.054993	2.506058	-0.441717	1.1486
MKP2	-2.485517	-1.802326	-1.20783	2.305037	-2.088473	0.438617
MEK4 (MAP2K4)	-0.590291	-0.659351	-0.22697	1.016706	-0.698462	0.226291
MEK6 (MAP2K6)	-0.761505	-0.631656	-0.520762	2.03918	-0.966093	0.319338
MEK3b (MAP2K3)	-0.728759	-0.485143	-0.707002	2.757088	2.325353	1.804679
Pyk2	-1.45977	-1.813892	-0.387773	2.059047	1.397269	1.686875
NMDAR2B	-0.821751	-1.189606	-0.55451	1.630476	0.572204	0.648914
Pyk2	-1.951041	-1.474617	-1.238349	3.531604	2.230718	0.988416
ILK1	-0.543595	-0.989285	0.789326	1.169073	2.010636	0.619987
MST3	-0.810771	-0.856942	0.691949	1.536015	1.186381	0.526412
Smad2/3	-3.503268	-2.395816	-1.954583	-0.71122	0.036338	1.613225
VEGFR2 (KDR)	-1.679586	-1.751728	-0.87986	0.244951	-0.039532	0.179672
ZIPK	-1.022111	-0.740629	-1.61761	-0.918463	0.822728	1.216546
FasL	-1.867587	-1.541067	-1.609083	-0.951751	1.395385	0.917357
STAT6	-1.575446	-1.300546	-1.597811	-0.547319	0.682964	0.363246
PKCm (PKD)	-1.370068	-0.250952	-1.239103	-0.224799	0.806516	0.900827
CK1d	-1.857824	-0.459427	-0.942899	-0.593865	1.023619	0.658055

Table 1*: Protein Kinases Microarray Indicate Cardiac Agonist and Antagonists, Continued.* The data in the table corresponds to the cluster image shown in Fig. 3. The boundaries denoted by the thick black lines correspond to the white lines in Fig. 3. Agonists are highlighted in blue and antagonists in yellow.

	Z-ratio					
	HA			11kPa PA		
Name	D3	D5	D11	D3	D5	D11
PDK1	-1.832064	-0.346846	-1.264894	-0.657584	0.893746	0.611151
PKCb2	-1.154032	-0.115537	-0.622879	-0.197305	0.224934	0.623178
Mcl1	-1.319301	-0.218202	-0.971265	-0.61945	1.424814	0.425025
Abl	-1.399569	-0.321737	-2.307207	0.127413	0.670179	1.309879
NFkappaB p65	-1.057321	-0.885754	-2.051806	0.320045	0.761837	1.006974
STAT5B	-2.272437	-0.722978	-2.952246	0.421225	0.985004	1.278741
STAT3	-2.535036	-0.999121	-2.773464	0.175419	1.415979	1.269999
STAT5A	-1.83704	-0.832961	-1.868501	-0.235185	1.076075	0.634091
STAT2	-2.419463	-0.901293	-3.996701	-0.269609	0.902753	0.895227
STAT4	-1.653014	-0.653023	-2.589441	-0.137029	0.628782	0.794242
Fos	-2.132183	-1.270737	-3.076954	-0.569609	0.602799	0.753295
NFkappaB p50	-1.646434	-0.781109	-1.624122	-0.227187	0.317804	0.732452
GSK3a+b	-1.100833	-0.763927	-1.083164	0.140016	0.193573	0.82517
Nek2	-0.662121	-0.68675	-1.107335	0.051373	0.082896	0.672394
Trail	-2.74235	-1.86363	-3.648386	0.008781	0.172514	0.664456
PAK1	-1.871039	-1.185871	-2.549705	0.032676	-0.065148	0.296416
PKCb1	-1.303128	-0.730947	-1.3375	-0.09781	-0.134037	0.277638
Catenin b1	-1.793364	-1.119445	-2.007365	-0.268435	-0.111805	0.217634
STAT1a+b	-1.729214	-1.294235	-1.765104	-0.119931	0.141772	0.152858
PTEN	-0.987824	-0.644651	-1.215845	-0.285324	-0.232666	0.006768
IkBa	-2.230398	-0.713355	-2.113096	-0.103292	-0.473585	0.115489
PP2A/Ca+Cb	-1.892122	-1.419836	-1.482832	-1.508824	0.598088	-0.322736
PKCm (PKD)	-2.131156	-1.222308	-1.830782	0.887954	0.491858	0.251773
PTP1D	-0.975557	-0.971189	-0.988516	1.150545	0.246225	-0.240427
PTP1C	-3.009337	-2.472423	-2.104736	2.531459	1.814942	0.060138
Rac1	-1.37083	-1.245224	-1.129863	1.258873	0.941889	-0.744528
PTP1B	-2.080339	-1.793426	-1.887101	0.031305	1.107104	-0.101787
Tyrosine Hydroxylase	-1.256523	-1.111868	-0.687271	-0.132243	0.391533	-0.169687
Rb	-2.824816	-2.666907	-1.904764	1.054273	1.202195	-0.625483
Rac1	-2.590589	-2.059583	-2.651311	0.780016	1.835245	-1.720305
Raf1	-1.496093	-1.064544	-0.876762	0.717639	0.300768	-1.026208
IkBb	-0.72104	0.312734	-1.713653	0.716927	0.958355	0.410461
PKCq	0.173988	-0.74191	-1.57076	0.611903	1.208336	0.203944
Erk1 + Erk2	-1.166351	-0.878663	0.636741	-0.39176	0.854204	0.44973
Rb	-0.466729	-0.064906	0.422701	0.514812	1.0059	-0.262417

3.7 References

1. Tse JR, Engler AJ (2011) Stiffness Gradients Mimicking In Vivo Tissue Variation Regulate Mesenchymal Stem Cell Fate. *PLoS ONE* 6(1):e15978.

2. Rowlands AS, George PA, Cooper-White JJ (2008) Directing osteogenic and myogenic differentiation of MSCs: interplay of stiffness and adhesive ligand presentation. *Am J Physiol Cell Physiol* 295(4):C1037–44.

3. Engler AJ, Sen S, Sweeney HL, Discher DE (2006) Matrix Elasticity Directs Stem Cell Lineage Specification. *Cell* 126(4):677–689.

4. Saha K, Keung AJ, Irwin EF, Li Y, Little L, Schaffer DV, Healy KE (2008) Substrate Modulus Directs Neural Stem Cell Behavior. *Biophysj* 95(9):4426–4438.

5. Holle AW, Engler AJ (2011) More than a feeling: discovering, understanding, and influencing mechanosensing pathways. *Current Opinion in Biotechnology* 22(5):648–654.

6. Hay ED (1981) *Cell biology of extracellular matrix* (Plenum Press, New York).

7. Nelson CM, Bissell MJ (2006) Of extracellular matrix, scaffolds, and signaling: tissue architecture regulates development, homeostasis, and cancer. *Annu Rev Cell Dev Biol* 22:287–309.

8. Montell DJ (2008) Morphogenetic cell movements: diversity from modular mechanical properties. *Science* 322(5907):1502–1505.

9. Jacot JG, McCulloch AD, Omens JH (2008) Substrate stiffness affects the functional maturation of neonatal rat ventricular myocytes. *Biophys J* 95(7):3479–3487.

10. Engler AJ, Carag-Krieger C, Johnson CP, Raab M, Tang HY, Speicher DW, Sanger JW, Sanger JM, Discher DE (2008) Embryonic cardiomyocytes beat best on a matrix with heart-like elasticity: scar-like rigidity inhibits beating. *Journal of Cell Science* 121(22):3794–3802.

11. Peyton SR, Putnam AJ (2005) Extracellular matrix rigidity governs smooth muscle cell motility in a biphasic fashion. *J Cell Physiol* 204(1):198–209.

12. Zaari N, Rajagopalan P, Kim SK, Engler AJ, Wong JY (2004) Photopolymerization in Microfluidic Gradient Generators: Microscale Control of Substrate Compliance to Manipulate Cell Response. *Adv Mater* 16(23-24):2133–2137.

13. Huebsch N, Arany PR, Mao AS, Shvartsman D, Ali OA, Bencherif SA, Rivera-

Feliciano J, Mooney DJ (2010) Harnessing traction-mediated manipulation of the cell/matrix interface to control stem-cell fate. *Nature Materials* 9(6):518–526.

14. Shih Y-RV, Tseng K-F, Lai H-Y, Lin C-H, Lee OK (2011) Matrix stiffness regulation of integrin-mediated mechanotransduction during osteogenic differentiation of human mesenchymal stem cells. *J Bone Miner Res* 26(4):730–738.

15. Ghosh K, Pan Z, Guan E, Ge S, Liu Y, Nakamura T, Ren X-D, Rafailovich M, Clark RAF (2007) Cell adaptation to a physiologically relevant ECM mimic with different viscoelastic properties. *Biomaterials* 28(4):671–679.

16. Evans ND, Minelli C, Gentleman E, LaPointe V, Patankar SN, Kallivretaki M, Chen X, Roberts CJ, Stevens MM (2009) Substrate stiffness affects early differentiation events in embryonic stem cells. *Eur Cell Mater* 18:1–13–discussion 13–14.

17. Marklein RA, Burdick JA (2010) Spatially controlled hydrogel mechanics to modulate stem cell interactions. *Soft Matter* 6(1):136–143.

18. Young JL, Engler AJ (2011) Hydrogels with time-dependent material properties enhance cardiomyocyte differentiation in vitro. *Biomaterials* 32(4):1002–1009.

19. Lutolf MP, Hubbell JA (2005) Synthetic biomaterials as instructive extracellular microenvironments for morphogenesis in tissue engineering. *Nat Biotechnol* 23(1):47–55.

20. Guo W-H, Frey MT, Burnham NA, Wang Y-L (2006) Substrate Rigidity Regulates the Formation and Maintenance of Tissues. *Biophysical Journal* 90(6):2213–2220.

21. Deroanne CF, Lapiere CM, Nusgens BV (2001) In vitro tubulogenesis of endothelial cells by relaxation of the coupling extracellular matrix-cytoskeleton. *Cardio Res* 49:647–658.

22. Jacot JG, Martin JC, Hunt DL (2010) Mechanobiology of cardiomyocyte development. *Journal of Biomechanics* 43(1):93–98.

23. Discher DE, Mooney DJ, Zandstra PW (2009) Growth factors, matrices, and forces combine and control stem cells. *Science* 324(5935):1673–1677.

24. Berry MF, Engler AJ, Woo YJ, Pirolli TJ, Bish LT, Jayasankar V, Morine KJ, Gardner TJ, Discher DE, and Sweeney HL (2006) Mesenchymal stem cell injection after myocardial infarction improves myocardial compliance. *Am J Physiol Heart Circ Physiol* 290(6):H2196–203.

25. Krieg M, Arboleda-Estudillo Y, Puech PH, Käfer J, Graner F, Müller DJ,

Heisenberg CP (2008) Tensile forces govern germ-layer organization in zebrafish. *Nature* 10(4):429–436.

26. Hibbs RG (1956) Electron microscopy of developing cardiac muscle in chick embryos. *Am J Anat* 99(1):17–51.

27. Zamir EA, Taber LA (2004) Material Properties and Residual Stress in the Stage 12 Chick Heart During Cardiac Looping. *J Biomech Eng* 126(6):823–830.

28. Zamir EA, Srinivasan V, Perucchio R, Taber LA (2003) Mechanical asymmetry in the embryonic chick heart during looping. *Ann Biomed Eng* 31(11):1327–1336.

29. Zamir EA, Taber LA (2004) On the Effects of Residual Stress in Microindentation Tests of Soft Tissue Structures. *J Biomech Eng* 126(2):276–283.

30. Wagner M, Siddiqui MAQ (2007) Signal Transduction in Early Heart Development (I): Cardiogenic Induction and Heart Tube Formation. *Experimental Biology and Medicine* 232(7):852–865.

31. Wagner M, Siddiqui MAQ (2007) Signal Transduction in Early Heart Development (II): Ventricular Chamber Specification, Trabeculation, and Heart Valve Formation. *Experimental Biology and Medicine* 232(7):866–880.

32. Rose BA, Force T, Wang Y (2010) Mitogen-Activated Protein Kinase Signaling in the Heart: Angels Versus Demons in a Heart-Breaking Tale. *Physiological Reviews* 90(4):1507–1546.

33. Bottcher RT (2005) Fibroblast Growth Factor Signaling during Early Vertebrate Development. *Endocrine Reviews* 26(1):63–77.

34. Dailey L, Ambrosetti D, Mansukhani A, Basilico C (2005) Mechanisms underlying differential responses to FGF signaling. *Cytokine & Growth Factor Reviews* 16(2):233–247.

35. Sheldahl LC, Slusarski DC, Pandur P, Miller JR, Kühl M, Moon RT (2003) Dishevelled activates Ca2+ flux, PKC, and CamKII in vertebrate embryos. *The Journal of Cell Biology* 161(4):769–777.

36. Pandur P, Lasche M, Eisenberg LM, Kuhl M (2002) Wnt-11 activation of a non-canonical Wnt signalling pathway is required for cardiogenesis. *Nature* 418(6898):636–641.

37. Schneider VA, Mercola M (2001) Wnt antagonism initiates cardiogenesis in Xenopus laevis. *Genes & Development* 15(3):304–315.

38. Naito AT, Akazawa H, Takano H, Minamino T, Nagai T, Aburatani H, Komuro I (2005) Phosphatidylinositol 3-Kinase–Akt Pathway Plays a Critical Role in Early

Cardiomyogenesis by Regulating Canonical Wnt Signaling. *Circulation Research* 97(2):144–151.

39. Tse JR, Engler AJ (2010) Preparation of hydrogel substrates with tunable mechanical properties. *Curr Protoc Cell Biol* Chapter 10:Unit 10.16.

40. Hamburger V, Hamilton HL (1992) A series of normal stages in the development of the chick embryo. *Dev Dyn* 195(4):231–272.

41. Cheadle C, Vawter MP, Freed WJ, Becker KG (2010) Analysis of Microarray Data Using Z Score Transformation. *The Journal of Molecular Diagnostics* 5(2):73–81.

42. Zambon AC, Gaj S, Ho I, Hanspers K, Vranizan K, Evelo CT, Conklin BR, Pico AR, Salomonis N (2012) GO-Elite: a flexible solution for pathway and ontology over-representation. *Bioinformatics* 28(16):2209–2210.

43. Botstein D, Cherry JM, Ashburner M, Ball CA, Blake JA, Butler H, Davis AP, Dolinski K, Dwight SS, Eppig JT, Harris MA, Hill DP, Issel-Tarver L, Kasarskis A, Lewis S, Matese JC, Richardson JE, Ringwald M, Rubin GM, Sherlock G (2000) Gene Ontology: tool for the unification of biology. *Nat Genet* 25(1):25–29.

44. Pico AR, Kelder T, van Iersel MP, Hanspers K, Conklin BR, Evelo C (2008) WikiPathways: Pathway Editing for the People. *PLoS Biol* 6(7):e184.

45. Allen DG, Kentish JC (1985) The cellular basis of the length-tension relation in cardiac muscle. *J Mol Cell Cardiol* 17(9):821–840.

46. Gomez J-P, Potreau D, Raymond G (1994) Intracellular calcium transients from newborn rat cardiomyocytes in primary culture. *Cell Calcium* 15(4):265–275.

47. Fujio Y, Nguyen T, Wencker D, Kitsis RN, Walsh K (2000) Akt Promotes Survival of Cardiomyocytes In Vitro and Protects Against Ischemia-Reperfusion Injury in Mouse Heart. *Circulation* 101(6):660–667.

Chapter 4

In Vivo Response to Dynamic Hyaluronic Acid Hydrogels

Abstract

Tissue-specific elasticity arises in part from developmental changes in extracellular matrix over time, e.g. ~10-fold myocardial stiffening in the chicken embryo. When this time-dependent stiffening has been mimicked *in vitro* with thiolated hyaluronic acid (HA-SH) hydrogels, improved cardiomyocyte maturation has been observed. However, host interactions, matrix polymerization, and the stiffening kinetics remain uncertain *in vivo*, and each plays a critical role in therapeutic applications using HA-SH. Hematological and histological analysis of subcutaneously injected HA-SH hydrogels showed minimal systemic immune response and host cell infiltration. Most importantly, subcutaneously injected HA-SH hydrogels exhibited time-dependent porosity and stiffness changes at a rate similar to hydrogels polymerized *in vitro*. When

injected intramyocardially host cells begin to actively degrade HA-SH hydrogels within 1 week post-injection, continuing this process while producing matrix to nearly replace the hydrogel within 1 month post-injection. While non-thiolated HA did not degrade after injection into the myocardium, it also did not elicit an immune response, unlike HA-SH, where visible granulomas and macrophage infiltration were present 1 month post-injection, likely due to reactive thiol groups. Altogether these data suggest that the HA-SH hydrogel responds appropriately in a less vascularized niche and stiffens as had been demonstrated *in vitro*, but in more vascularized tissues, *in vivo* applicability appears limited.

4.1 Introduction

Matrix elasticity is an important cue regulating a variety of cellular responses, including 'durotaxis' (1-3), adhesion (4-6), proliferation (7-9), and differentiation (1, 4, 10, 11). Stem or progenitor cellular responses can be further improved when extracellular matrix (ECM) cues are presented in a developmentally appropriate context, i.e. matrices with appropriate temporal (12-14) or spatial changes in stiffness (1, 9, 13, 15) to encourage cell alignment, cell fusion (15), or striation assembly (16). On the other hand, matrices that are stiffer than normal to mimic *in vivo* tissue fibrosis (17-19) result in aberrant cell behavior *in vitro* (20, 21). In the case of myocardial infarction (MI), stem cell-based interventions post-MI, i.e. cellular cardiomyoplasty, are intended to attenuate negative remodelling, but have demonstrated mixed results (22-24), potentially due to consequences of stiffening (18) inducing transdifferentiation (25).

To protect cells from these adverse conditions, a variety of cell-adhesive scaffolds have been employed, including fibrin (26, 27), collagen (28), matrigel (29-31), alginate (32, 33), and de-cellularized matrix (34, 35). Each scaffold has been tailored to display unique properties suitable for its application, e.g. injectability, stiffness, cellularity, etc. For example, stiffness increases ~10-fold during development, and mimicking this change *in vitro* using a thiolated hyaluronic acid (HA-SH)/poly(ethylene glycol) diacrylate (PEGDA) hydrogel improved cardiomyocyte maturation by more than 60% (12). Though HA is a glycosaminoglycan that can be modified with chemistries to present specific spatial and temporal properties (9, 12, 14, 36, 37), it is not clear whether thiolated HA remains as non-immunogenic as unmodified HA *in vivo* (38). Recently free thiols have been implicated in hematopoietic stem cell differentiation and subsequent lymphocyte activation (39), which may negatively impact the *in vivo* performance of HA-SH hydrogels. Moreover, it is not certain if the HA-SH hydrogel will have similar crosslinking dynamics as was reported *in vitro* (12). To answer these questions and determine its utility as a cardiac tissue engineering scaffold, we sought to determine the biocompatibility and temporal stiffening of the HA-SH/PEGDA material *in vivo* using subcutaneous and intramyocardial injections. Although the material stiffens with the same kinetics and does not elicit an immune response in a subcutaneous niche, we found an unforeseen inflammatory reaction after injecting into the healthy heart, likely resulting from adverse host interaction with free thiols on HA. While use in the failing heart post-MI would have been ideal, biocompability issues in healthy myocardium may limit its further *in vivo* use; nonetheless, the dynamics of this hydrogel system makes it a useful *in vitro* tool to study dynamic effects on cellular behavior in a wide variety of applications.

4.2 Materials and Methods

4.2.1 Hyaluronic Acid Gelation

Thiolated hyaluronic was obtained directly from a commercial source (Glycosan Biosystems). The sample was analyzed via ^{1}H nuclear magnetic resonance (NMR) spectroscopy (JEOL ECA 500) to assess thiol substitution. To prepare appropriately stiff HA hydrogels to mimic heart stiffening, 4.53% (w/v) PEGDA with M_w ~ 3400 Da (polydispersity index or PDI ~ 3, Glycosan Biosystems) in de-gassed (DG) PBS and 1.25% thiolated HA (Glycosan BioSystems) in DG PBS were separately mixed at 37°C with gentle shaking for up to 30 minutes. To initiate polymerization, solutions were combined at a volume ratio of 1 PEGDA solution: 4 HA solution to yield a 1% HA/0.9% PEGDA hydrogel, unless otherwise indicated.

4.2.2 Subcutaneous and Intramyocardial Injections

All animals received humane care in compliance with University of California, San Diego's Institutional Animal Care and Use Committee (protocol #S08172 and #S10026) and the American Association for the Accreditation of Laboratory Animal Care. HA hydrogels were prepared as above but using aseptic methods and materials warmed at 37°C for ~5 mins until the solution became viscous. For subcutaneous injections, animals were anesthetized with 5% isoflurane and maintained at 2.5% isoflurane with a nose cone throughout the procedure. Prior to injection, 3mg/kg Bupivacaine Hydrochloride (Hospira), a local anesthetic, was delivered to the injection

sites in order to minimize pain. Two 200 μL injections were made on the backside of Sprague-Dawley (SD) rats opposite the spinal cord using a 25 G needle attached to a 1mL luer lock syringe (BD Biosciences). Boluses were visible at the injection sites. Samples from four animals per time point were removed 1, 3, 5, 7 and 14 days after injection and subject to mechanical (AFM) and histological analysis.

For intramyocardial injections, pre-gelation time was carefully regulated because when injected too early, the gel solution dispersed interstitially and could not be identified via histology (< ~3 min); when injected too late, the syringe resistance was too great to deliver the increasingly crosslinked hydrogel (> ~5 min). For comparison, three other materials were also examined for intramyocardial injection. Human clinical grade HA (Restylane®) was injected as a 1% pre-gelled solution to be able to best compare its results with HA hydrogels lacking thiols. In order to examine effects of the PEGDA crosslinker, a mixture containing 1/10 PEGDA and the regular amount of HA-SH, i.e. 0.09% PEGDA/1% HA-SH hydrogel, was prepared along with a 2% HA-SH mixture without crosslinker. Both samples were prepared aseptically the day before injection and allowed to gel in the syringe at 37°C overnight due to slow gelation time when acrylate crosslinker concentration is dramatically reduced or absent.

Before injection, animals were anesthetized with 5% isoflurane, intubated, and maintained at 2.5% isoflurane throughout the procedure. After anesthetization, animals were given 3 ml of lactated Ringers solution (Hospira) for hydration during surgery. Injections were performed using a procedure described previously (26). Briefly, an incision was made in the abdomen, the diaphragm was cut to expose the heart and the heart was held steady using forceps. A single injection of 50-75 μL of the hydrogel was

delivered into the left ventricular free wall of healthy SD rats using a 27 G needle attached to a 1 mL slip tip syringe (BD Biosciences). Blanching was observed after injection, which ensured material injection into the myocardium, though some extrusion was not uncommon. After injection, suction of the chest cavity was performed in order to ensure the diaphragm was tight, the abdomen was stitched up, and animals were allowed to recover. Once alert and sternal, animals were given 0.05 mg/kg of buprenorphine hydrochloride (Reckitt Benckiser Healthcare), an analgesic, prior to recovery from anesthesia. Hearts from 3-6 animals per time point were removed after 1 hr or less and 3, 7, 14 and 30 days after injection and subjected to histological analysis. A statistical power analysis set to a threshold of 0.8 was performed by "PS - Power and Sample Size Calculation" software indicated at least 3 rats per condition were required per experiment.

4.2.3 Hematology

For subcutaneous injections, 25μL of blood was drawn from the saphenous vein of anesthetized (5% isoflurane and maintained at 2.5% isoflurane with a nose cone) rats prior to subcutaneous injection and prior to removal of the gel according to the time course. Four control rats underwent the same blood withdrawal procedure without any injection. Blood samples were examined on a Hemavet Hematology Analyzer (UCSD Hematology Core). Whole blood cell, neutrophil and monocyte counts were examined by comparing pre- vs. post-injection values for each time point. Statistical analyses compared each time point of non-injected and HA-injected samples.

4.2.4 Histology

For subcutaneous injections, one of the bilateral injections was removed from each rat at the indicated time points and frozen in Tissue Tek Optimal Cutting Temperature (OCT) solution. Subcutaneous injection samples were sectioned on a Cryocut 1800 (Leica) at 10 μm and mounted on glass slides. Intramyocardial injection samples and *in vitro* hydrogels were frozen in the same manner as mentioned and sectioned at 10μm. Alternating slides were stained with hematoxylin and eosin (H&E). Briefly, samples were rehydrated in DH_2O for 3 min, stained in hematoxylin (Fisher Scientific) for 2.5 min, rinsed in water for 3 min, dipped in bluing reagent (Protocol) 20 times, dehydrated in EtOH, stained in Eosin (Fisher Scientific) for 2.5 min, dehydrated once more, and cleared in Histoclear (National Diagnostics). Samples were mounted with Cytoseal-60 (Richard-Allan Scientific), examined using a Carl Zeiss Observer D.1, and analyzed with AxioVision software. H&E stained samples were corrected for white balance.

4.2.5 Immunohistochemistry

Remaining slides from subcutaneous and intramyocardial injections were stained with antibodies for a lymphocyte marker, CD45 (ab10558, Abcam), or a macrophage marker, CD68 (ab31630, Abcam), and Hoescht (33342, Invitrogen) as indicated in order to visualize any inflammatory cell response present in the samples. Briefly, samples were fixed in acetone for 1.5 min, rinsed in 1X PBS, blocked with staining buffer (0.3% Triton-100X and 2% goat serum in 1X PBS) for 20 min, and incubated with primary

antibody at 1:200 in staining buffer for 1hr, anti-mouse Alexa Fluor® 488 (A11001, Invitrogen) for 30 min, and Hoescht for 10 min at room temperature. Samples were mounted with fluoromount-G (SouthernBiotech). Samples were examined using a BD Carv II confocal microscope (BD Biosciences; San Jose, CA) mounted on a Nikon Eclipse TE2000-U microscope with Metamorph 7.6 software. Since the hydrogels were not stained, they could be visualized using bright field in order to confirm injected hydrogel and host tissue position for fluorescence imaging.

4.2.6 Atomic Force Microscopy

The other subcutaneous bilateral injection was removed intact, rinsed in 1X PBS and mounted on a glass slide for AFM analysis. AFM indentation was performed as previously described (40) using 20 pN/nm pyramidal tips (Olympus TR400PB) or 2 μm radius 120pN/nm spherical tips (Novascan), a tip approach velocity of 2 μm/s, and a deflection trigger of 100 nm. To minimize tip-sample interaction, measurements were performed in 1% bovine serum albumin in PBS. Force vs. displacement curves were analyzed using a non-contact, linearized Hertz method (41), assuming a Poisson's ratio ~ 0.5. No significant difference was observed between values obtained from the two different cantilever geometries for all hydrogels.

4.2.7 Statistical Analysis

All experiments were performed using three biological replicates unless otherwise noted and reported as a mean ± standard error of the mean. Significance was assessed by

student's t-test at a significance threshold of $p < 0.05$ or lower as indicated. Data where $p > 0.05$ is not statistically different and is reported to emphasize similarities between treated and sham conditions in hematological analysis.

4.3 Results

4.3.1 Subcutaneous Injections

Hematological analysis of total white blood cell as well as monocyte and neutrophil counts, normalized to their pre-injection value, were not found to be elevated in either the HA-SH/PEGDA injected or non-injected conditions (Fig. 1). Given the lack of statistical difference between injected and non-injected rats for our sample size, sham-injected rats were not measured. Hydrogel polymerization and local immune response were also assessed in order to examine hydrogel biocompatibility after injection into the host. The HA-SH and PEGDA crosslinker formed a continuous network subcutaneously (Fig. 2, top). Lymphocytes were present at low levels within and surrounding the hydrogel as indicated by CD45 staining (Fig. 2, middle, white arrows).

HA-SH hydrogels have been previously shown to undergo time-dependent stiffening *in vitro* (12), and thus the dynamics previously measured *in vitro* were verified in this subcutaneous injection model. Hydrogel porosity was compared via histological sections between identical samples either injected *in vivo* or maintained *in vitro* with both conditions resulting in comparable changes in porosity over time (Fig. 3). Similar crosslinking dynamics between *in vivo* and *in vitro* samples should result in similar

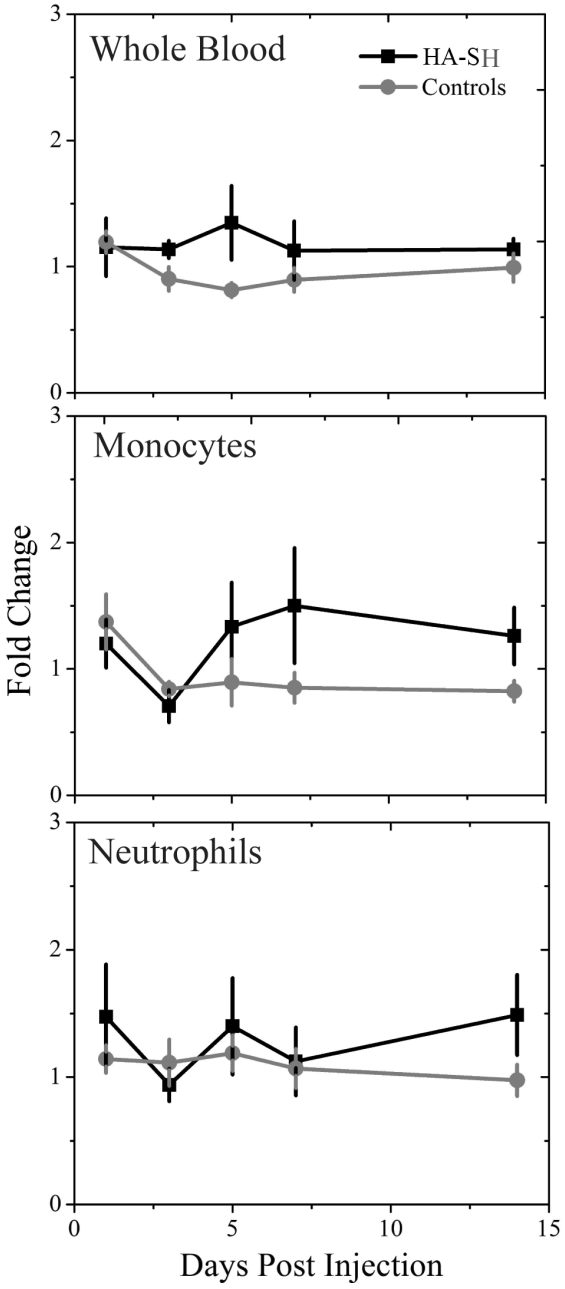

Figure 1: *Hematological Analysis of Subcutaneously HA-Injected vs. Non-Injected Rats.* Hematological cell counts of subcutaneously HA-injected (black) and non-injected rats (gray) for whole blood (top), monocytes (middle) and neutrophils (bottom). Values are post-injection at each indicated time point, were always taken prior to sample removal, and were normalized to pre-injection values. None of the subcutaneous HA-injected data was statistically different from non-injected rats as determined by Student's *t*-test: whole blood, $p > 0.06$; monocytes,$p > 0.14$; neutrophils $p > 0.16$. $n = 4$ for each group.

changes in stiffness over time; after removing subcutaneously injected samples, direct comparison of the two samples by AFM indicated that HA-SH/PEGDA stiffening dynamics were preserved after injection (Fig. 4).

4.3.2 Intramyocardial Injections

HA-SH hydrogel stiffening mimics cardiac developmental stiffening (12), so HA-SH hydrogels were also examined after intramyocardial injection into the healthy heart. HA-SH hydrogels were found to be intact and well distributed throughout the injection site through 1-week post-intramyocardial injection with host cells beginning to infiltrate and degrade the material (Fig. 5, 1 week; nuclei stained blue). The hydrogel appeared to be more porous at early time points compared to subcutaneous or *in vitro* controls (Fig. 5, 30 min vs. Fig. 3, 1 day). At one month, degraded hydrogel with host cell infiltration was observed along with new matrix deposition (Fig. 5, 1 month); however, the response was indicative of chronic inflammation.

To determine the inflammatory source, hydrogels comprised of non-thiolated HA (Restylane®), HA-SH, or HA-SH with high or low PEGDA crosslinker were injected into the myocardium. Restylane® did not elicit a significant, chronic immune response surrounding the injection site, as assessed by H&E staining and the lack of lymphocytes (CD45) and macrophages (CD68) within the injection site (Fig. 6A, leftmost column). In contrast, staining of standard HA-SH hydrogels, i.e. 0.9% PEGDA/1% HA-SH, indicated a dramatic increase in host cell infiltration from H&E staining and the presence of CD45 and CD68 positive cells within the injection site (Fig. 6A, left center column). These data

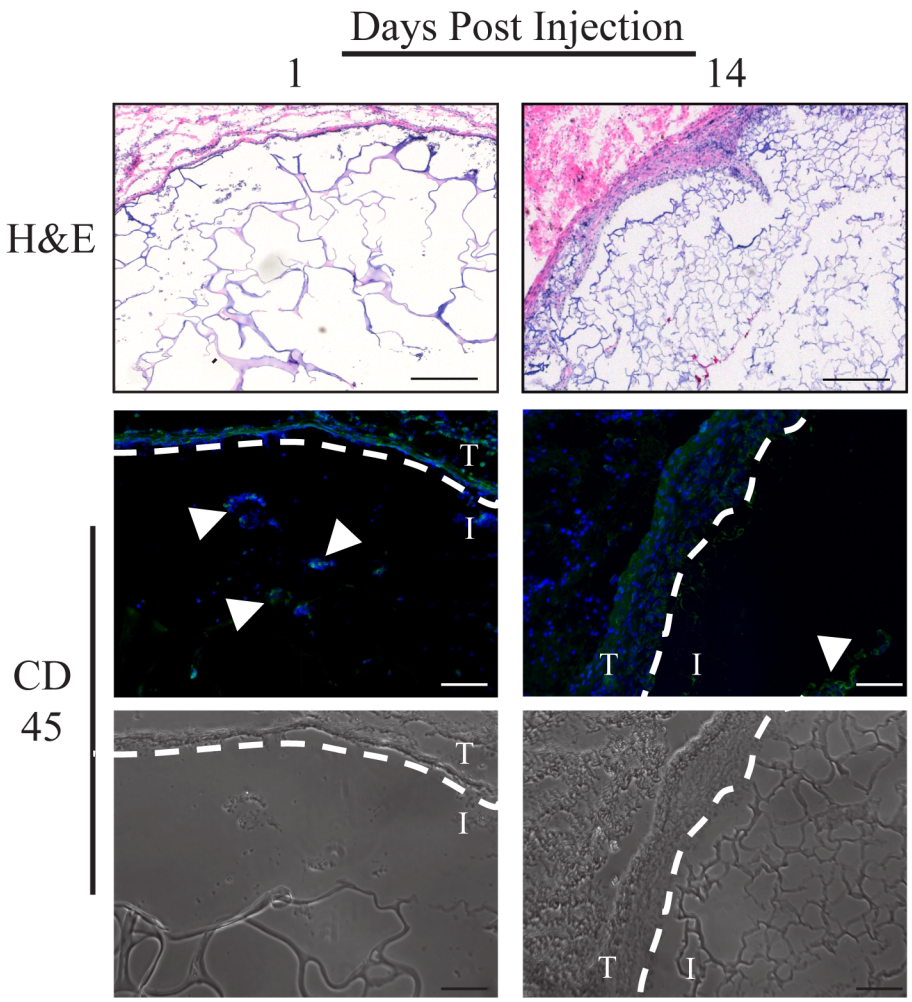

Figure 2: *Histology of Subcutaneously HA-Injected Rats.* (Top) Hematoxylin and eosin (H&E) stained sections of subcutaneously-injected samples (left) 1 and (right) 14 days post-injection. (Middle) Immunohistochemical staining with CD45 (green) and Hoescht (blue) shows the presence of a limited number of inflammatory cells within and around the hydrogel (arrowheads). (Bottom) Accompanying bright field images for the middle panel of images. Scale bars 500 μm for the top and 100 μm for the middle and bottom images. The dashed white line denotes the host tissue (T) and injection (I) regions.

implicated thiol and acrylate groups within the hydrogel as the inflammatory source. Therefore, a hydrogel with lower crosslinking concentration (0.09% PEGDA) was injected to determine if free acrylates induced inflammation, and a similar immune response with CD45 and CD68 positive cells was observed within weeks of injection (Fig. 6A right center column). In the absence of PEGDA but with a higher HA-SH concentration (to allow gelation via thiol-thiol bonding), CD45 and CD68 positive cells were still visible, indicating that the thiol may be an inflammatory source (Fig. 6A, rightmost column). A lack of CD45 and CD68 staining in non-injected regions of the heart ensured that no inflammation was present outside of the injection area (Fig. 6B).

4.4 Discussion

HA is a durable glycosaminoglycan for tissue engineering due to its ECM-derivation and ease of modification, e.g. methacrylation (9), thiolation (37), etc. More specifically, thiol modification of HA and subsequent crosslinking with acrylates in a Michael-type addition reaction has been well described by Prestwich and co-workers (36, 37, 42). Recently using specific HA-SH and PEGDA concentrations and molecular weights, time-dependent crosslinking dynamics have been described where slow thiol-acrylate and thiol-thiol reactions account for the temporal change in stiffness (12). We documented here that in a less vascularized, subcutaneous niche, these same formulations are capable of time-dependent changes in porosity and stiffness without significant immunogenicity. In much more vascularized tissues, an adverse host interaction, likely due to the presence of free thiols, and perhaps subsequent oxidation (43, 44), created an inflammatory reaction that will limit its myocardial compatibility. Despite these results in

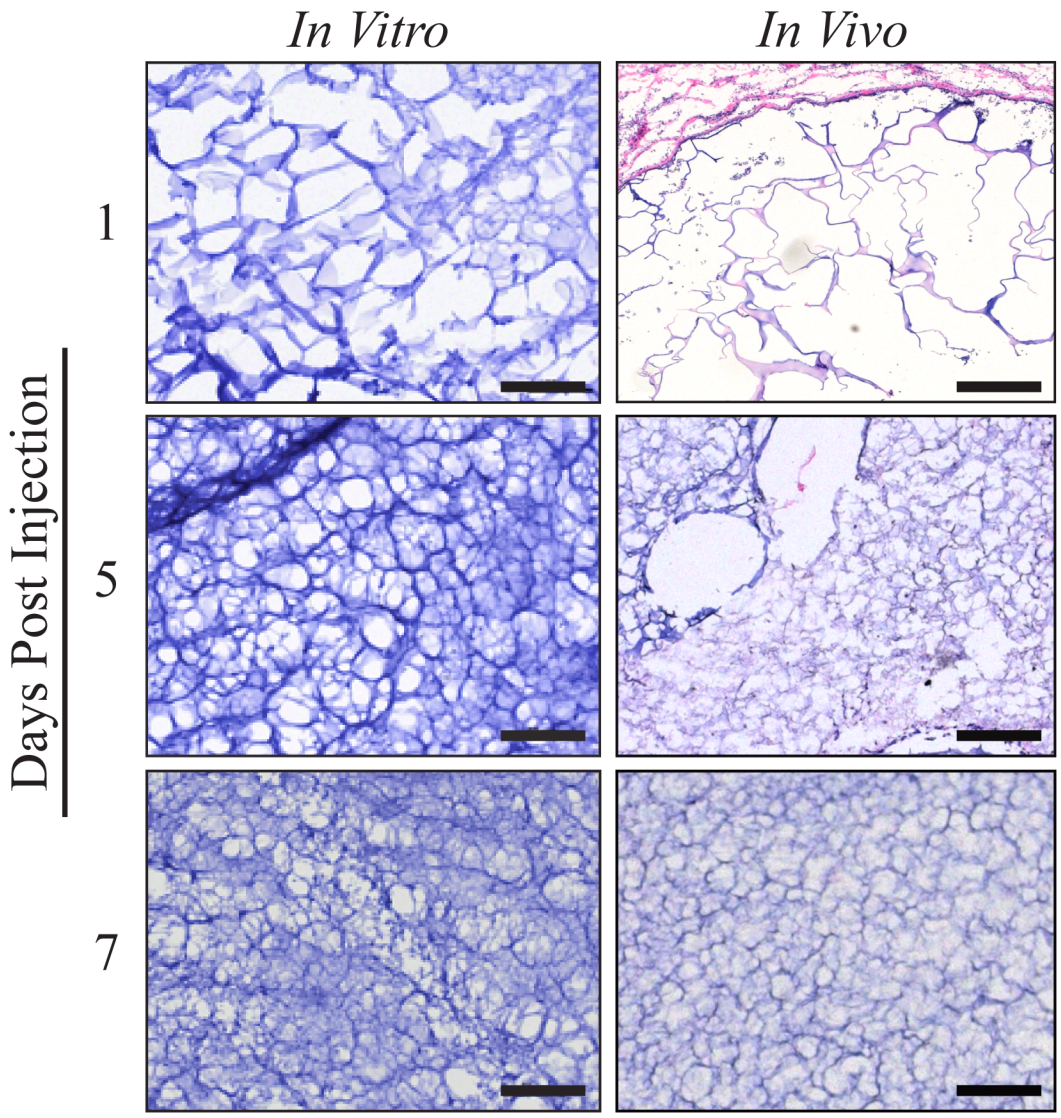

Figure 3: *Histology of Subcutaneously-Injected In Vivo vs. In Vitro Polymerized HA Hydrogels Shows Porosity Similarities.* H&E stained cross-sections of (left) *in vitro* and (right) subcutaneously *in vivo* injected samples are shown as a function of time. Scale bars 500 μm.

vascularized tissues, less vascularized niche where dynamic changes occur, e.g. cartilage (45), may be suitable for thiolated HA hydrogels.

4.4.1 Subcutaneous versus Intramyocardial HA-SH Injections

Assessment of local and systemic immune responses after subcutaneous and intramyocardial HA-SH injection provides important information on host interactions, matrix polymerization, and stiffening kinetics *in vivo*. Subcutaneously, limited systemic immune response and small fibrotic capsule surrounding the material demonstrate that the hydrogel does not elicit a significant local and systemic response. These results are consistent with prior subcutaneously-injected hydrogels composed of other thiolated glycosaminoglycans (46), though specific formulations, concentrations, and crosslinkers differ. Most importantly, AFM and porosity measurements confirm that the HA-SH hydrogel's temporal stiffening occurs when injected subcutaneously *in vivo*. However, direct evaluation of porosity may be limited by host cell infiltration and potential sectioning differences between tissues. Despite this, AFM data was consistent between *in vitro*-polymerized and subcutaneously-polymerized measurements, though both are subject to little strain when compared to the myocardium in which the gel is more compressed and subject to rhythmic contraction. In the higher strain niche of the myocardium, non-linear strain stiffening may occur, which could alter gelation kinetics, although significant cell infiltration and hydrogel degradation precludes measurement.

In more vascularized tissues, i.e. myocardium, the formation of large, CD68 - positive granulomas and inflammatory cells within and surrounding the hydrogel were observed, indicating a significant immune response not present in subcutaneous

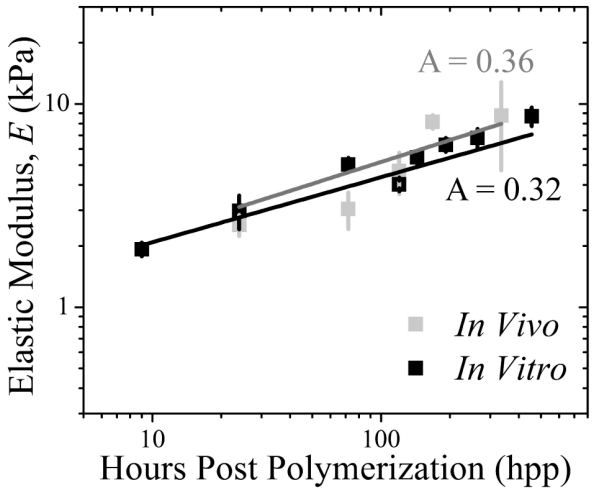

Figure 4: *AFM Analysis of Subcutaneously-Injected HA Hydrogels Shows Stiffening Kinetics Similar to In Vitro Polymerized HA Hydrogels.* Elastic modulus of *in vivo* (gray) subcutaneously-injected HA compared with (black) *in vitro* on a log–log plot. Data points were fitted using the power law $y = x^A$, where $A = 0.36$ *in vivo* and $A = 0.32$ *in vitro.* Student's *t*-test analyses indicate that these data are not statistically different ($p > 0.97$). For *in vitro* and *in vivo* samples, $n = 3$ and 6, respectively.

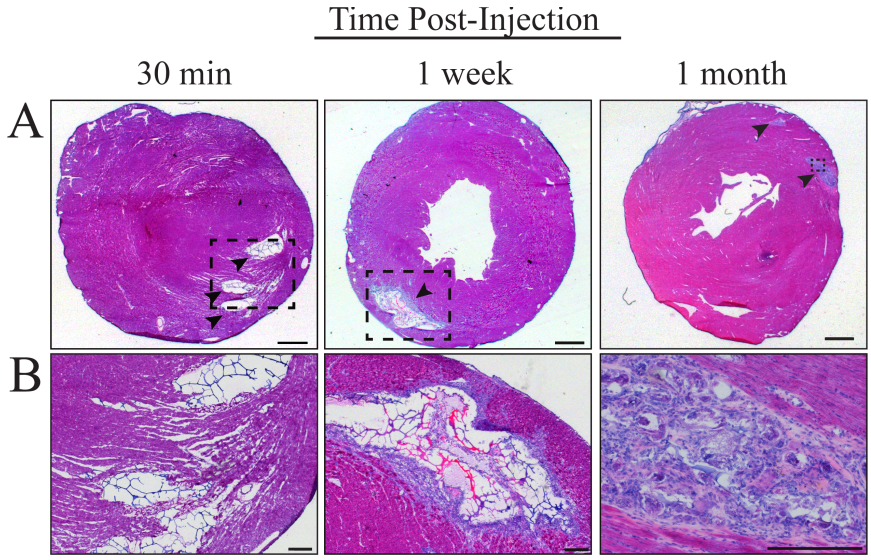

Figure 5: *Histology of Intramyocardially-Injected HA Hydrogel Over 1 Month Shows Immune Response.* (A) HA-SH hydrogel in myocardium (left) 30 min, (middle) 1 week and (right) 1 month post-injection (indicated by arrowheads in the top panel). (B) Enlarged images of the area indicated by the black dashed box. 1 month post-injection shows material degradation and cell infiltration. Scale bars: (A) 500 μm; (B) 250 μm.

injections. Though non-thiolated HA did not elicit the same adverse response intramyocardially, such hydrogels lack the benefit of cell-mediated degradation and HA-SH's temporal stiffening. Closer inspection of the biocompatibility issue appears to indicate that the adverse interaction was specific to thiol-containing hydrogels. Thiol oxidation is cytotoxic *in vitro* (43, 44), and while capping exposed groups post-polymerization *in vivo* via iodoacetamide would limit oxidation, it would also prevent additional Michael-type reactions and thus block beneficial temporal stiffening of the hydrogel. While thiol-based Michael-type reactions *in vitro* have been extensively documented (47-49) and cells typically interact with a matrix layer covalently attached to the hydrogel's surface (12), there are limited studies using these materials *in vivo* (46) with results that show mixed biocompatibility, particularly in highly vascularized locations such as the eye (50) or in the myocardium of immune-compromised mice post-infarct (51). This study, along with some of these recent studies, suggests that thiols may not produce biocompatible responses in highly vascularized tissues, and therefore this crosslinking mechanism may be limited to *in vitro* applications or specific tissues.

4.4.2 Alternative Approaches

Despite limitations in vascularized tissues, HA-SH hydrogels appear useful in less vascular settings and as an *in vitro* culture substrate. We have previously shown that varying hydrogel components, e.g. HA concentration, crosslinker concentration, and crosslinker molecular weight, can affect overall stiffness as well as stiffening kinetics (12); therefore, HA-SH hydrogels could be used in conjunction with soluble factors to guide *in vitro* cell behavior for applications that require softer or stiffer hydrogels with

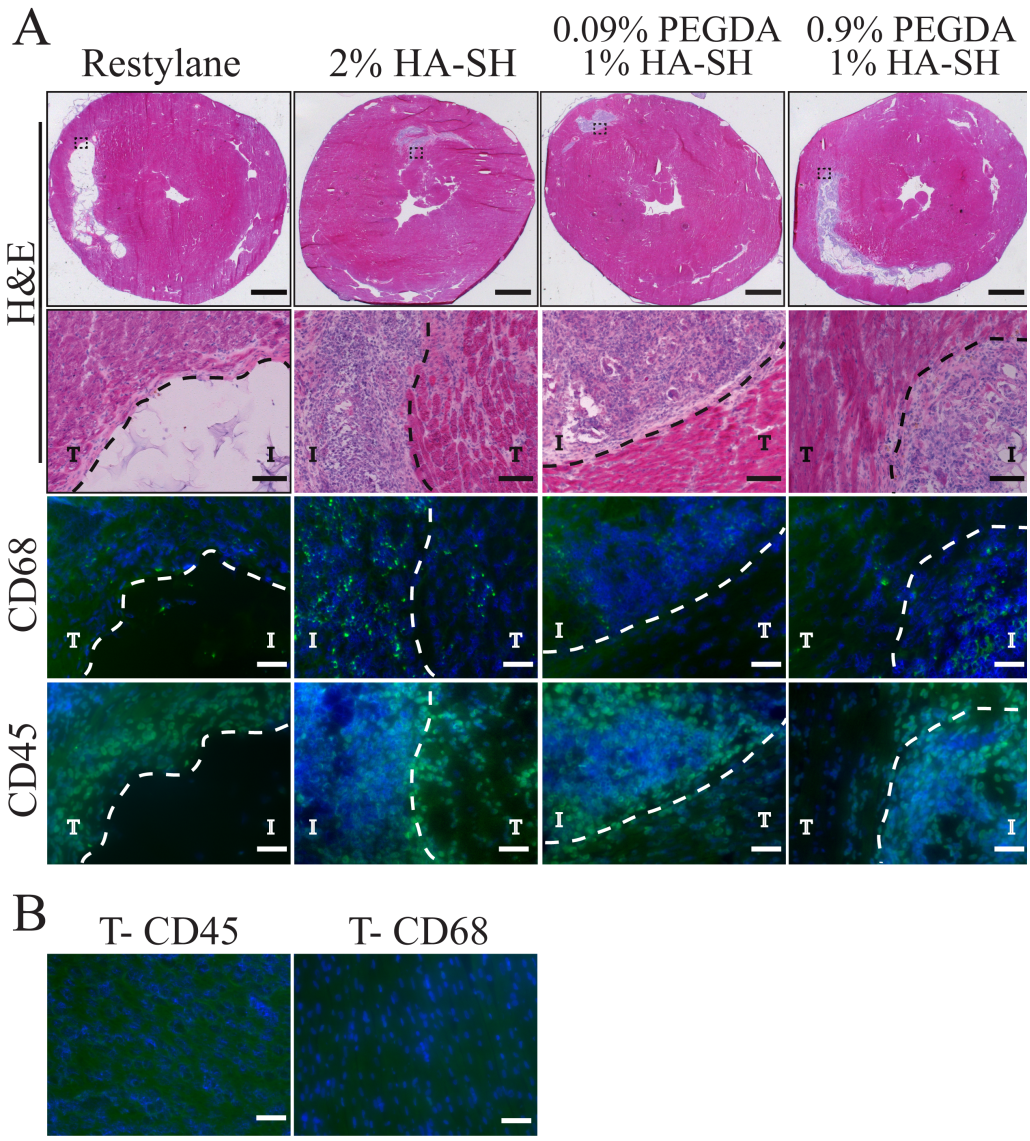

Figure 6: *Histology of Different Formulations of HA Shows Thiol Group Toxicity.* (A) Histological sections of hearts injected with (left) Restylane®, (left center) 2% HA-SH hydrogels, (right center) 0.09% PEGDA/1% HA-SH hydrogel, and (right) 0.9% PEGDA/1% HA-SH (original formulation) are shown 3 weeks post-intramyocardial injection. For H&E stained sections, the black dashed box in the top row (scale bar 2000 μm) indicates the enlarged area depicted in the second row (scale bar 100 μm). Immunohistochemical staining for CD68 (green, third row) and CD45 (green, fourth row) show macrophages and lymphocytes, respectively, as well as other invasive cells (Hoescht-labeled nuclei in blue) present within and around the hydrogels as indicated. The dashed line separates the site of injection (I) from the surrounding host tissue (T). (B) Immunohistochemical staining for CD45 (left) and CD68 (right) in non-injected regions of the myocardium. Image intensity is scaled according to the injected images in (A). Scale bars 50 μm for all immunofluorescent images.

slower or faster kinetics. For example, dynamic culture conditions could be utilized for stem cell cardiac differentiation, wound healing or fibrosis (12, 18, 52) keeping in mind that *in vitro*, cells attach to a layer of collagen covalently bound to the HA-SH hydrogel.

An alternative approach to our hydrogel system may be to modify HA with thioethyl ether derivatives, which appear to protect against oxidation as it reduces cell apoptosis upon exposure to hydrogen peroxide *in vitro* (36). To ensure that it would have dynamic stiffening like the HA-SH hydrogel, such material would need to have approximately the same substitution efficiency of HA-SH, e.g. ~40% (12), be used at the same concentrations, etc.

4.5 Conclusions

It has previously been shown that time-dependent stiffening enhances cardiomyocyte maturation (12) and thus, the combination of cells and developmentally appropriate matrix cues in regenerative therapies may significantly restore tissue function relative to cell-only therapies, e.g. cellular cardiomyoplasty. Injections into less vascularized tissues here indicate that these same HA-SH hydrogels can at least achieve stiffening and crosslinking as *in vitro* hydrogels, without significant host response, and therefore may be useful as a subcutaneous *in vivo* model. In highly vascularized regions, i.e. myocardium, injections show that HA-SH can assemble and degrade over time; however, the continual recruitment of inflammatory cells likely due to interactions with free thiol in the scaffold implies that HA-SH based hydrogels have limited biocompatibility, adding to recent evidence that popular thiol-based Michael-type

reactions may not be suitable for many *in vivo* applications. However, these materials may still be applicable as an *in vitro* tool to study the effects of dynamic mechanical cues on cellular behaviors where cells on top of the hydrogel bind to a covalently attached matrix layer and 'feel' the stiffening beneath them rather than interact with the free thiols within the hydrogel.

4.6 Acknowledgements

Chapter 4, in full, is a reformatted version of the published article in *Acta Biomaterialia,* http://dx.doi.org/10.1016/j.actbio.2013.03.019, 2013. The dissertation author was the primary investigator and author of this paper, and thanks co-authors Jeremy Tuler, Rebecca Braden, Pamela Schüp-Magoffin, Jacquelyn Schaefer, Kyle Kretchmer, Dr. Karen Christman and Dr. Adam Engler for their contributions. The authors would like to thank Dr. Alex Furhmann (UC San Diego) for use of his AFM analysis code, Dr. Marek Dobke for his kind gift of Restylane® samples and pathology expertise in examining the data shown here, Kenneth Kim and Qiongyu Chen (UCSD Hematology Core) for their hematology expertise, and Dr. William D. Dupont (Vanderbilt University) for use of his statistical power analysis software. This work was supported in part by the National Institutes of Health (R21HL106529 to A.J.E.), American Heart Association (0865150F to A.J.E. and 10PRE4160143 to J.L.Y.), and Achievement Rewards for College Scientists (ARCS; to J.L.Y.).

4.7 References

1. Tse JR, Engler AJ (2011) Stiffness gradients mimicking in vivo tissue variation regulate mesenchymal stem cell fate. *PLoS One* 6(1):e15978.

2. Peyton SR, Putnam AJ (2005) Extracellular matrix rigidity governs smooth muscle cell motility in a biphasic fashion. *J Cell Physiol* 204(1):198-209.

3. Zaari N, Rajagopalan P, Kim SK, Engler AJ, Wong JY (2004) Photopolymerization in microfluidic gradient generators: Microscale control of substrate compliance to manipulate cell response. *Advanced Materials* 16(23-24):2133-2137.

4. Rowlands AS, George PA, Cooper-White JJ (2008). Directing osteogenic and myogenic differentiation of MSCs: interplay of stiffness and adhesive ligand presentation. *Am J Physiol Cell Physiol* 295(4):C1037-1044.

5. Huebsch N, Arany PR, Mao AS, Shvartsman D, Ali OA, Bencherif SA, Rivera-Feliciano J, Mooney D (2010) Harnessing traction-mediated manipulation of the cell/matrix interface to control stem-cell fate. *Nat Mater* 9(6):518-526.

6. Shih YR, Tseng KF, Lai HY, Lin CH, Lee OK (2010). Matrix stiffness regulation of integrin-mediated mechanotransduction during osteogenic differentiation of human mesenchymal stem cells. *J Bone Miner Res* 26(4):730-738.

7. Ghosh K, Pan Z, Guan E, Ge S, Liu Y, Nakamura T, Ren X-D, Rafailovich M, Clark RAF (2007) Cell adaptation to a physiologically relevant ECM mimic with different viscoelastic properties. *Biomaterials* 28(4):671-679.

8. Evans ND, Minelli C, Gentleman E, LaPointe V, Patankar SN, Kallivretaki M, Chen X, Roberts CJ, Stevens MM (2009) Substrate stiffness affects early differentiation events in embryonic stem cells. *Eur Cell Mater* 18:1-13; discussion 13-14.

9. Marklein RA, Burdick JA (2010) Spatially controlled hydrogel mechanics to modulate stem cell interactions. *Soft Matter* 6(1):136-143.

10. Engler AJ, Sen S, Sweeney HL, Discher DE (2006). Matrix elasticity directs stem cell lineage specification. *Cell* 126(4):677-689.

11. Saha K, Keung AJ, Irwin EF, Li Y, Little L, Schaffer DV, Healy KE (2008) Substrate modulus directs neural stem cell behavior. *Biophys J* 95(9):4426-4438.

12. Young JL, Engler AJ (2011) Hydrogels with time-dependent material properties enhance cardiomyocyte differentiation in vitro. *Biomaterials* 32(4):1002-1009.

13. Kloxin AM, Kasko AM, Salinas CN, Anseth KS (2009) Photodegradable hydrogels for dynamic tuning of physical and chemical properties. *Science* 324(5923):59-63.

14. Guvendiren M, Burdick JA (2012) Stiffening hydrogels to probe short- and long-term cellular responses to dynamic mechanics. *Nature communications* 3:792-799.

15. Choi YS, Vincent LG, Lee AR, Kretchmer KC, Chirasatitsin S, Dobke MK, Engler AJ (2012) The alignment and fusion assembly of adipose-derived stem cells on mechanically patterned matrices. *Biomaterials* 33(29):6943–6951.

16. Engler AJ, Griffin MA, Sen S, Bonnemann CG, Sweeney HL, Discher DE (2004) Myotubes differentiate optimally on substrates with tissue-like stiffness: pathological implications for soft or stiff microenvironments. *J Cell Biol* 166(6):877-887.

17. Zhang S, Sun A, Ma H, Yao K, Zhou N, Shen L, Zhang C, Zou Y, Ge J (2011) Infarcted myocardium-like stiffness contributes to endothelial progenitor lineage commitment of bone marrow mononuclear cells. *Journal of cellular and molecular medicine* 15(10):2245-2261.

18. Berry MF, Engler AJ, Woo YJ, Pirolli TJ, Bish LT, Jayasankar V, Morine KJ, Gardner TJ, Discher DE, Sweeney HL (2006) Mesenchymal stem cell injection after myocardial infarction improves myocardial compliance. *Am J Physiol Heart Circ Physiol* 290(6):H2196-203.

19. Georges PC, Hui JJ, Gombos Z, McCormick ME, Wang AY, Uemura M, Mick R, Janmey PA, Furth EE, Wells RG (2007) Increased stiffness of the rat liver precedes matrix deposition: implications for fibrosis. *Am J Physiol Gastrointest Liver Physiol* 293(6):G1147-1154.

20. Engler AJ, Carag-Krieger C, Johnson CP, Raab M, Tang HY, Speicher DW, Sanger JW, Sanger JM, Discher DE. (2008) Embryonic cardiomyocytes beat best on a matrix with heart-like elasticity: scar-like rigidity inhibits beating. *J Cell Sci* 121(22):3794-3802.

21. Jacot JG, McCulloch AD, Omens JH (2008) Substrate stiffness affects the functional maturation of neonatal rat ventricular myocytes. *Biophys J* 95(7):3479-3487.

22. Lunde K, Solheim S, Aakhus S, Arnesen H, Abdelnoor M, Forfang K (2005)

Autologous stem cell transplantation in acute myocardial infarction: The ASTAMI randomized controlled trial. Intracoronary transplantation of autologous mononuclear bone marrow cells, study design and safety aspects. *Scand Cardiovasc J* 39(3):150-158.

23. Chachques JC, Acar C, Herreros J, Trainini JC, Prosper F, D'Attellis N, Fabiani JN, and Carpentier AF (2004) Cellular cardiomyoplasty: clinical application. *Ann Thorac Surg* 77(3):1121- 1130.

24. Janssens S, Dubois C, Bogaert J, Theunissen K, Deroose C, Desmet W, Kalantzi M, Herbots L, Sinnaeve P, Dens J, Maertens J, Rademakers F, Dymarkowski S, Gheysens O, Van Cleemput J, Bormans G, Nuyts J, Belmans A, Mortelmans L, Boogaerts M, Van de Werf F (2006) Autologous bone marrow-derived stem-cell transfer in patients with ST-segment elevation myocardial infarction: double-blind, randomised controlled trial. *Lancet* 367(9505):113-121.

25. Breitbach M, Bostani T, Roell W, Xia Y, Dewald O, Nygren JM, Fries JW, Tiemann K, Bohlen H, Hescheler J, Welz A, Bloch W, Jacobsen SE, Fleischmann BK (2007) Potential risks of bone marrow cell transplantation into infarcted hearts. *Blood* 110(4):1362-1369.

26. Christman KL, Fok HH, Sievers RE, Fang Q, Lee RJ (2004) Fibrin glue alone and skeletal myoblasts in a fibrin scaffold preserve cardiac function after myocardial infarction. *Tissue Eng* 10(3-4):403-409.

27. Christman KL, Vardanian AJ, Fang Q, Sievers RE, Fok HH, Lee RJ (2004) Injectable fibrin scaffold improves cell transplant survival, reduces infarct expansion, and induces neovasculature formation in ischemic myocardium. *J Am Coll Cardiol* 44(3):654-660.

28. Huang NF, Yu J, Sievers R, Li S, Lee RJ (2005) Injectable biopolymers enhance angiogenesis after myocardial infarction. *Tissue Eng* 11(11-12):1860-1866.

29. Laflamme MA, Chen KY, Naumova AV, Muskheli V, Fugate JA, Dupras SK, Reinecke H, Xu C, Hassanipour M, Police S, O'Sullivan C, Collins L, Chen Y, Minami E, Gill EA, Ueno S, Yuan C, Gold J, Murry CE (2007) Cardiomyocytes derived from human embryonic stem cells in pro-survival factors enhance function of infarcted rat hearts. *Nature Biotechnology* 25(9):1015-1024.

30. Kofidis T, de Bruin JL, Hoyt G, Lebl DR, Tanaka M, Yamane T, Chang C-P, Robbins RC (2004) Injectable bioartificial myocardial tissue for large-scale intramural cell transfer and functional recovery of injured heart muscle. *J Thorac Cardiovasc Surg* 128(4):571-578.

31. Zhang P, Zhang H, Wang H, Wei Y, Hu S (2006) Artificial matrix helps neonatal

cardiomyocytes restore injured myocardium in rats. *Artif Organs* 30(2):86-93.

32. Yu J, Christman KL, Chin E, Sievers RE, Saeed M, Lee RJ (2009) Restoration of left ventricular geometry and improvement of left ventricular function in a rodent model of chronic ischemic cardiomyopathy. *J Thorac Cardiovasc Surg* 137(1):180-187.

33. Mukherjee R, Zavadzkas JA, Saunders SM, McLean JE, Jeffords LB, Beck C, Stroud RE, Leone AM, Koval CN, Rivers WT, Basu S, Sheehy A, Michal G, Spinale FG (2008) Targeted myocardial microinjections of a biocomposite material reduces infarct expansion in pigs. *Ann Thorac Surg* 86(4):1268-1276.

34. French KM, Boopathy AV, Dequach JA, Chingozha L, Lu H, Christman KL, Davis ME (2012) A naturally derived cardiac extracellular matrix enhances cardiac progenitor cell behavior in vitro. *Acta biomaterialia* 2012 8(12):4357-4364.

35. Singelyn JM, Sundaramurthy P, Johnson TD, Schup-Magoffin PJ, Hu DP, Faulk DM, Wang J, Mayle KM, Bartels K, Salvatore M, Kinsey AM, Demaria AN, Dib N, Christman KL (2012) Catheter-deliverable hydrogel derived from decellularized ventricular extracellular matrix increases endogenous cardiomyocytes and preserves cardiac function post-myocardial infarction. *J Am Coll Cardiol* 59(8):751-763.

36. Serban MA, Yang G, Prestwich GD (2008) Synthesis, characterization and chondroprotective properties of a hyaluronan thioethyl ether derivative. *Biomaterials* 29(10):1388-1399.

37. Shu XZ, Liu YC, Luo Y, Roberts MC, Prestwich GD (2002) Disulfide cross-linked hyaluronan hydrogels. *Biomacromolecules* 3(6):1304-1311.

38. Burdick JA, Prestwich GD (2011) Hyaluronic Acid Hydrogels for Biomedical Applications. *Advanced Materials* 23(12):H41-H56.

39. Grek CL, Townsend DM, Tew KD (2011) The impact of redox and thiol status on the bone marrow: Pharmacological intervention strategies. *Pharmacol Ther* 129(2):172-184.

40. Engler AJ, Rehfeldt F, Sen S, Discher DE (2007) Microtissue elasticity: measurements by atomic force microscopy and its influence on cell differentiation. *Methods Cell Biol* 83:521-545.

41. Kaushik G, Fuhrmann A, Cammarato A, Engler AJ (2011) In situ mechanical analysis of myofibrillar perturbation and aging on soft, bilayered Drosophila myocardium. *Biophys J* 101(11):2629-2637.

42. Kuo JW, Prestwich GD (2010) Materials of Biological Origin – Materials Analysis and Implant Uses. In: Ducheyne P, Healy KE, Hutmacher D, Kirkpatrick J, editors. *Comprehensive Biomaterials*: Elsevier.

43. Held KD, Biaglow JE (1994) Mechanisms for the oxygen radical-mediated toxicity of various thiol-containing compounds in cultured mammalian cells. *Radiat Res* 139(1):15-23.

44. Munday R (1989) Toxicity of thiols and disulphides: involvement of free-radical species. *Free Radic Biol Med* 7(6):659-673.

45. Wilson R, Norris EL, Brachvogel B, Angelucci C, Zivkovic S, Gordon L, Bernardo BC, Stermann J, Sekiguchi K, Gorman JJ, Bateman JF (2012) Changes in the chondrocyte and extracellular matrix proteome during post-natal mouse cartilage development. *Mol Cell Proteomics* 11(1):M111.014159.

46. Shu XZ, Ahmad S, Liu Y, Prestwich GD (2006) Synthesis and evaluation of injectable, in situ crosslinkable synthetic extracellular matrices for tissue engineering. *J Biomed Mater Res A* 79(4):902-912.

47. Liu Y, Shu XZ, Gray SD, Prestwich GD (2004) Disulfide-crosslinked hyaluronan-gelatin sponge: growth of fibrous tissue in vivo. *J Biomed Mater Res* A 68(1):142-149.

48. Shu XZ, Ghosh K, Liu Y, Palumbo FS, Luo Y, Clark RA, Prestwich GD (2004) Attachment and spreading of fibroblasts on an RGD peptide-modified injectable hyaluronan hydrogel. J *Biomed Mater Res A* 68(2):365-75.

49. Shu XZ, Liu Y, Palumbo F, Prestwich GD (2003) Disulfide-crosslinked hyaluronan-gelatin hydrogel films: a covalent mimic of the extracellular matrix for in vitro cell growth. *Biomaterials* 24(21):3825-34.

50. Tao Y, Tong X, Zhang Y, Lai J, Huang Y, Jiang YR, Guo BH (2012) Evaluation of an in situ chemically crosslinked hydrogel as a long-term vitreous substitute material. *Acta biomaterialia* 9(2):5022-5030

51. Cheng K, Blusztajn A, Shen D, Li TS, Sun B, Galang G, Zarembinski TI, Prestwich GD, Marbán E, Smith RR, Marbán L (2012) Functional performance of human cardiosphere-derived cells delivered in an in situ polymerizable hyaluronan-gelatin hydrogel. *Biomaterials* 33(21):5317-24.

52. Goffin JM, Pittet P, Csucs G, Lussi JW, Meister JJ, Hinz B (2006) Focal adhesion size controls tension-dependent recruitment of alpha-smooth muscle actin to stress fibers. *J Cell Biol* 172(2):259-68.

Chapter 5

Conclusion

Understanding the developmental mechanics of various tissues can be useful for both stem cell differentiation and regenerative medicine strategies. In the myocardium, a stiff, fibrotic scar forms after injury, which impairs the ability of transplanted stem cells to properly differentiate into functional muscle cells (1). As it has been shown *in vitro* that cells can sense and respond to matrix-mediated mechanical stimuli (2), it has become apparent that mechanics must receive attention when devising differentiation studies or therapeutic interventions. The aims of this dissertation were first to characterize the stiffening dynamics of the developing myocardium, to mimic these mechanics *in vitro* using a hydrogel-based approach, to characterize biomaterial properties of the hydrogel and to investigate maturation of embryonic cardiomyocytes on dynamically-stiffening hydrogels compared to static hydrogels, which was covered in Chapter 2. Chapter 3 focused on investigating activation of mechanosensitive pathways based on matrix mechanics in order to better understand how stiffness is tied to protein kinase signaling within the cell. Lastly, Chapter 4 focused on investigating the *in vivo* feasibility of the

hydrogel system to be utilized in a regenerative medicine approach for treating myocardial infarction. As a final summary, the conclusions of this dissertation will be outlined here.

In order to test the hypothesis that time-dependent material properties can improve cell maturation, mechanical parameters of the developing chicken embryo heart were first characterized by atomic force microscopy (AFM), and it was found that the heart undergoes a ~9-fold increase in elastic modulus, i.e. $E \sim 0.9 \pm 0.2$ kPa at 36 HPF to $E \sim 8.2 \pm 1.3$ kPa at 408 HPF. Concomitant with this stiffness change was an increase in the extracellular matrix (ECM) protein collagen, which also went from being peripherally-localized to being uniformly distributed. Though peripherally-localized collagen is likely mechanically important during heart formation (3), uniform collagen expression throughout the heart may enable a consistent set of material properties for heart maturation.

In order to recapitulate the dynamic stiffness change *in vitro* that we saw in *ex vivo* samples, we used a modified hyaluronic acid (HA) hydrogel. HA is a natural, non-immunogenic (4) ECM component that can be easily modified to display various chemistries (5). HA was thiolated (~40% efficiency) and crosslinked with poly(ethylene glycol) diacrylate (PEGDA) in order to initiate a Michael-type addition reaction. Addition reaction dynamics can be controlled by PEGDA molecular weight: hydrogels composed of higher molecular weight PEGDA reduced their mass swelling ratio, i.e. the ratio of swollen to dried polymer weight (Q_m), and stiffened faster than lower molecular weight PEGDA hydrogels. This could imply that a higher molecular weight PEGDA bound at one end may diffuse through greater space and thus is more likely to find an

unbound thiol site faster to form a crosslink. Michael-type addition as well as disulfide bond formation contributed to crosslink formation, and via AFM, the hydrogel was found to stiffen from 1.9 ± 0.1 to 8.2 ± 1.1 kPa. Hydrogel degradation via ester bond hydrolysis, which would actually soften the hydrogel, could compete with time-dependent crosslinking that stiffens the material; however hydrogel stiffness, thickness, swelling and surface topography were not greatly affected by hydrolysis, even in more basic conditions in which hydrolysis would occur more rapidly. In contrast to time-dependent hydrogels, polyacrylamide (PA) hydrogel crosslinking is provided by persulfate-generated free radical polymerization, which creates hydrogels with stiffness that remains constant over time, making this system a suitable control for HA hydrogels.

To examine to what extent material stiffening regulates cardiomyocyte development, embryonic cells were isolated from embryonic myocardial tissues at 72, 120, 168, 240, and 288 HPF and cultured *in vitro* on both hydrogel systems until reaching a total age of 312 HPF. After 312 HPF, expression of mature cardiac marker Troponin T was 3-fold higher on HA than PA hydrogels in cells isolated before 150 HPF. A better assessment of cardiac muscle formation, however, is the assembly of contractile units, i.e. myofibrils, which can be described by three major stages to indicate muscle maturity: pre-myofibrils, maturing myofibrils, and mature myofibrils where the alternating pattern of α-actinin is less than 1 μm, 1–1.8 μm, and 1.8–2.2 μm (6), respectively. Quantifying myofibril striation distance indicated that greater than 75% of pre-cardiac cells plated on HA hydrogels contained maturing or mature myofibrils for cells isolated before 150 HPF while these same cells on PA hydrogels mostly contained pre-myofibrils (40–85%) at these early time points, resulting in up to a 60% difference. Myofibril alignment with

respect to the long axis of the cell is also an indication of muscle maturity (6) and was found that for cells isolated before 168 HPF, HA hydrogels produced cells with better aligned myofibrils compared to PA hydrogels. Calcium imaging demonstrates the power spectral density remains relatively constant over time for HA and 11 kPa PA hydrogels, but greatly decreases on 1 and 34 kPa PA hydrogels.

We next wanted to determine biomolecular consequences of dynamic vs. static stiffness in the development of embryonic cardiomyocytes. In order to examine a wide range of intracellular targets, we employed an 854 protein kinase microarray to compare differences between embryonic cardiomyocytes plated on dynamic HA and static 11 kPa PA hydrogels. Through microarray analysis using clustering and GO-ELITE software (7), we observed the up-regulation of many pathways important to cardiac development, e.g. PI3K/Akt, Wnt signaling and MAPKs/ERKs. While cardiomyocyte development involves a multitude of varied signals, understanding the link between mechanical and molecular signals could be harnessed in many applications-from basic cellular biology to cellular therapeutics.

Lastly, we examined the use of our HA hydrogel system for a tissue engineering-based approach. The idea was to utilize embryonic stem cells and co-inject with our stiffening HA hydrogel to guide their differentiation into cardiomyocytes, which would in turn regenerate the damaged myocardium post-heart attack. We documented here that in a less vascularized, subcutaneous niche, these same formulations are capable of time-dependent changes in porosity and stiffness without significant immunogenicity. In much more vascularized tissues, however, an adverse host interaction, likely due to the presence of free thiols, and perhaps subsequent oxidation (8), created an inflammatory

reaction that will limit its myocardial compatibility. Despite these results in vascularized tissues, a less vascularized niche where dynamic changes occur may be suitable for thiolated HA hydrogels.

References

1. Breitbach M, Bostani T, Roell W, Xia Y, Dewald O, Nygren JM, Fries JW, Tiemann K, Bohlen H, Hescheler J, Welz A, Bloch W, Jacobsen SE, Fleischmann BK (2007) Potential risks of bone marrow cell transplantation into infarcted hearts. *Blood* 110(4):1362–1369.

2. Engler AJ, Sen S, Sweeney HL, Discher DE (2006) Matrix elasticity directs stem cell lineage specification. *Cell* 126(4):677–689.

3. Zamir EA, Srinivasan V, Perucchio R, Taber LA (2003) Mechanical asymmetry in the embryonic chick heart during looping. *Ann Biomed Eng* 31(11):1327–1336.

4. Humphrey JH (1943) Antigenic properties of hyaluronic acid. *Biochem J* 37(4):460–463.

5. Shu XZ, Liu Y, Luo Y, Roberts MC, Prestwich GD (2002) Disulfide cross-linked hyaluronan hydrogels. *Biomacromolecules* 3(6):1304–1311.

6. Sanger JW, Kang S, Siebrands CC, Freeman N, Du A, Wang J, Stout AL, Sanger JM (2005) How to build a myofibril. *J Muscle Res Cell Motil* 26(6–8):343–354.

7. Zambon AC, Gaj S, Ho I, Hanspers K, Vranizan K, Evelo CT, Conklin BR, Pico AR, Salomonis N (2012) GO-Elite: a flexible solution for pathway and ontology over-representation. *Bioinformatics* 28(16):2209–2210.

8. Munday R (1989) Toxicity of thiols and disulphides: involvement of free-radical species. *Free Radic Biol Med* 7(6):659-73.